ROLE OF NANOMATERIAL PHYSICOCHEMICAL PROPERTIES ON FATE AND TOXICITY IN BACTERIA AND PLANTS

Danielle Slomberg

A dissertation submitted to the faculty of the University of North Carolina at Chapel Hill in the partial fulfillment of the requirements for the degree of Doctor of Philosophy in the Department of Chemistry (Analytical Chemistry).

Chapel Hill
2013

Approved by:

Mark H. Schoenfisch

Royce W. Murray

James W. Jorgenson

Ann G. Matthysse

Bo Li

ABSTRACT

Danielle Slomberg: Role of Nanomaterial Physicochemical Properties on Fate and Toxicity in Bacteria and Plants
(Under the direction of Mark H. Schoenfisch)

Nanomaterials, defined as having at least one dimension <100 nm, are ubiquitous in nature. However, engineered nanomaterials have gained increasing attention for use in drug-delivery applications and consumer goods. Examination of nanomaterial toxicity, both beneficial (e.g., drug delivery to bacterial pathogens) and detrimental (e.g., death of terrestrial plants), thus warranted. Herein, I present the evaluation of nitric oxide-releasing nanomaterial toxicity to bacteria and silica particle toxicity to plants as a function of nanomaterial physicochemical properties.

Nanomaterial toxicity toward planktonic (i.e., free-floating) *Pseudomonas aeruginosa* and *Staphylococcus aureus* bacteria was evaluated as a function of scaffold size, shape, and exterior functionality using nitric oxide-releasing (NO) silica particles, dendrimers, and chitosan oligosaccharides. Improved bactericidal efficacy was observed for silica particles with decreased size and increased aspect ratio due to improved particle–cell interactions. Likewise, better nanomaterial–bacteria association and biocidal action was noted for more hydrophobic NO-releasing dendrimers and chitosan oligosaccharides. Planktonic bacterial killing was not dependent on chitosan molecular

weight due to rapid association between the cationic scaffolds and negatively-charged bacterial cell membranes.

Given the importance of nanomaterial physicochemical properties in planktonic bacterial killing, the NO-releasing scaffolds were also evaluated against clinically-relevant bacterial biofilms. Similar to planktonic studies, smaller particle sizes proved more efficient in delivering NO throughout the biofilm. Particles with rod-like shape also eradicated biofilms more effectively. The role of NO-releasing dendrimer and chitosan oligosaccharide hydrophobicity was prominent in scaffold diffusion through the biofilm and subsequent NO delivery, with scaffolds modified with hydrophobic functionalities generally exhibiting better bacterial association. Lastly, biofilm eradication was more effective for NO-releasing dendrimers exhibiting sustained NO-release compared to delivery of NO via an initial burst.

Phytotoxicity and uptake of silica nanoparticles was evaluated for the plant *Arabidopsis thaliana* as a function of particle size, surface composition, and shape (i.e., spherical versus rod-like particles). Overall, the silica nanoparticles examined were found to be relatively non-toxic to *A. thaliana* plants when pH effects were mitigated. Size-dependent uptake of the silica particles was observed, with smaller particles concentrating more heavily in the roots, rosette, and stem; however no shape-dependent uptake was noted at the low exposure concentration examined.

ACKNOWLEDGEMENTS

I would first like to thank my advisor, Dr. Mark Schoenfisch, for providing guidance and very practical knowledge and training that will last throughout the years.

I thank Dr. Alexis Carpenter, Dr. Bin Sun, and Dr. Yuan Lu for allowing me to assist in their NO-releasing nanomaterial projects early on. I thank Angela Broadnax for helping to synthesize particles for phytotoxicity experiments. I thank Dr. Wallace Ambrose for assistance with sample sectioning and thoughtful discussion. I also thank Dr. Neal Kramarcy and Dr. Michael Chua for assistance with confocal microscopy.

To the past and present Schoenfisch lab members: I thank you for making work an enjoyable and inspiring place to be. To my non-chemistry friends: I thank you for reminding me to keep balance in my life.

I thank my Mom, Dad, Christine, and Jim, as well as my siblings Allen, Ashley, and Zack for always supporting me through thick and thin…no matter what crazy ideas I may come up with. I can truly say that I wouldn't be where I am today without you.

TABLE OF CONTENTS

LIST OF TABLES

LIST OF FIGURES

LIST OF ABBREVIATIONS AND SYMBOLS

%	percentage
[…]	concentration
[NO]max	maximum NO flux
~	approximately
°C	degree(s) Celsius
µg	microgram(s)
µL	microliter(s)
µmol	micromole
AEAI	N-(2-aminoethyl)-3-amino-isobutyl-dimethyl methoxysilane
AHAP	N-(6-aminohexyl)aminopropyltrimethoxysilane
Ar	argon
atm	atmosphere(s)
ATTC	American Type Culture Collection
BET	Brunauer-Emmett-Teller
CDC	Centers for Disease Control and Prevention
CFU	colony forming units
cm	centimeter(s)
CO_2	carbon dioxide
Cu	copper

d	day(s)
DAF-2	4,5-diaminofluorescein
DAF-2 DA	4,5-diaminofluorescein diacetate
DLS	dynamic light scattering
DMF	N,N-dimethylformamide
E. coli	Escherichia coli
e.g.	for example
ED	1,2-epoxy-9-decene
EPS	exopolysaccharide
et al.	and others
etc.	and so forth
EtOH	ethanol
g	gravitational force
h	hour(s)
H_2O	water
HCl	hydrochloric acid
i.e.	that is
ICP-OES	inductively coupled plasma-optical emission spectroscopy
kg	kilogram
KOH	potassium hydroxide
LMW	low molecular weight

m	meter(s)
M	molar
MAP	3-methylaminopropyltrimethoxysilane
MBC	3-methylaminopropyltrimethoxysilane
MeOH	methanol
mg	milligram(s)
min	minute(s)
mL	milliliter(s)
mm	millimeter(s)
mM	millimolar
mmol	millimole(s)
mol	mole
mol%	percent of total moles
N_2	nitrogen
N_2O_3	nitrogen
NaCl	sodium chloride
NaOH	sodium hydroxide
NaOMe	sodium methoxide
NH_4OH	ammonium hydroxide
nm	nanometer(s)
nmol	nanomole(s)
NMR	nuclear magentic resonance spectroscopy

NO	nitric oxide analyzer
NO_2	nitrogen dioxide
NO_2^-	nitrite
NOA	nitric oxide analyzer
O_2	oxygen
OH-	hydroxide ion
ONOO-	peroxynitrite
P. *aeruginosa*	*Pseudomonas aeruginosa*
PAMAM	poly(amidoamine)
PBS	phosphate buffered saline, pH 7.4
PDI	polydispersity index
PEG	poly(ethylene glycol)
PI	propidium iodide
pmol	picomole(s)
PO	propylene oxide
ppb	parts per billion
PPI	poly(propylene imine)
ppm	parts per million
PROLI/NO	N-diazeniumdiolate-modified L-proline
RSNO	S-nitrosothiol
s	second(s)

S. aureus	*Staphylococcus aureus*
S. epidermidis	*Staphylococcus epidermidis*
SEM	scanning electron microscope/microscopy
SO	styrene oxide
t	time
$t_{1/2}$	half-life
TEM	transmission electron microscope/microscopy
TEOS	tetraethoxysilane
THF	tetrahydrofuran
t_{max}	time to max NO flux
TMOS	tetramethoxysilane
TSA	tryptic soy agar
TSB	tryptic soy broth
v/v	volume/volume
w/w	weight/weight
wt%	weight percent

CHAPTER 1: RECENT ADVANCES IN EVALUATION OF NANOMATERIAL TOXICITY TOWARD BACTERIA AND PLANTS

In 1959, physicist and Nobel laureate, Richard Feynman, challenged the scientific community to think small, noting that "[a]toms on a small scale behave like nothing on a large scale."[1] Feynman also suggested that "[the] problems of chemistry and biology [could] be greatly helped" if the ability "to do things on an atomic level, [was] ultimately developed." Inspired by these challenges, the field of nanotechnology has rapidly developed as researchers work to create materials with new molecular organization, properties, and functions relative to the bulk material.[2] However, evaluation of the toxicity of these engineered nanomaterials toward biological systems has only begun in recent years. In this introductory chapter, nanomaterial toxicity, both beneficial (e.g., drug delivery to bacterial pathogens) and detrimental (e.g., death of terrestrial plants), will be discussed as a function of the material's physicochemical properties.

1.1 Overview of nanomaterial toxicity

1.1.1 Engineered nanomaterials

Since the advent of nanotechnology, a wide variety of nanomaterials have been developed for a range of applications including drug delivery, biotechnology, water decontamination, and communication technologies.[3, 4] These engineered nanomaterials (ENMs) have at least one dimension between 1 and 100 nm.[5] Nanomaterials synthesized

for distinct applications include metal (e.g., Fe and Ag) and metal oxide nanoparticles (e.g., TiO_2 and SiO_2), dendrimers, carbon nanotubes, and quantum dots among others.[6] As the quantities and types of ENMs increase and consumers begin to use nanomaterial-containing products with greater frequency, the need for an improved understanding of nanomaterial physicochemical behavior and prevention of unintended biological and environmental consequences will also rise.[7] Humans and a myriad of other organisms will be exposed to ENMs through intended (e.g., common therapeutic use) or incidental routes (e.g., release into atmosphere, rivers, soil, etc). Thus, proactive measures are necessary to fully evaluate both the beneficial and detrimental implications associated with ENMs.

The behavior of ENMs, and ultimately their toxicity, is influenced by several physicochemical properties, such as increased surface area to volume ratio,[8] size, shape, exterior functionality,[9] and drug-release kinetics.[10] Each of these characteristics is significant in dictating how a nanomaterial will interact with cells and the surrounding environment. Generally, nanomaterials exhibit increased reactivity and toxicity compared to their bulk counterparts.[8] Midander et al. reported increased DNA damage in human lung cells exposed to nano-copper compared to micron-sized copper particles.[11] However, in some cases there is no difference in toxicity between nanomaterials and bulk formulations. Heinlaan et al. noted no significant differences in ecotoxicity to select bacteria and crustaceans exposed to ZnO, TiO_2, and CuO nanoparticles and their bulk oxides.[12] Likewise, nanoparticulate and bulk ZnO exhibited comparable toxicity to the freshwater microalga, *Pseudokirchneriella subcapitata*, with the toxicity attributed to

dissolved Zn and not nanoparticle effects.[13] Evaluation of nanomaterial toxicity relative to the corresponding bulk material on a case by case basis is thus warranted.

1.1.2 Nanomaterial-cell interactions

Nanomaterial-cell interactions will greatly depend on nanomaterial size, shape, surface characteristics, and drug-release properties (if any). Generally, improved penetration of cell membranes is observed for smaller nanoparticles. Association of nanomaterials with the cell membrane may also be governed by nanomaterial shape. Nanomaterial surface charge is important in that the cell membrane is negatively-charged and will associate more readily with positively-charged materials. In addition, more hydrophobic ENMs are better able to penetrate the lipophilic membrane.

After association with the cell, nanomaterials can cause DNA damage, degrade the membrane, or interrupt key processes for cellular function. The mechanism of action varies with nanomaterial composition, size, and shape. For example, Yang et al. studied the cytotoxicity, oxidative stress, and genotoxicity as a function of ENM composition (i.e., carbon nanotubes and silica and ZnO nanoparticles), size, and shape.[14] Particle composition played the primary role in cytotoxicity, and genotoxicity was significantly influenced by ENM shape. However, no significant toxicity was attributed to size. The effects of nanomaterial physicochemical properties on their interactions with cells is clear, thus researchers are currently focused on further developing methodology to understand and evaluate these interactions and any resulting toxicity.

1.1.3 Evaluation of nanomaterial toxicity

Given the importance of assessing ENM parameters in toxicity, a variety of in vitro and in vivo assays are currently used for screening risk. In vitro systems are ideal in that they are cost effective and generate rapid, reproducible results.[15] Common methods for screening new ENMs include the LDH (cell membrane integrity) and MTT assays (mitochondrial function), as well as assays for measuring cell-generated reactive oxygen species and immunochemistry markers (apoptosis and necrosis).[15, 16] Due to the variety of physiological environments and applications in which ENMs may be encountered, these in vitro assays are tested against numerous cell types including phagocytic, neural, hepatic, epithelial, endothelial, and red blood cells.[16] Despite the toxicity data generated with in vitro tests, determinations of safety need to be made based on the final fate of ENMs in biological systems.[15] Thus, tests to evaluate ENM absorption, distribution, transformation, and excretion in vivo are ultimately warranted. Researchers are now focused on a predictive toxicological approach in which high-throughput screening is used in vitro and in vivo to determine ENM structure-activity relationships and hazard risk.[17-19]

Understanding the nano-bio interface is crucial to elucidating potential ENM toxicity in environmental applications as well.[20] The transformation and fate of ENMs and the potential for biomagnification and biodistribution within a multitude of ecosystems necessitate evaluation as risk of exposure is likely to increase.[7] Whether viewed as beneficial or detrimental, nanomaterial toxicity is likely to play an ever increasing role in our daily lives.[21]

1.2 Nanomaterial toxicity toward bacteria

1.2.1 Bacteria in clinical settings

Although bacteria are ubiquitous in aquatic and soil-based ecosystems, their prevalence in clinical settings has become particularly problematic, with hospital-acquired infections being the fourth-leading cause of death in the United States.[22, 23] Open wounds[24, 25] and implanted medical devices such as prosthetic heart valves,[23] orthopedic implants, and catheters are frequent sites of microbial infection despite aseptic procedures and instrument sterilization.[23, 26, 27] With >99% of all bacteria existing in a biofilm state, these infections are increasingly difficult to treat.[28] Bacterial biofilms have shown decreased susceptibility to antibacterials compared to their planktonic (i.e., free-floating) counterparts.[28-31] Consequently, infected medical implants often necessitate device removal,[32] and hospital-acquired infections can result in sepsis,[33] and even death. Current research is focused on developing nanomaterial-based drugs to address these problems. Furthermore, understanding the clinical significance of nanomaterial toxicity to bacteria will aid in the design of future antibacterial and anti-biofilm agents.

Bacterial biofilm formation occurs in several sequential phases as shown in Figure 1.1.[34] Prior to bacterial adhesion, organic and inorganic nutrients first adsorb to the surface. When bacteria come into contact with this conditioned surface, they

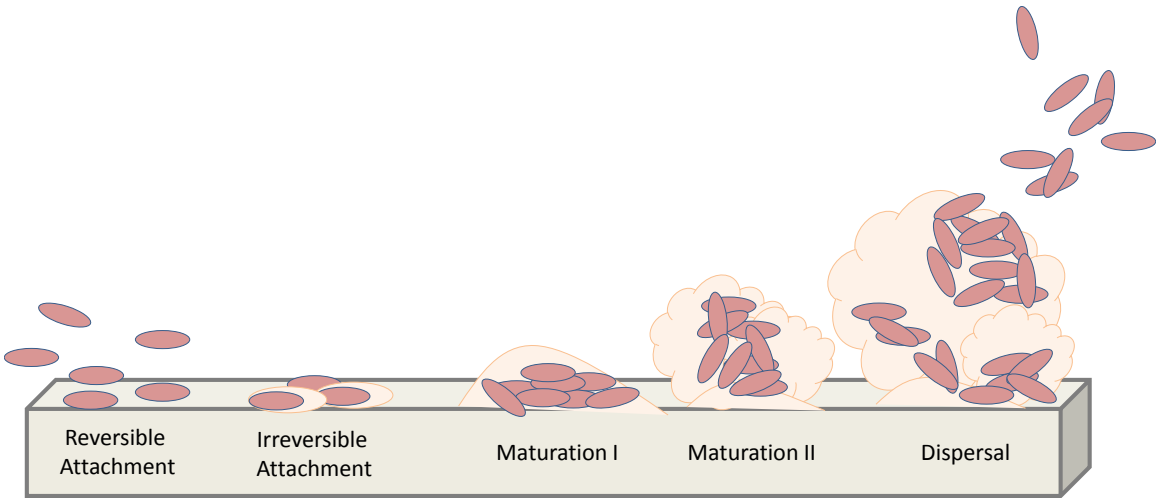

Figure 1.1 Stages of bacterial adhesion to a substrate and subsequent biofilm formation.

reversibly attach via gravitational, electrostatic, and van der Waals forces. Short range (i.e., hydrogen boding, dipole-dipole, ionic, and hydrophobic) interactions also influence the degree of bacterial adhesion. After a few hours, the bacteria begin to secrete extracellular polymeric substances (EPS) and form cell-to-cell bridges, thus irreversibly attaching to the surface.[35, 36] Maturation of the biofilm continues as bacterial cells grow, divide, and form microcolonies (clusters of bacteria).[37] The biofilm formation process continues over hours to days depending on several abiotic (e.g., nutrient conditions and pH) and biotic (e.g., quorum-sensing) factors. Following maturation, detachment of biofilm bacteria from microcolonies may occur via regulated dispersal mechanisms to release planktonic cells that can further colonize surfaces.[34, 38]

Given the frequency and complexity of bacterial surface colonization, and the rate at which bacterial biofilms are increasingly difficult to treat, research into antibacterial resistance mechanisms has continued to garner attention. The traditional antibacterial resistance mechanisms attributed to planktonic bacteria include efflux pumps, modifying enzymes, and target mutations, but these mechanisms do not always explain the resistance of biofilm-embedded bacteria.[39] Genetic mutation of the biofilm bacteria is not likely the main cause of resistance since biofilm cells will once again exhibit susceptibility to antibacterial agents upon dispersal.[40, 41] Three proposed mechanisms for the increased resistance of biofilms are slow antibacterial penetration beyond surface layers of the biofilm, differentiation of cells into a resistant phenotype, and reduced antibacterial action in altered microenvironments (e.g., regions of nutrient depletion).[39]

As a result, complete eradication of biofilms using common antibacterials has been met with increasing difficulty and is often not feasible.

1.2.2 Current bacteria eradication strategies

Ideally, hospital-acquired infections would be controlled by eliminating initial bacteria attachment to a surface and thus preventing biofilm formation by adherent cells.[34] However, superhydrophobic,[42] heparin-coated,[43] and antibacterial-doped substrates[44, 45] have met varied success in eliminating bacterial adhesion and reducing clinical infection. These strategies are also often not amenable to implanted sensor applications, which can hinder their utility. As such, additional bacteria eradication strategies have been implemented for cases in which surface colonization cannot be prevented. Bacterial biofilm formation has been minimized through interference of iron metabolism,[46, 47] enhancement of macrophage phagocytosis of the bacteria,[48] or disruption of quorum-signaling.[23, 34] Another biofilm control strategy has focused on targeting the EPS layer. Hatch and Schiller observed enhanced diffusion of the antibiotics, gentamicin and tobramycin, after the enzyme, alginate lyase, degraded the EPS layer of *P. aeruginosa* biofilms.[49] Lastly, several researchers are working toward the development of new antibacterial agents, that will be effective against current and emerging multi-drug resistant bacteria strains.[50-53] Successful new antibacterial agents will need to not only prevent initial adhesion or eradicate established biofilms, but must do so without fostering resistance or harming healthy host cells.

1.2.3 Nitric oxide as an antibacterial agent

Nitric oxide (NO) is an endogenously-produced, diatomic free radical that participates in several concentration-dependent processes within the body.[54-56] At low concentrations (~pM–nM), NO mediates vasodilation, angiogenesis, and neurotransmission.[57-59] However, at higher concentrations (~μM), NO can serve as a potent antibacterial agent, inducing oxidative and nitrosative stresses that damage the bacteria membrane.[60-62] In the presence of bacterial pathogens, macrophages utilize inducible nitric oxide synthase (iNOS) to generate NO. Once formed, NO can react with oxygen or other reactive oxygen intermediates (e.g., superoxide) to yield antibacterial byproducts (e.g., peroxynitrite, nitrogen dioxide, and dinitrogen trioxide).[60] These reactive species can then induce oxidative stress, resulting in lipid peroxidation, tyrosine nitrosation, and oxidative DNA cleavage. Concurrently, thiol nitrosation, deamination of cellular proteins, and nitrosamine formation occur via nitrosative stress. Through disruption of bacterial components and disabling of crucial cell functions, NO and its reactive byproducts have proven effective as antibacterial agents against both Gram-positive and Gram-negative species.[63, 64] Additionally, NO is a known anti-biofilm agent, capable of eradicating a variety of microbial strains including *P. aeruginosa*, *E. coli*, *S. aureus*, *S. epidermidis*, and *C. albicans*.[62] The utility of NO as an antibacterial and anti-biofilm agent is demonstrated by its broad-spectrum and multi-mechanistic killing, thereby reducing the chance for bacteria resistance to treatment.

Although NO exerts the desired toxicity against both planktonic and biofilm-based bacteria, candidate therapeutics must also exhibit limited toxicity toward healthy mammalian cells. Nitric oxide toxicity to mammalian cells is mitigated by a series of

antioxidant enzymes, including superoxide dismutase, catalase, and peroxidase.[65] Superoxide dismutase converts superoxide formed from the reaction of NO and oxygen into hydrogen peroxide. Catalase and peroxidase then convert the produced hydrogen peroxide into water. Using these enzymatic pathways, mammalian cells are able to turn superoxide and hydrogen peroxide into water, thus reducing NO-induced toxicity. Of note, some bacterial cells (e.g., *S. aureus*) produce lower levels of antioxidant enzymes and can adapt to oxidative stress via NO-mediated cytoprotection; however, bacteria are generally unable to mitigate the toxic effects of NO and its reactive byproducts as readily as mammalian cells.[66]

In addition to NO produced endogenously by immune cells, exogenous gaseous NO has proven effective in eradicating bacterial infections.[67] However, control over the dose and location of delivery is challenging due to the highly reactive nature of gaseous NO. While administration of gaseous NO is appropriate for topical and pulmonary treatments, the use of NO in other clinical applications necessitates greater control of dosage and delivery.[68] As such, compounds (NO donors) that store NO and release it upon an appropriate trigger (e.g., pH change, light, heat) have been developed.[56]

1.2.4 Nitric oxide donors

Several types of NO donors have been synthesized to store and controllably release NO, with major donor classes including metal-NO complexes, nitrosamines, nitrosothiols, and diazeniumdiolates. *N*-diazeniumdiolates, specifically, have found widespread use in biomedical applications due to their stability, ability to release NO

under physiological conditions, and varied NO-release kinetics.[69] The *N*-diazeniumdiolate moieties are formed on amine sites of the donor compound upon reaction with high pressures (~10 atm) of gaseous NO in the presence of a strong base (Figure 1.2 A).[70] In the more generally accepted mechanism, the amine reacts with an NO dimer (N_2O_2) to form the *N*-diazeniumdiolate. Release of NO then occurs via proton-intitiated decomposition, in which the *N*-diazeniumdiolate decomposes under aqueous conditions to yield 2 moles of NO and the parent secondary amine (Figure 1.2 B). Overall, the *N*-diazeniumdiolate functionality is stable in the absence of a proton source and at low temperature, making it an appropriate NO donor for a variety of clinically-relevant applications.

N-diazeniumdiolate NO donors have been formed on small molecules such as proline (PROLI/NO) and diethylenetriamine (DETA/NO) for treatment of cardiovascular disease and respiratory distress.[55, 71] However, low molecular weight (LMW) donors diffuse rapidly, exhibit short circulation times, and often necessitate higher doses of NO to elicit an effect.[56] Side effects including hypotension, headaches, and possible tolerance have been noted during clinical use.[72] Given these shortcomings, macromolecular scaffolds can instead be utilized to obtain controlled and localized NO delivery, facilitate targeting, and decrease potential for tolerance.[56, 61]

Relative to LMW donors, macromolecular NO-releasing scaffolds have numerous advantages including increased NO payload, targeted and localized delivery, and tunable NO-release kinetics.[73] With many clinical applications utilizing the benefits of NO,

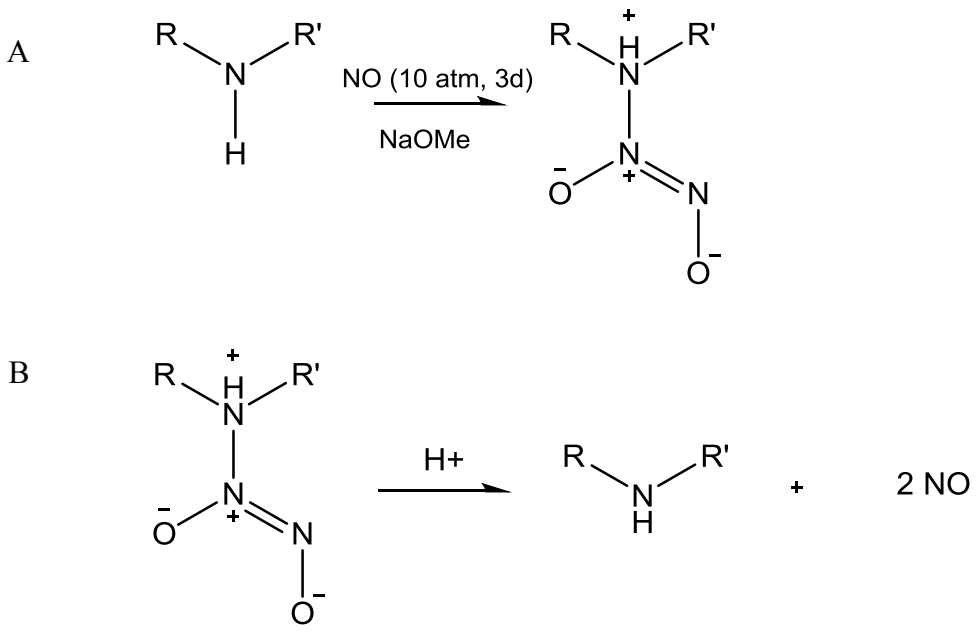

Figure 1.2 *N*-diazeniumdiolate (A) formation and (B) proton-initiated decomposition.

control over the concentration, location, timing, and duration of NO release can decrease the potential for tolerance and unwanted toxic side effects. As such, several types of NO-releasing protein, organic, inorganic, and hybrid polymer macromolecular scaffolds have been designed.[73] An ideal NO-releasing macromolecular scaffold would be functionalized with multiple NO donors and/or targeting ligands to achieve localized release with the desired payload while controlling toxicity. The NO-releasing macromolecular scaffolds presented in this work include silica nanoparticles, dendrimers, and chitosan oligosaccharides. These NO-release vehicles allow for the tuning of size, shape, hydrophobicity, and NO-release kinetics to evaluate the effects of nanomaterial physicochemical properties on bactericidal efficacy to planktonic bacteria and biofilms.

Silica nanoparticles are appealing drug delivery scaffolds in that they are chemically stabile, allow for covalent modification, and generally exhibit low cytotoxicity.[74] Additionally, their size and shape can be tuned to improve nanoparticle–cell interactions. Silica particles are commonly synthesized via sol-gel chemistry, where silane precursors undergo hydrolysis and condensation under basic conditions to form a solid silica network.[75] Briefly, the sol-gel process begins when a silane precursor is hydrolyzed upon attack by a hydroxide ion (Figure 1.3 A). A second hydrolyzed silane can then condense with the first to form a siloxane bond (Figure 1.3 B). As hydrolysis and condensation continue, a solid silica network forms. Reaction conditions can be tailored to control silica particle formation and growth. Specifically, the Stöber method offers a facile approach for synthesizing silica particles in a “one-pot” reaction.

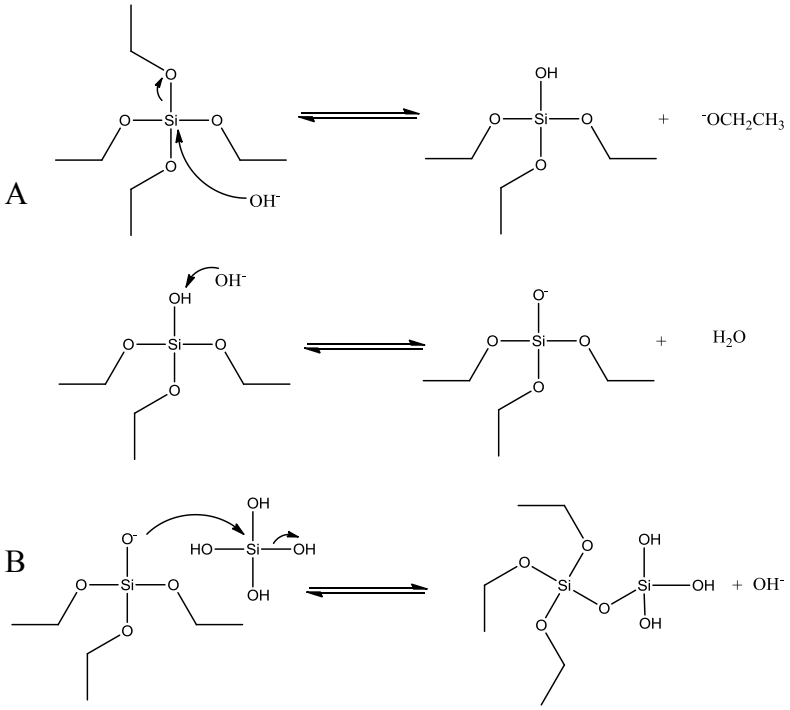

Figure 1.3 Representative formation of silica particles via (A) hydrolysis and (B) condensation under basic conditions.

Silica particles can be synthesized via the Stöber method through the hydrolysis and condensation of a tetraalkoxysilane in a solution of water, an alcohol solvent (e.g., ethanol), and a base catalyst.[76] Monodispersity of the synthesized particles is dependent on the rates of nucleation and growth during the reaction. Conditions favoring simultaneous formation of particle nuclei, with similar subsequent growth result in particles with narrow distributions in size. Silica particles synthesized via the Stöber method are generally ≥100 nm as the conditions favor particle growth over nucleation. Alternatively, silica particles with sizes on the low end of the nanoparticle regime (i.e., <100 nm) can be synthesized by a reverse microemulsion approach in which particles are confined to micelles of a pre-determined size as they form.[77] Tuning of particle size is critical in biomedical applications since effective drug delivery is generally inversely proportional to particle size.

Particle size can be tuned by varying the concentration of water or ammonia, the chain length of the alcohol solvent, and the reaction temperature.[76, 78] Increasing water concentration (>9 M) of the reaction promotes hydrolysis, and thus reduces particle size, while decreasing the water concentration favors nuclei aggregation and growth of the silica particles. Ammonia also influences size and morphology, with larger, non-spherical particles observed at low concentrations due to instability of the suspended particles. During particle formation, the size is also dictated by the choice of solvent. Long-chain (i.e., larger molecular weight) water-miscible alcohol solvents slow hydrolysis and result in increased particle size. Similarly, decreasing the reaction temperature hinders hydrolysis and increases particle size.

In addition to size, the aspect ratio of silica particles can be altered to evaluate drug delivery efficiency and nanoparticle–cell interactions as a function of shape. Rod-like particles of various compositions (e.g., poly(ethylene glycol), silica, and poly(lactide-co-glycotide)) have demonstrated increased mammalian cell internalization and circulation time compared to spherical particles, thus improving their capacity for drug delivery.[79-83] Silica nanorods of varied aspect ratio (i.e., 1–8) have been synthesized via a surfactant-templated synthesis, where the nanorods are grown along micelles. Control over the shape and geometry of the micelle ultimately impacts the final shape of the silica nanorod. Particle aspect ratio has been tuned by altering the type of surfactant, reaction temperature, ammonia concentration, or solution volume. Despite previous studies on mammalian cell interactions and uptake, there is a lack of understanding on how nanoparticle shape influences bactericidal efficacy against planktonic and biofilm-based bacteria.

Loading of NO onto the aforementioned silica particles and nanorods via *N*-diazeniumdiolation necessitates modification of the scaffold with a secondary amine. Secondary amine-modified silica particles can either be achieved via co-condensation of an aminosilane and a "backbone" silane (e.g., tetraalkoxysilane) or via surface-grafting onto an already formed silica scaffold. These NO-releasing hybrid silica particles are capable of storing large payloads of NO, with tunable NO-release to maximize bactericidal efficacy.[61, 84, 85]

To fully explore the effects of NO-releasing nanomaterial characteristics on toxicity toward bacteria, dendrimers have been evaluated as a second type of delivery scaffold. Dendrimers are highly-branched, nano-scale macromolecules.[86] Bonds emanate from a central core at the interior of the dendrimer, forming a hyper-branched, multivalent structure. A wide range of dendritic scaffolds have been used in drug delivery,[87] gene transfection,[88, 89] tissue engineering,[90] and even antibacterial applications. For example, quaternary ammonium-modified dendrimers have demonstrated efficacy in bacterial killing, but their inherent positive charge resulted in significant toxicity to mammalian cells.[91] Masking this charge with poly(ethylene glycol) (PEG) helped mitigate the cytotoxicity while still providing potent antibacterial efficacy. Poly(amidoamine) (PAMAM) dendrimers and partially PEG-modified dendrimers were also proven effective against planktonic bacteria, with complete eradication of *P. aeruginosa* and *S. aureus* at μg/mL concentrations.[92]

The multi-valency and amine-loading capabilities of dendrimers make them great candidates for coupling with NO release to further improve biocidal action. Taite et al. synthesized NO-releasing PEG-lysine dendrimers for cell proliferation applications, but low NO storage and lack of control over release kinetics make them non-ideal as antibacterial agents.[93] Instead, the Schoenfisch lab has designed NO-releasing poly(propylene imine) (PPI) and PAMAM dendrimers that can store and deliver increased NO payloads (~2–5.6 μmol/mg).[94-96] The reaction of secondary amine sites on the PAMAM dendrimers with high pressures of NO to form *N*-diazeniumdiolates is detailed in Figure 1.4.

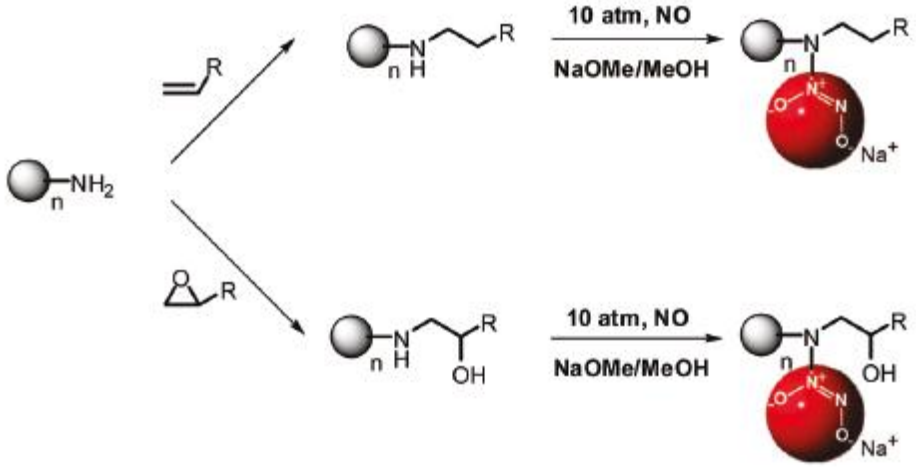

Figure 1.4 Formation of secondary amine sites on dendrimers via Michael addition or ring-opening reaction and subsequent *N*-diazeniumdiolation.

In drug delivery applications, important dendrimer parameters to evaluate are size (i.e., generation), surface functionalization, and cytotoxicity. Unlike silica particles that range from ~10–1000 nm, dendrimers can be reproducibly synthesized with sizes <10 nm. Of note, as dendrimer generation is increased, the number of surface groups at the exterior also increases, likely enhancing biocidal action. The type of functional group bound to the dendrimer scaffold has also been shown to influence NO-release properties. For example, NO-releasing PAMAM dendrimers functionalized with varied carbon chain lengths (i.e., C1–C7) exhibited half-lives of 2.5–86 min, with the longer chain resulting in extended NO release.[94]

Silica particles and dendrimers are both effective NO delivery vehicles, allowing for tailored NO-release through varied size, exterior functionality, and kinetics. However, after the NO release has expired, select applications may necessitate degradation of the scaffold. Biodegradable scaffolds are best suited for pulmonary,[97] oral, and parenteral drug delivery,[98] as well as tissue engineering.[99] The natural biopolymer, chitosan, has already shown promise in these applications due to its biocompatibility and biodegradability. Chitosan also exhibits antimicrobial properties toward bacteria, fungi, and viruses.[100] Furthermore, as shown in Figure 1.5, the high secondary amine content of the chitosan backbone lends itself to *N*-diazeniumdiolate modification and subsequent NO release, thus increasing potential for antibacterial action. In previous reports, low *N*-diazeniumdiolate conversion and NO storage (~0.2 μmol/mg) were observed for chitosan polysaccharides (~60–220 kD), likely due to their insolubility in the necessary basic conditions. Chitosan oligosaccharides (<20 kD), however, are soluble in basic conditions

and thus offer a better approach for designing NO-releasing scaffolds with improved conversion efficiency and total storage.

Similar to NO-releasing silica and dendrimer scaffolds, the physicochemical properties (e.g., molecular weight and exterior functionality) of chitosan oligosaccharides can be tailored to influence NO-release kinetics and bactericidal action. The molecular weight (MW) of chitosan oligosaccharides can be controlled through the oxidative degradation of chitosan using hydrogen peroxide. Hydrogen peroxide concentration, (0.5–3.5%), reaction temperature (≥80 °C), and reaction time (~2.5–12 h) have all been shown to influence the degree of chitosan degradation and the resulting chitosan oligosaccharide MW.[101] Additionally, a variety of functional groups can be introduced to the chitosan oligosaccharides via covalent modification. For example, secondary amine functionality can be imparted to the chitosan oligosaccharides via a cationic ring opening reaction with 2-methyl aziridine (MAz), after which PEG modification can be achieved via the Michael addition.

1.2.5 Tuning properties of nitric oxide-releasing nanomaterials

The physicochemical properties of NO-releasing scaffolds are critical in improving NO delivery efficiency and bactericidal action while minimizing cytotoxicity to healthy host cells. Nanomaterial size, shape, exterior functionality, and NO-release kinetics are all important parameters to consider in evaluating nanomaterial–bacteria interactions. Particles of small size exhibit increased surface area to volume ratios compared to their larger counterparts. Thus, smaller NO-releasing particles have a greater

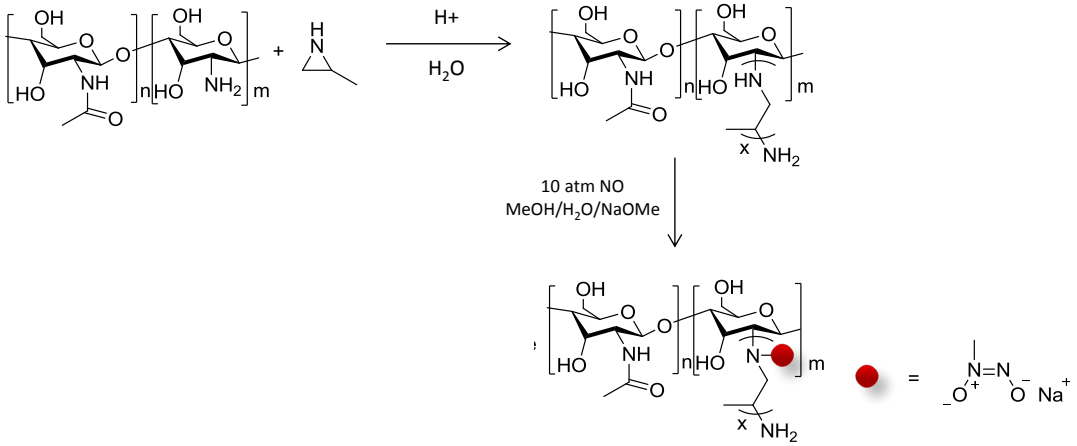

Figure 1.5 Formation of secondary amine-modified chitosan oligosaccharides and subsequent *N*-diazeniumdiolation.

number of their *N*-diazeniumdiolates at the particle surface, likely promoting faster NO release and bacterial killing. Smaller nanoparticles are also likely to exhibit improved bactericidal efficacy due to more rapid diffusion to the bacterial cell surface. Particles with high aspect ratios (i.e., rod-like) may also enhance the efficiency of NO delivery given the potential for an increased surface area of interaction between the nanoparticle and bacterial membrane. Increased bactericidal efficacy of nanomaterials with more hydrophobic character will likely be observed due to improved association with the lipid-containing bacterial membrane; however, cytotoxicity may present a challenge. Lastly, evaluating scaffold NO-release kinetics will be crucial to understanding the desired release profile (i.e., short burst of NO versus low sustained levels) for eradication of planktonic bacteria versus biofilms.

1.3 Nanomaterial toxicity toward plants

1.3.1 Phytotoxicity and uptake of nanomaterials

Although just recently gaining attention in biomedical and commercial applications, nanomaterials have been a part of the environment for most of the Earth's history.[102, 103] Natural nanoparticles have been found in areas as diverse as volcanic dust and 10,000 year old glacial ice cores.[102] These naturally occurring nanoparticles have shown toxicity to some life forms, raising concerns that engineered nanoparticles will exhibit similar toxicity. Engineered nanoparticles (ENPs) incorporated into consumer goods are now making their way into atmospheric, aquatic, and terrestrial environments due to incidental and direct release/disposal (Figure 1.6).[104-106] However, while natural

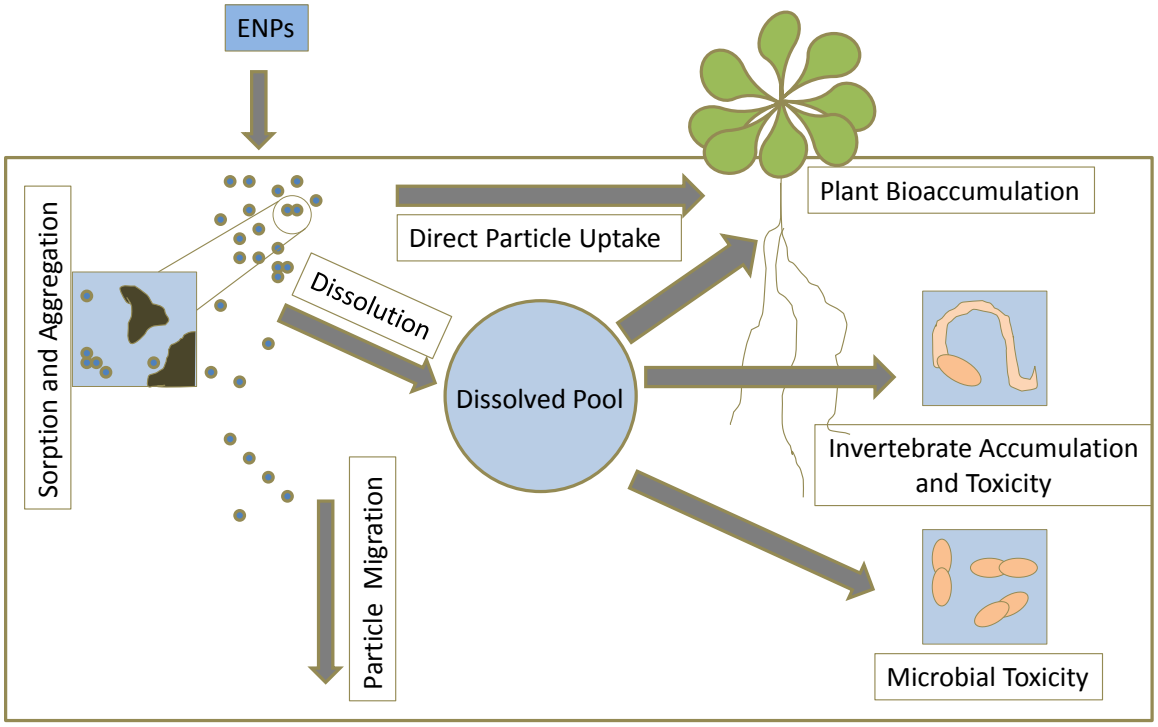

Figure 1.6 Transformation and key processes of engineered nanoparticles in soil (modified from Klaine et al).[10]

nanoparticles tend to be transient in the environment, disappearing by either dissolution or aggregation, some ENPs have been shown to persist due to stabilization by surfactants or organic matter. A better understanding of particle fate, behavior, and potential toxicity in the environment is thus warranted. As such, researchers are evaluating ENP mobility, fate, and bioavailability in the environment as a function of size, shape, and surface charge.[10, 102] Prior studies have assessed the toxicity of ENPs toward mammalian cells, bacteria, aquatic invertebrates, and other terrestrial organisms. However, plant toxicity (i.e., phytotoxicity) and potential uptake due to nanoparticle exposure have received less attention to date, especially with regard to ENP physicochemical properties.[107, 108] Of note, ENP–plant interactions may not always result in toxicity, as some nanoparticles (e.g., mesoporous silica) have been used for target-specific delivery of proteins, nucleotides, or other chemicals for plant biotechnology applications.[109]

Previous work with plants has evaluated the toxicity of silica (SiO_2), zinc oxide (ZnO), nickel hydroxide ($Ni(OH)_2$), copper (Cu), cerium oxide (CeO_2), titanium dioxide (TiO_2), iron oxide (Fe_3O_4), gold (Au), silver (Ag), and iron (Fe) nanoparticles, as well as CdSe/ZnS quantum dots and carbon nanotubes to *Arabidopsis thaliana*,[105, 110] rye grass,[111, 112] mesquite,[113] and select edible plant species including wheat and mung bean,[106] alfalfa, tomato, corn, and cucumber.[114, 115] Although current research has made some progress in determining the effects of nanomaterials on terrestrial plants, systematic studies are still lacking in the literature.

1.3.2 Nanomaterial physicochemical properties in phytotoxicity

Some researchers have started to evaluate phytotoxicity as a function of nanomaterial physicochemical properties such as size, shape, and surface charge. Nanoparticle size has been the most readily examined parameter, with increased phytotoxicity generally observed in correlation with decreased particle size. Lee et al. noted that ZnO nanoparticles (~44 nm) were more toxic to *Arabidopsis thaliana* than micron-sized counterparts.[105] Similarly, smaller (~3.5 nm) Au NPs were more toxic to tobacco plants and exhibited greater uptake compared to larger (~18 nm) particles.[116] After 7 d exposure to silver NPs (20 and 100 nm), size-dependent NP toxicity was observed in *L. minor*.[117] However, no significant difference in toxicity was noted between the 20 and 100 nm particles after a 14 d exposure.

The importance of nanoparticle shape and surface charge in phytotoxicity have also been noted, but studies systematically investigating these parameters are not currently available.[118] Phytotoxicity observed in cabbage, tomato, red spinach, and lettuce seedlings exposed to graphene sheets was attributed to the nanomaterial morphology and aggregation.[119] The graphene sheet form of the carbon-based nanomaterial exhibited similar growth inhibition to carbon nanotubes, demonstrating the role of nanomaterial shape on phytotoxicity. Aluminum nanoparticle surface charge has been shown to vary with environmental conditions (e.g., pH).[120] Neutral species resulted in NP flocculation while negatively-charged species remained stable in solution. Despite evaluations of stability and transport in aqueous media, aluminum species of distinct surface charge have not yet been investigated for phytotoxic effects.[120]

1.3.3 Silica nanoparticle phytotoxicity

Silica nanoparticles (SiNPs) have received special interest in toxicology studies due to their prominence in cosmetic and biomedical applications.[121-123] In one study, 12.5 and 27.0 nm SiNPs (20.0 and 28.8 mg L^{-1}, respectively) were shown to reduce growth of green alga by 20% after 72 h.[124] Phytotoxicity assays with *Cucurbita pepo* (zucchini), however, showed no significant difference in germination percent, root elongation, or biomass after exposure to 1000 mg L^{-1} bulk silicon powder and SiNPs (< 100 nm) for 5–14 d.[125] Lee and coworkers found that 42.8 nm SiNPs promoted *Arabidopsis thaliana* root elongation at a low concentration (400 mg L^{-1}), but resulted in toxicity at higher concentrations (≥ 2000 mg L^{-1}).[105] While prior work on the phytotoxicity of SiNPs to higher plants has established a strong foundation, lack of toxicity examination as a function of increased SiNP size range (i.e., < 42.8 nm and > 100 nm), shape (i.e., rod-like versus spherical), duration of exposure, and surface composition necessitated further investigation. Additionally, visualization of SiNPs in the plant cells and determination of uptake location (i.e., roots, rosette, and stem) had not been previously observed.

1.4 Summary of dissertation research

The goal of my dissertation research was to evaluate how nanomaterial physical and chemical properties influence toxicity toward biological systems such as bacteria and plants. The specific aims of my research were to:

1. determine the bactericidal efficacy of NO-releasing silica, dendrimer, and chitosan scaffolds against planktonic and biofilm bacteria as a function of size, shape, and surface exterior functionality;

2. evaluate the mechanisms of antibacterial activity for these scaffolds using confocal microscopy; and,

3. determine the phytotoxicity and uptake of silica nanoparticles for *Arabidopsis thaliana* as a function of the physical properties of this scaffold.

In this introductory chapter, the potential of NO-releasing silica, dendrimer, and chitosan scaffolds are justified for antibacterial applications. The physicochemical properties of these NO-release vehicles are critical for tuning the influence of nanomaterial–cell interactions and drug (i.e., NO) delivery efficiency. Likewise, these properties prove important in dictating nanoparticle toxicity to plants. In order to develop safe nanomaterials with minimal risk, we must examine how they act in the body and on the environment. In Chapter 2, planktonic bacterial killing with NO using three distinct sizes and shapes of silica nanoparticles, dendrimers with varied exterior functionalities, and chitosans of different molecular weights and hydrophobicities is described. Subsequent studies in Chapter 3 utilize these NO-releasing scaffolds to evaluate the eradication of more clinically-relevant bacterial biofilms as a function of nanomaterial size, shape, exterior functionality, and molecular weight. In Chapter 4, NO-releasing dendrimers with identical NO storage but varied NO-release kinetics are used to evaluate the desired NO-release profiles for killing of planktonic and biofilm bacteria. The

importance of size and shape on silica nanoparticle phytotoxicity to *Arabidopsis thaliana* is described in Chapter 5. Finally, Chapter 6 provides an overall summary of my dissertation work and details possible future directions in evaluating nanomaterial physicochemical properties and their relation to potential toxicity.

REFERENCES

1. Feynman, R. P., There's plenty of room at the bottom. *Caltech Engineering and Science* **1960**, pp 22-36.

2. Alvarez, P., Nanotechnology in the Environment: The good, the bad, and the ugly. *Journal of Environmental Engineering* **2006,** *132*, 1233.

3. Roco, M. C.; Mirkin, C. A.; Hersam, M. C., *Nanotechnology research directions for societal needs in 2020*. New York, **2011**.

4. Cañas, J. E.; Long, M.; Nations, S.; Vadan, R.; Dai, L.; Luo, M.; Ambikapathi, R.; Lee, E. H.; Olszyk, D., Effects of functionalized and nonfunctionalized single-walled carbon nanotubes on root elongation of select crop species. *Environ*. *Toxicol*. *Chem*. **2008,** *27*, 1922-1931.

5. Handy, R.; Kammer, F.; Lead, J.; Hassellov, M.; Owen, R.; Crane, M., The ecotoxicology and chemistry of manufactured nanoparticles. *Ecotoxicol*. **2008,** *17*, 287-314.

6. Wiesner, M. R.; Lowry, G. V.; Alvarez, P.; Dionysiou, D.; Biswas, P., Assessing the risks of manufactured nanomaterials. *Environ*. *Sci*. *Technol*. **2006,** *40*, 4336-4345.

7. Colvin, V. L., The potential environmental impact of engineered nanomaterials. *Nat*. *Biotechnol*. **2003,** *21*, 1166-1170.

8. Rotello, V., *Nanoparticles: Building Blocks for Nanotechnology*. Springer: New York, 2004.

9. Kim, S. T.; Saha, K.; Kim, C.; Rotello, V. M., The role of surface functionality in determining nanoparticle cytotoxicity. *Accounts of Chemical Research* **2013,** *46*, 681-691.

10. Klaine, S. J.; Alvarez, P. J. J.; Batley, G. E.; Fernandes, T. F.; Handy, R. D.; Lyon, D. Y.; Mahendra, S.; McLaughlin, M. J.; Lead, J. R., Nanomaterials in the environment: Behavior, fate, bioavailability, and effects. *Environ*. *Toxicol*. *Chem*. **2008,** *27*, 1825-1851.

11. Midander, K.; Cronholm, P.; Karlsson, H. L.; Elihn, K.; Möller, L.; Leygraf, C.; Wallinder, I. O., Surface characteristics, copper release, and toxicity of nano- and micrometer-sized copper and copper(II) oxide particles: A cross-disciplinary study. *Small* **2009,** *5*, 389-399.

12. Heinlaan, M.; Ivask, A.; Blinova, I.; Dubourguier, H.-C.; Kahru, A., Toxicity of nanosized and bulk ZnO, CuO and TiO2 to bacteria *Vibrio fischeri* and crustaceans *Daphnia magna* and *Thamnocephalus platyurus*. *Chemosphere* **2008,** *71*, 1308-1316.

13. Franklin, N. M.; Rogers, N. J.; Apte, S. C.; Batley, G. E.; Gadd, G. E.; Casey, P. S., Comparative toxicity of nanoparticulate ZnO, Bulk ZnO, and $ZnCl_2$ to a freshwater microalga (*Pseudokirchneriella subcapitata*): The importance of particle solubility. *Environ*. *Sci*. *Technol*. **2007,** *41*, 8484-8490.

14. Yang, H.; Liu, C.; Yang, D.; Zhang, H.; Xi, Z., Comparative study of cytotoxicity, oxidative stress and genotoxicity induced by four typical nanomaterials: the role of particle size, shape and composition. *J*. *Appl*. *Toxicol*. **2009,** *29*, 69-78.

15. Sharifi, S.; Behzadi, S.; Laurent, S.; Forrest, M. L.; Stroeve, P.; Mahmoudi, M., Toxicity of nanomaterials. *Chem*. *Soc*. *Rev*. **2012,** *41*, 2323-2343.

16. Jones, C. F.; Grainger, D. W., In vitro assessments of nanomaterial toxicity. *Adv*. *Drug Deliv*. *Rev*. **2009,** *61*, 438-456.

17. Nel, A.; Xia, T.; Meng, H.; Wang, X.; Lin, S.; Ji, Z.; Zhang, H., Nanomaterial toxicity testing in the 21st century: use of a predictive toxicological approach and high-throughput screening. *Accounts of Chemical Research* **2012,** *46*, 607-621.

18. Sun, B.; Li, R.; Wang, X.; Xia, T., Predictive toxicological paradigm and high throughput approach for toxicity screening of engineered nanomaterials. *Int*. *J*. *Biomed*. *Nanosci*. *Nanotechnol*. **2013,** *3*, 4-18.

19. Nel, A.; Zhao, Y.; MÃ¤dler, L., Environmental health and safety considerations for nanotechnology. *Accounts of Chemical Research* **2013,** *46*, 605-606.

20. Gagner, J. E.; Shrivastava, S.; Qian, X.; Dordick, J. S.; Siegel, R. W., Engineering Nanomaterials for biomedical applications requires understanding the nano-bio interface: A perspective. *J*. *Phys*. *Chem*. *Lett*. **2012,** *3*, 3149-3158.

21. Ray, P. C.; Singh, A. K.; Senapati, D.; Fan, Z.; Yu, H., Toxicity and environmental risks of nanomaterials: An Update. *Bio-Nanotechnology*, Blackwell Publishing Ltd.: 2013; 733-748.

22. Neal, A. L., What can be inferred from bacterium-nanoparticle interactions about the potential consequences of environmental exposure to nanoparticles? *Ecotoxicol*. **2008,** *17*, 362-371.

23. Bryers, J. D., Medical biofilms. *Biotechnol*. *Bioeng*. **2008,** *100*, 1-18.

24. D'Avignon, L. C.; Hogan, B. K.; Murray, C. K.; Loo, F. L.; Hospenthal, D. R.; Cancio, L. C.; Kim, S. H.; Renz, E. M.; Barillo, D.; Holcomb, J. B.; Wade, C. E.; Wolf, S. E., Contribution of bacterial and viral infections to attributable mortality in patients with severe burns: An autopsy series. *Burns* **2010,** *36*, 773-779.

25. Goswami, A. P.; Goswami, N.; Patel, T.; Tripathi, C.; Trivedi, H., Antibiotic sensitivity profile of bacterial pathogens in postoperative wound infections at a tertiary care hospital in Gujarat, India. *J*. *Pharmacol*. *Pharmacother*. **2011,** *2*, 158-164.

26. Nablo, B. J.; Prichard, H. L.; Butler, R. D.; Klitzman, B.; Schoenfisch, M. H., Inhibition of implant-associated infections via nitric oxide release. *Biomaterials* **2005,** *26*, 6984-6990.

27. Rutala, W. A.; Weber, D. J., Infection control: the role of disinfection and sterilization. *Journal of Hospital Infection* **1999,** *43, Supplement 1*, S43-S55.

28. Smith, A. W., Biofilms and antibiotic therapy: Is there a role for combating bacterial resistance by the use of novel drug delivery systems? *Adv*. *Drug Deliv*. *Rev*. **2005,** *57*, 1539-1550.

29. Anderl, J. N.; Franklin, M. J.; Stewart, P. S., Role of antibiotic penetration limitation in *Klebsiella pneumoniae* biofilm resistance to ampicillin and ciprofloxacin. *J*. *Antimicrob*. *Chemother*. **2000,** *44*, 1818-1824.

30. Nickel, J. C.; Ruseska, I.; Wright, J. B.; Costerton, J. W., Tobramycin resistance of *Pseudomonas aeruginosa* cells growing as a biofilm on urinary catheter material. *J*. *Antimicrob*. *Chemother*. **1985,** *27*, 619-624.

31. Cerca, N.; Martins, S.; Cerca, F.; Jefferson, K. K.; Pier, G. B.; Oliveira, R.; Azeredo, J., Comparative assessment of antibiotic susceptibility of coagulase-negative staphylococci in biofilm versus planktonic culture as assessed by bacterial enumeration or rapid XTT colorimetry. *Journal of Antimicrobial Chemotherapy* **2005,** *56*, 331-336

32. Mack, D.; Rohde, H.; Harris, L. G.; Davies, A. P.; Hortskotte, M. A.; Knobloch, J. K., Biofilm formation in medical-device related infection. *Int*. *J*. *Artif*. *Organs* **2006,** *29*, 343-359.

33. Alberti, C.; Brun-Buisson, C.; Burchardi, H.; Martin, C.; Goodman, S.; Artigas, A.; Sicignano, A.; Palazzo, M.; Moreno, R.; Boulmé, R.; Lepage, E.; Le Gall, J.,

Epidemiology of sepsis and infection in ICU patients from an international multicentre cohort study. *Intensive Care Medicine* **2002,** *28*, 108-121.

34. Lindsay, D.; von Holy, A., Bacterial biofilms within the clinical setting: what healthcare professionals should know. *J*. *Hosp*. *Infect*. **2006,** *64*, 313-325.

35. Donlan, R. M., Biofilms: microbial life on surfaces. *Emerging Infectious Diseases* **2002,** *8*, 881-90.

36. Hall-Stoodley, L.; Costerton, J. W.; Stoodley, P., Bacterial biofilms: from the natural environment to infectious diseases. *Nat*. *Rev*. *Microbiol*. **2004,** *2*, 95-108.

37. Costerton, J. W.; Stewart, P. S.; Greenberg, E. P., Bacterial biofilms: A common cause of persistent infections. *Science* **1999,** *284*, 1318-1322.

38. Parsek, M. R.; Fuqua, C., Biofilms 2003: Emerging themes and challenges in studies of surface-associated microbial life. *Journal of bacteriology* **2004,** *186*, 4427-4440.

39. Stewart, P. S.; William Costerton, J., Antibiotic resistance of bacteria in biofilms. *The Lancet* **2001,** *358*, 135-138.

40. Anwar, H.; van Biesen, T.; Dasgupta, M.; Lam, K.; Costerton, J. W., Interaction of biofilm bacteria with antibiotics in a novel in vitro chemostat system. *Antimicrob*. *Agents Chemother*. **1989,** *33*, 1824-1826.

41. Barraud, N.; Hassett, D. J.; Hwang, S.-H.; Rice, S. A.; Kjelleberg, S.; Webb, J. S., Involvement of nitric oxide in biofilm dispersal of *Pseudomonas aeruginosa*. *J*. *Bacteriol*. **2006,** *188*, 7344-7353.

42. Fadeeva, E.; Truong, V. K.; Stiesch, M.; Chichkov, B. N.; Crawford, R. J.; Wang, J.; Ivanova, E. P., Bacterial retention on superhydrophobic titanium surfaces fabricated by femtosecond laser ablation. *Langmuir* **2011,** *27*, 3012-3019.

43. Appelgren, P.; Ransjö, U.; Bindslev, L.; Larm, O., Does surface heparinisation reduce bacterial colonisation of central venous catheters? *The Lancet* **1995,** *345*, 130.

44. Chilukuri, D. M.; Shah, J. C., Local delivery of vancomycin for the prophylaxis of prosthetic device-related infections. *Pharm*. *Res*. **2005,** *22*, 563-572.

45. Morris, N. S.; Stickler, D. J., Encrustation of indwelling urethral catheters by *Proteus mirabilis* biofilms growing in human urine. *J*. *Hosp*. *Infect*. **1998,** *39*, 227-234.

46. Narasimhan, J.; Antholine, W. E.; Chitambar, C. R., Effect of gallium on the tyrosyl radical of the iron-dependent M2 subunit of ribonucleotide reductase. *Biochem*. *Pharmacol*. **1992,** *44*, 2403-2408.

47. Singh, P., Iron sequestration by human lactoferrin stimulates *P*. *aeruginosa* surface motility and blocks biofilm formation. *Biometals* **2004,** *17*, 267-270.

48. Krishnamurthy, V. M.; Quinton, L. J.; Estroff, L. A.; Metallo, S. J.; Isaacs, J. M.; Mizgerd, J. P.; Whitesides, G. M., Promotion of opsonization by antibodies and phagocytosis of Gram-positive bacteria by a bifunctional polyacrylamide. *Biomaterials* **2006,** *27*, 3663-3674.

49. Hatch, R. A.; Schiller, N. L., Alginate lyase promotes diffusion of aminoglycosides through the extracellular polysaccharide of mucoid *Pseudomonas aeruginosa*. *Antimicrob*. *Agents Chemother*. **1998,** *42*, 974-977.

50. Saravanakumari, P.; Mani, K., Structural characterization of a novel xylolipid biosurfactant from Lactococcus lactis and analysis of antibacterial activity against multi-drug resistant pathogens. *Bioresource Technol*. **2010,** *101*, 8851-8854.

51. Norrby, S. R.; Nord, C. E.; Finch, R., Lack of development of new antimicrobial drugs: a potential serious threat to public health. *The Lancet Infectious Diseases* **2005,** *5*, 115-119.

52. Khan, R.; Islam, B.; Akram, M.; Shakil, S.; Ahmad, A. A.; Ali, S. M.; Siddiqui, M.; Khan, A., Antimicrobial activity of five herbal extracts against multi drug resistant (MDR) strains of bacteria and fungus of clinical origin. *Molecules* **2009,** *14*, 586-597.

53. Malka, E.; Perelshtein, I.; Lipovsky, A.; Shalom, Y.; Naparstek, L.; Perkas, N.; Patick, T.; Lubart, R.; Nitzan, Y.; Banin, E.; Gedanken, A., Eradication of multi-drug resistant bacteria by a novel Zn-doped CuO nanocomposite. *Small* **2013**, doi: 10.1002/smll.201301081.

54. Ignarro, L. J.; Buga, G. M.; Wood, K. S.; Byrns, R. E.; Chaudhuri, G., Endothelium-derived relaxing factor produced and released from artery and vein is nitric oxide. *Proc*. *Natl*. *Acad*. *Sci*. **1987,** *84*, 9265-9269.

55. Ignarro, L. J.; Napoli, C.; Loscalzo, J., Nitric oxide donors and cardiovascular agents modulating the bioactivity of nitric oxide: An overview. *Circ*. *Res*. **2002,** *90*, 21-28.

56. Carpenter, A. W.; Schoenfisch, M. H., Nitric oxide release: Part II. Therapeutic applications. *Chem*. *Soc*. *Rev*. **2012,** *41*, 3742-3752.

57. Ferrari, C. K. B.; Franca, E. L.; Honorio-Franca, A. C., Nitric oxide, health and disease. *J*. *Appl*. *Biomed*. **2009,** *7*, 163-173.

58. Hill, B. G.; Dranka, B. P.; Bailey, S. M.; Lancaster, J. R.; Darley-Usmar, V. M., What part of NO don't you understand? Some answers to the cardinal questions in nitric oxide biology. *J*. *Biol*. *Chem*. **2010,** *285*, 19699-19704.

59. Ziche, M.; Morbidelli, L.; Masini, E.; Amerini, S.; Granger, H.; Maggi, C.; et al.; Geppetti, P.; Ledda, F., Nitric oxide mediates angiogenesis in vivo and endothelial cell growth and migration in vitro promoted by substance P. *Journal of Clinical Investigation* **1994,** *94*, 2036-2044.

60. Fang, F. C., Perspectives series: host/pathogen interactions. Mechanisms of nitric oxide-related antimicrobial activity. *J*. *Clin*. *Invest*. **1997,** *99*, 2818-2825.

61. Hetrick, E. M.; Shin, J. H.; Stasko, N. A.; Johnson, C. B.; Wespe, D. A.; Holmuhamedov, E.; Schoenfisch, M. H., Bactericidal efficacy of nitric oxide-releasing silica nanoparticles. *ACS Nano* **2008,** *2*, 235-246.

62. Hetrick, E. M.; Shin, J. H.; Paul, H. S.; Schoenfisch, M. H., Anti-biofilm efficacy of nitric oxide-releasing silica nanoparticles. *Biomaterials* **2009,** *30*, 2782-2789.

63. De Groote, M. A.; Fang, F. C., NO inhibitions: antimicrobial properties of nitric oxide. *Clinical Infectious Diseases* **1995,** *21*, S162-S165.

64. Privett, B. J.; Deupree, S. M.; Backlund, C. J.; Rao, K. S.; Johnson, C. B.; Coneski, P. N.; Schoenfisch, M. H., Synergy of nitric oxide and silver sulfadiazine against gram-negative, gram-positive, and antibiotic-resistant pathogens. *Mol*. *Pharm*. **2010,** *7*, 2289-2296.

65. Weydert, C. J.; Cullen, J. J., Measurement of superoxide dismutase, catalase and glutathione peroxidase in cultured cells and tissue. *Nature protocols* **2009,** *5*, 51-66.

66. Gusarov, I.; Nudler, E., NO-mediated cytoprotection: Instant adaptation to oxidative stress in bacteria. *Proc*. *Natl*. *Acad*. *Sci*. **2005,** *102*, 13855-13860.

67. Ghaffari, A.; Miller, C.; McMullin, B.; Ghahary, A., Potential application of gaseous nitric oxide as a topical antimicrobial agent. *Nitric Oxide* **2006,** *14*, 21-29.

68. Eroy-Reveles, A. A.; Mascharak, P. K., Nitric oxide-donating materials and their potential in pharmacological applications for site-specific nitric oxide delivery. *Future Medicinal Chemistry* **2009,** *1*, 1497-1507.

69. Wang, P. G.; Xian, M.; Tang, X.; Wu, X.; Wen, Z.; Cai, T.; Janczuk, A. J., Nitric oxide donors: chemical activities and biological applications. *Chem*. *Rev*. **2002,** *102*, 1091-1134.

70. Hrabie, J. A.; Keefer, L. K., Chemistry of the nitric oxide-releasing diazeniumdiolate ("nitrosohydroxylamine") functional group and its oxygen-substituted derivatives. *Chem*. *Rev*. **2002,** *102*, 1135-1154.

71. Lam, C.-F.; van Heerden, P. V.; Blott, J.; Roberts, B.; Ilett, K. F., The selective pulmonary vasodilatory effect of inhaled DETA/NO, a novel nitric oxide donor, in ARDS–a pilot human trial. *J*. *Crit*. *Care* **2004,** *19*, 48-53.

72. Yamamoto, T.; Kakar, N. R.; Vina, E. R.; Johnson, P. E.; Bing, R. J., The effect of aspirin and two nitric oxide donors on the infarcted heart in situ. *Life Sciences* **2000,** *67*, 839-846.

73. Riccio, D. A.; Schoenfisch, M. H., Nitric oxide release: Part I. Macromolecular scaffolds. *Chem*. *Soc*. *Rev*. **2012,** *41*, 3731-3741.

74. Lee, J. E.; Lee, N.; Kim, T.; Kim, J.; Hyeon, T., Multifunctional mesoporous silica nanocomposite nanoparticles for theranostic applications. *Accounts of Chemical Research* **2011,** *44*, 893-902.

75. Brinker, C. J.; Scherer, G. W., *Sol-gel science: the physics and chemistry of sol-gel processing*. Elsevier: 1990.

76. Stöber, W.; Fink, A.; Bohn, E., Controlled growth of monodisperse silica spheres in micron size range. *J*. *Colloid Interf*. *Sci*. **1968,** *26*, 62-69.

77. Carpenter, A. W.; Slomberg, D.L.; Rao, K.S.; Schoenfisch, M.H., Influence of scaffold size on bactericidal activity of nitric oxide-releasing silica nanoparticles. *ACS Nano* **2011,** *5*, 7235-7244.

78. Bogush, G. H.; Tracy, M. A.; Zukoski Iv, C. F., Preparation of monodisperse silica particles: Control of size and mass fraction. *J*. *Non-Cryst*. *Solids* **1988,** *104*, 95-106.

79. Yoo, J. W.; Doshi, N.; Mitragotri, S., Endocytosis and intracellular distribution of PLGA particles in endothelial cells: effect of particle geometry. *Macromolecular rapid communications* **2010,** *31*, 142-148.

80. Huang, X.; Li, L.; Liu, T.; Hao, N.; Liu, H.; Chen, D.; Tang, F., The shape effect of mesoporous silica nanoparticles on biodistribution, clearance, and biocompatibility in vivo. *ACS Nano* **2011,** *5*, 5390-5399.

81. Huang, X.; Teng, X.; Chen, D.; Tang, F.; He, J., The effect of the shape of mesoporous silica nanoparticles on cellular uptake and cell function. *Biomaterials* **2010,** *31*, 438-448.

82. Meng, H.; Yang, S.; Li, Z.; Xia, T.; Chen, J.; Ji, Z.; Zhang, H.; Wang, X.; Lin, S.; Huang, C., Aspect ratio determines the quantity of mesoporous silica nanoparticle uptake by a small GTPase-dependent macropinocytosis mechanism. *ACS Nano* **2011,** *5*, 4434-4447.

83. Kolhar, P.; Doshi, N.; Mitragotri, S., Polymer nanoneedle–mediated intracellular drug delivery. *Small* **2011,** *7*, 2094-2100.

84. Shin, J. H.; Metzger, S. K.; Schoenfisch, M. H., Synthesis of nitric oxide-releasing silica nanoparticles. *J*. *Am*. *Chem*. *Soc*. **2007,** *129*, 4612-4619.

85. Shin, J. H.; Schoenfisch, M. H., Inorganic/organic hybrid silica nanoparticles as a nitric oxide delivery scaffold. *Chem*. *Mater*. **2007,** *20*, 239-249.

86. Tomalia, D. A.; Naylor, A. M.; Goddard, W. A., Starburst dendrimers: molecular-level control of size, shape, surface chemistry, topology, and flexibility from atoms to macroscopic matter. *Angewandte Chemie International Edition in English* **1990,** *29*, 138-175.

87. Patri, A. K.; Kukowska-Latallo, J. F.; Baker Jr, J. R., Targeted drug delivery with dendrimers: comparison of the release kinetics of covalently conjugated drug and non-covalent drug inclusion complex. *Adv*. *Drug Deliv*. *Rev*. **2005,** *57*, 2203-2214.

88. Patil, M. L.; Zhang, M.; Taratula, O.; Garbuzenko, O. B.; He, H.; Minko, T., Internally cationic polyamidoamine PAMAM-OH dendrimers for siRNA delivery: effect of the degree of quaternization and cancer targeting. *Biomacromolecules* **2009,** *10*, 258-266.

89. Taratula, O.; Garbuzenko, O. B.; Kirkpatrick, P.; Pandya, I.; Savla, R.; Pozharov, V. P.; Minko, T., Surface-engineered targeted PPI dendrimer for efficient intracellular and intratumoral siRNA delivery. *J*. *Controlled Release* **2009,** *140*, 284-293.

90. Wathier, M.; Jung, P. J.; Carnahan, M. A.; Kim, T.; Grinstaff, M. W., Dendritic macromers as in situ polymerizing biomaterials for securing cataract incisions. *J*. *Am*. *Chem*. *Soc*. **2004,** *126*, 12744-12745.

91. Chen, C. Z.; Beck-Tan, N. C.; Dhurjati, P.; van Dyk, T. K.; LaRossa, R. A.; Cooper, S. L., Quaternary ammonium functionalized poly (propylene imine) dendrimers as effective antimicrobials: structure-activity studies. *Biomacromolecules* **2000,** *1*, 473-480.

92. Calabretta, M. K.; Kumar, A.; McDermott, A. M.; Cai, C., Antibacterial activities of poly(amidoamine) dendrimers terminated with amino and poly(ethylene glycol) groups. *Biomacromolecules* **2007,** *8*, 1807-1811.

93. Taite, L. J.; West, J. L., Poly(ethylene glycol)-lysine dendrimers for targeted delivery of nitric oxide. *J*. *Biomater*. *Sci*., *Polymer Edition* **2006,** *17*, 1159-1172.

94. Stasko, N. A.; Schoenfisch, M. H., Dendrimers as a scaffold for nitric oxide release. *J*. *Am*. *Chem*. *Soc*. **2006,** *128*, 8265-8271.

95. Lu, Y.; Sun, B.; Li, C.; Schoenfisch, M. H., Structurally diverse nitric oxide-releasing poly(propylene imine) dendrimers. *Chem*. *Mater*. **2011,** *23*, 4227-4233.

96. Stasko, N. A.; Fischer, T. H.; Schoenfisch, M. H., *S*-Nitrosothiol-modified dendrimers as nitric oxide delivery vehicles. *Biomacromolecules* **2008,** *9*, 834-841.

97. Yang, Y.; Bajaj, N.; Xu, P.; Ohn, K.; Tsifansky, M. D.; Yeo, Y., Development of highly porous large PLGA microparticles for pulmonary drug delivery. *Biomaterials* **2009,** *30*, 1947-1953.

98. Jameela, S. R.; Jayakrishnan, A., Glutaraldehyde cross-linked chitosan microspheres as a long acting biodegradable drug delivery vehicle: studies on the in vitro release of mitoxantrone and in vivo degradation of microspheres in rat muscle. *Biomaterials* **1995,** *16*, 769-775.

99. Agrawal, C. M.; Ray, R. B., Biodegradable polymeric scaffolds for musculoskeletal tissue engineering. *J*. *Biomed*. *Mater*. *Res*. **2001,** *55*, 141-150.

100. Rabea, E. I.; Badawy, M. E. T.; Stevens, C. V.; Smagghe, G.; Steurbaut, W., Chitosan as antimicrobial agent: Applications and mode of action. *Biomacromolecules* **2003,** *4*, 1457-1465.

101. Chang, K. L. B.; Tai, M.-C.; Cheng, F.-H., Kinetics and products of the degradation of chitosan by hydrogen peroxide. *J*. *Agric*. *Food Chem*. **2001,** *49*, 4845-4851.

102. Handy, R.; Owen, R.; Valsami-Jones, E., The ecotoxicology of nanoparticles and nanomaterials: current status, knowledge gaps, challenges, and future needs. *Ecotoxicol*. **2008,** *17*, 315-325.

103. Nowack, B.; Bucheli, T. D., Occurrence, behavior and effects of nanoparticles in the environment. *Environ*. *Pollut*. **2007,** *150*, 5-22.

104. Navarro, E. B., A.; Behra, R.; Hartmann, N. B.; Filser, J.; Miao, A.; Quigg, A.; Santschi, P.H.; Sigg, L., Environmental behavior and ecotoxicity of engineered nanoparticles to algae, plants, and fungi. *Ecotoxicol*. **2008,** *17*, 372-386.

105. Lee, C. W. M., S.; Zodrow, K.; Li, D.; Tsai, Y.; Braam, J.; Alvarez, P. J. J. , Developmental phytotoxicity of metal oxide nanoparticles to *Arabidopsis thaliana*. *Environ*. *Toxicol*. *Chem*. **2010,** *29*, 669-675.

106. Lee, W.; An, Y.; Yoon, H.; Kweon, H., Toxicity and bioavailability of copper nanoparticles to the terrestrial plants mung bean (*Phaseolus radiatus*) and wheat (*Triticum aestivum*): Plant agar test for water-insoluble nanoparticles. *Environ*. *Toxicol*. *Chem*. **2008,** *27*, 1915-1921.

107. Peralta-Videa, J. R. Z., L.; Lopez-Moreno, M. L.; de la Rosa, G.; Hong, J.; Gardea-Torresdey, J.L., Nanomaterials and the environment: A review for the biennium 2008-2010. *J*. *Hazard*. *Mater*. **2011,** *186*, 1-15.

108. Klaine, S. J.; Alvarez, P. J.; Batley, G. E.; Fernandes, T. F.; Handy, R. D.; Lyon, D. Y.; Mahendra, S.; McLaughlin, M. J.; Lead, J. R., Nanomaterials in the environment: Behavior, fate, bioavailability, and effects. *Environ*. *Toxicol*. *Chem*. **2008,** *27*, 1825-1851.

109. Torney, F.; Trewyn, B.G.; Lin, V. S.-Y.; Wang, K., Mesoporous silica nanoparticles deliver DNA and chemicals into plants. *Nat*. *Nanotechnol*. **2007,** *2*, 295-300.

110. Navarro, D. A.; Bisson, M. A.; Aga, D. S., Investigating uptake of water-dispersible CdSe/ZnS quantum dot nanoparticles by *Arabidopsis thaliana* plants. *J*. *Hazard*. *Mater*. **2012,** *211-212*, 427-435.

111. Lin, D.; Xing, B., Root uptake and phytotoxicity of ZnO nanoparticles. *Environ*. *Sci*. *and Technol*. **2008,** *42*, 5580-5585.

112. Yin, L.; Cheng, Y.; Espinasse, B.; Colman, B. P.; Auffan, M.; Wiesner, M.; Rose, J.; Liu, J.; Bernhardt, E. S. , More than the ions: The effects of silver nanoparticles on *Lolium multiflorum*. *Environ*. *Sci*. *and Technol*. **2011,** *45*, 2360-2367.

113. Parsons, J. G.; Lopez, M. L.; Gonzalez, C. M.; Peralta-Videa, J. R.; Gardea-Torresdey, J. L., Toxicity and biotransformation of uncoated and coated nickel hydroxide nanoparticles on mesquite plants. *Environ*. *Toxicol*. *Chem*. **2010,** *29*, 1146-1154.

114. Lopez-Moreno, M. L.; de la Rosa, G.; Hernandez-Viezcas, J. A.; Peralta-Videa, J. R.; Gardea-Torresdey, J. L., X-ray absorption spectroscopy (XAS) corroboration of the uptake and storage of CeO_2 nanoparticles and assessment of their differential toxicity in four edible plant species. *J*. *Agric*. *Food Chem*. **2010,** *58*, 3689-3693.

115. Rico, C. M.; Majumdar, S.; Duarte-Gardea, M.; Peralta-Videa, J. R.; Gardea-Torresdey, J. L., Interaction of nanoparticles with edible plants and their possible implications in the food chain. *J*. *Agric*. *Food Chem*. **2011,** *59*, 3485-3498.

116. Sabo-Attwood, T.; Unrine, J. M.; Stone, J. W.; Murphy, C. J.; Ghoshroy, S.; Blom, D.; Bertsch, P. M.; Newman, L. A., Uptake, distribution and toxicity of gold nanoparticles in tobacco (Nicotiana xanthi) seedlings. *Nanotoxicol*. **2012,** *6*, 353-360.

117. Gubbins, E. J.; Batty, L. C.; Lead, J. R., Phytotoxicity of silver nanoparticles to Lemna minor L. *Environ*. *Pollut*. **2011,** *159*, 1551-1559.

118. Ma, X.; Geiser-Lee, J.; Deng, Y.; Kolmakov, A., Interactions between engineered nanoparticles (ENPs) and plants: Phytotoxicity, uptake and accumulation. *Sci*. *Tot*. *Environ*. **2010,** *408*, 3053-3061.

119. Begum, P.; Ikhtiari, R.; Fugetsu, B., Graphene phytotoxicity in the seedling stage of cabbage, tomato, red spinach, and lettuce. *Carbon* **2011,** *49*, 3907-3919.

120. Darlington, T. K.; Neigh, A. M.; Spencer, M. T.; Guyen, O. T. N.; Oldenburg, S. J., Nanoparticle characteristics affecting environmental fate and transport through soil. *Environ*. *Toxicol*. *Chem*. **2009,** *28*, 1191-1199.

121. Xu, H.; Yan, F.; Monson, E. E.; Kopelman, R., Room-temperature preparation and characterization of polyethylene-glycol coated silica nanoparticles for biomedical applications. *J*. *Biomed*. *Mater*. *Res*., *Part A* **2003,** *66A*, 870-879.

122. Anselmann, R., Nanoparticles and nanolayers in commercial applications. *J*. *Nanopart*. *Res*. **2001,** *3*, 329-336.

123. Meyer, D. E.; Curran, M. A.; Gonzalez, M. A., An examination of existing data for the industrial manufacture and use of nanocomponents and their role in the life cycle impact of nanoproducts. *Environ*. *Sci*. *and Technol*. **2009,** *43*, 1256-1263.

124. Hoecke, K. V.; de Schamphelaere, K. A. C.; van der Meeren, P.; Lucas, S.; Janssen, C. R., Ecotoxicity of silica nanoparticles to the green alga *Psuedokirchneriella subcapitata*: Importance of surface area. *Environ*. *Toxicol*. *Chem*. **2008,** *27*, 1948-1957.

125. Stampoulis, D.; Sinha, S.; White, J., Assay-dependent phytotoxicity of nanoparticles to plants. *Environ*. *Sci*. *and Technol*. **2009,** *43*, 9473-9479.

CHAPTER 2: ROLE OF NITRIC OXIDE-RELEASING SCAFFOLD PROPERTIES ON ANTIBACTERIAL EFFICACY AGAINST PLANKTONIC BACTERIA

2.1 Introduction

The prevalence of bacteria in clinical settings has become particularly problematic, with hospital-acquired infections being the fourth-leading cause of death in the United States.[1, 2] Open wounds[3, 4] and implanted medical devices such as prosthetic heart valves,[2] orthopedic implants, and catheters are frequent sites of microbial infection despite aseptic procedures and instrument sterilization.[2, 5, 6] While several antibacterial agents have proven effective against planktonic (i.e., free-floating) bacteria,[4, 7] there is concern of the bacteria developing resistance to the treatment over time.[8-10] Indeed, antibacterial resistance mechanisms including efflux pumps, modifying enzymes, and target mutations have been attributed to planktonic bacteria.[11] Clinically-relevant infections including those associated with medical implants, non-healing wounds, diabetic mellitus, and cystic fibrosis are often the result of bacterial biofilms, which are generally more resistant than their planktonic counterparts.[12-14] Since >99% of bacteria exist in the biofilm state, researchers are ultimately aiming to develop potent anti-biofilm agents.[15] However, prior to treating biofilms, a proposed antibacterial agent must prove effective at eradicating planktonic bacteria, without fostering resistance. Thus,

understanding the clinical significance of nanomaterial toxicity to planktonic bacteria will aid in the design of future antibacterial and anti-biofilm agents.

Nitric oxide (NO) is an endogenously-produced, diatomic free radical that serves various roles in the body.[16-18] Specifically, at higher concentrations (μM), NO can serve as a potent antibacterial agent, inducing oxidative and nitrosative stresses that can damage the bacteria membrane of both Gram-positive and Gram-negative species.[19-23] The broad-spectrum and multi-mechanistic killing of nitric oxide further demonstrate its potential as an antibacterial agent, with a reduced chance for bacterial resistance to treatment. Due to the reactive nature of gaseous NO, several *N*-diazeniumdiolate-modified scaffolds (e.g., silica particles,[20] dendrimers,[24] and chitosans[25]) have been designed to store and controllably release NO. Selective tuning of the physicochemical properties (e.g., size, shape, and exterior functionality) of NO-releasing scaffolds to enhance killing of planktonic bacteria is a necessary first step in realizing a successful therapeutic. Herein, the evaluation of the bactericidal efficacy of several NO-releasing nanomaterials (i.e., silica particles, dendrimers, and chitosan oligosaccharides) to planktonic *Pseudomonas aeruginosa* and *Staphylococcus aureus* is reported as a function of nanomaterial size, shape, exterior functionality, and molecular weight.

2.1.1 Nitric oxide-releasing silica particles

Silica nanoparticles are attractive antibacterial scaffolds due to the capability for functionalization and their generally low toxicity to healthy host cells.[26] *N*-diazeniumdiolate-modified silica nanoparticles (~100 nm) have thus been developed to

deliver large NO payloads and kill planktonic bacteria.[20] However, these scaffolds could be further tuned to enhance efficacy, as particle size and shape have previously been shown to influence bacterial killing. Morones et al. observed improved killing of *E. coli* for small silver particles (1–10 nm).[27] Size-dependent bacterial killing was also examined by Nair et al., with the smaller particles exhibiting greater biocidal action.[28] Additionally, Pal et al. studied the role of silver nanoparticle shape (i.e., nanoplates, spherical, or rod-shaped) in the eradication of *E. coli*.[29] Given the observed effects of nanomaterial size and shape in bacterial eradication, the role of NO-releasing silica nanoparticle size (i.e., 50, 100, 200 nm) and shape (i.e., aspect ratio 1, 4, and 8) on the killing of planktonic Gram-negative *Pseudomonas aeruginosa* and Gram-positive *Staphylococcus aureus* was investigated.

2.1.2 Nitric oxide-releasing dendrimers

In addition to exploring the effects of silica nanoparticle physicochemical properties on bactericidal efficacy, dendrimers have been evaluated as an NO-releasing scaffold. Dendrimers are highly-branched, nano-scale macromolecules with bonds emanating from a central core at the interior of the dendrimer.[30] Dendritic scaffolds have been used in drug delivery,[31] gene transfection,[32, 33] tissue engineering,[34] and even antibacterial applications. For example, Chen et al. demonstrated the efficacy of quaternary ammonium-modified dendrimers in bacterial killing, but the inherent positive charge of the dendrimers resulted in significant toxicity to mammalian cells.[35] Cytotoxicity was subsequently reduced by masking the charge with poly(ethylene glycol)

(PEG). Poly(amidoamine) (PAMAM) dendrimers and partially PEG-modified dendrimers have also proven effective against planktonic bacteria, with complete eradication of *P. aeruginosa* and *S. aureus* at μg/mL concentrations.[36]

Due to the inherent biocidal action of dendrimers, NO-release has been coupled to these scaffolds to further enhanace their efficacy. For example, NO-releasing poly(propylene imine) (PPI) and PAMAM dendrimers that can store and deliver increased NO payloads (~2–5.6 μmol/mg) have been reported.[24, 37, 38] In drug delivery applications, important dendrimer parameters to evaluate are size (i.e., generation), surface functionalization, and cytotoxicity. Dendrimers can be reproducibly synthesized with sizes <10 nm, likely improving their bactericidal activity compared to silica particles (~100 nm) that have been previously evaluated.[20] The exterior functionality of the dendrimers may also prove important in both bacterial killing and cytotoxicity. As such, NO-releasing PPI dendrimers were evaluated against planktonic *P. aeruginosa* and *S. aureus* as a function of dendrimer size (i.e., generation 2 or 5) and exterior modification (i.e., propylene oxide, styrene oxide, or poly(ethylene glycol)).

2.1.3 Nitric oxide-releasing chitosan oligosaccharides

Although silica particles and dendrimers enable tuning of NO-release through varied size, shape, and exterior functionality, pulmonary,[39] oral, and parenteral drug delivery,[40] as well as tissue engineering[41] applications necessitate biodegradable scaffolds. The natural biopolymer, chitosan, has already shown promise in these applications due to its biocompatibility and biodegradability. Chitosan also exhibits

antimicrobial properties toward bacteria, fungi, and viruses.[42] Furthermore, the high secondary amine content of the chitosan backbone lends itself to *N*-diazeniumdiolate modification and subsequent NO release, thus increasing potential for antibacterial action. Chitosan oligosaccharides (<20 kD) are soluble in the basic conditions necessary for *N*-diazeniumdiolation and thus offer a promising approach for designing biodegradable NO-releasing therapeutics.

Similar to NO-releasing silica and dendrimer scaffolds, the physicochemical properties (e.g., molecular weight and exterior functionality) of chitosan oligosaccharides can be tailored to influence NO-release kinetics and bactericidal action. The molecular weight (MW) of chitosan oligosaccharides can be controlled through the oxidative degradation of chitosan using hydrogen peroxide.[43] Additionally, a variety of functional groups (e.g., secondary amines and PEG) can be introduced to the chitosan oligosaccharides via covalent modification. Herein, the bactericidal efficacy of NO-releasing chitosan oligosaccharides was evaluated against planktonic *P. aeruginosa* as a function of molecular weight (i.e., 2.5k, 5k, and 10k) and exterior hydrophobicity.

2.2 Materials and Methods

Note: Silica particle, dendrimer, and chitosan synthesis, characterization, and evaluation of cytotoxicity were supported by other members of the Schoenfisch lab

Tetraethylorthosilicate (TEOS), *N*-(6-aminohexyl)aminopropyltrimethoxysilane (AHAP), and *N*-(2-aminoethyl)-3-amino-isobutyl-dimethyl-methoxysilane (AEAI) were purchased from Gelest (Morrisville, PA). Triton X-100, 1-hexanol, heptane, pentane,

N,N-dimethylformamide (DMF), methanol, cetyltrimethylammonium bromide (CTAB), was obtained from Acros Organics (Geel, Belgium). Ethanol (EtOH), butanol, 1-propanol, and ammonium hydroxide (28 wt%) were purchased from Fisher Scientific (Fair Lawn, NJ). Sodium methoxide (5.4 M in methanol), sulfanilamide, *N*-1-napthylethylenediamine dihydrochloride, rhodamine B isothiocyanate (RITC), propidium iodide (PI), fetal bovine serum (FBS), Dulbecco's Modified Eagle's Medium (DMEM), phenazine methosulfate (PMS), 3-(4,5-dimethylthiazol-2-yl)-5-(3-carboxymethoxyphenyl)-2-(4-sulfophenyl)-2H-tetrazolium inner salt (MTS), trypsin, phosphate buffered saline (PBS) used for cell culture, and Pen Strep solution (10,000 u/mL penicillin, 10,000 μg/mL streptomycin), propylene oxide (PO), styrene oxide (SO), medium molecular weight chitosan, 2-methyl aziridine (MAz), and poly(ethylene glycol) methyl ether acrylate (average Mn = 480) (PEG) were purchased from the Sigma Aldrich Corp. (St. Louis, MO). Tryptic soy broth (TSB) and tryptic soy agar (TSA) were obtained from Becton, Dickinson, and Company (Franklin Lakes, NJ). *Pseudomonas aeruginosa* (ATCC #19143) and *Staphylococcus aureus* (ATCC# 29231) were obtained from the American Type Culture Collection (Manassas, VA). L929 mouse fibroblasts (ATCC #CCL-1) were purchased from the University of North Carolina Tissue Culture Facility (Chapel Hill, NC). Spectra/Por Float-A-Lyzers for dialysis of the dendrimers were purchased from Spectrum Laboratories, Inc. (Rancho Dominguez, CA). 4,5-Diaminofluorescein diacetate (DAF-2 DA) was purchased from Calbiochem (San Diego, CA). Glass bottom microscopy dishes were received from MatTek Corporation (Ashland, MA). Nitric oxide (NO) was purchased from Praxair (Bethlehem, PA). Argon (Ar) gas

was obtained from Airgas National Welders (Raleigh, NC). A Millipore Milli-Q UV Gradient A10 System (Bedford, MA) was used to purify distilled water to a final resistivity of 18.2 MΩ·cm and a total organic content of ≤6 parts per billion (ppb). Other solvents and chemicals were analytical-reagent grade and used as received. Nuclear magnetic resonance (NMR) spectra were recorded on a 400 MHz Bruker instrument. Elemental (carbon, hydrogen, nitrogen or CHN) analysis was performed using a PerkinElmer Elemental Analyzer Series 2400 instrument (Waltham, MA).

2.2.1 Synthesis of nitric oxide-releasing silica particles

To evaluate the effects of nanoparticle size on bactericidal efficacy, secondary amine-functionalized silica nanoparticles of select sizes (i.e., 50, 100, and 200 nm) were synthesized using a reverse-microemulsion technique.[44] Size was controlled by varying the type (i.e., pentane or heptane) and volume of the organic solvent used in the reverse microemulsion. Seed particles (TEOS) were formed in the reverse micelles and AHAP was subsequently added to impart secondary amine functionality. The three particle sizes (i.e., 50, 100, and 200 nm) were then functionalized with *N*-diazeniumdiolates by suspending the particles in a 1:9 (v/v) mixture of DMF and methanol (5 mg/mL) and adding sodium methoxide (5.4 M in MeOH). Vials of the suspensions were then placed in a Parr hydrogenation vessel and stirred. Residual oxygen in the suspensions was removed by purging the vessel with argon (Ar) three times quickly, followed by three longer (10 min) Ar purges. The vessel was then pressurized to 10 atm with purified gaseous NO. The hydrogenation vessel was maintained at 10 atm throughout a 3 d period after which

the Ar purging procedure was repeated to remove unreacted NO prior to removal of the vials from the vessel. The *N*-diazeniumdiolated particles were recollected by centrifugation (3645 *g* for 5 min, 25 °C), washed three times with EtOH, dried under vacuum, and stored at -20 °C until use.

Silica particles of three distinct aspect ratios (AR1, AR4, and AR8) were synthesized via a surfactant-templated approach as previously described by varying reaction temperature and ammonia concentration.[45] Elevated temperature (30 vs. 20 °C) was used to increase the aspect ratio of the particles (AR8), while a greater ammonia concentration (1.0 vs. 0.5 M) allowed for the synthesis of a more spherical particle (AR1). Of note, cetyltrimethylammonium bromide (CTAB) removal was confirmed via CHN analysis prior to surface grafting. Monoalkoxysilane, *N*-(2-aminoethyl)-3-amino-isobutyl-dimethyl-methoxysilane (AEAI) was then surface grafted onto the particle/rods to impart secondary amine functionality for *N*-diazeniumdiolation as described below. *N*-diazeniumdiolate-functionalized AR1, AR4, and AR8 silica particles were prepared by suspending the AEAI-functionalized particles (15 mg) in a 9:1 (v/v) solution of DMF and MeOH, and adding 50 μL sodium methoxide (5.4 M in MeOH). Vials of the suspensions were placed in the Parr hydrogenation vessel, purged with Ar, exposed to NO, and the resulting particles were recollected and stored following the same protocol.

2.2.2 Synthesis of nitric oxide-releasing PPI dendrimers

Secondary amine-functionalized PPI dendrimers (G2 and G5) of varied exterior functionality were synthesized as described previously.[46] Briefly, 100 mg primary amine-

functionalized G2-PPI dendrimer 7 (G2-PPI-NH2) was dissolved in methanol (2 mL). A total of 1 molar equivalent of PO, SO, or PEG was then added to the G2-PPI-NH2 solution (methanol) with constant stirring at room temperature for 4 d to yield the secondary amine-functionalized G2-PPI conjugates (i.e., G2-PPI-PO 1, G2-PPI-PEG 3, G2-PPI-SO 5). Likewise, secondary amine-functionalized G5-PPI conjugates (i.e., G5-

PPI-PO 2, G5-PPI-PEG 4, G5-PPI-SO 6) were formed via the reactions of G5-PPI-NH2 8 with PO, PEG, and SO, respectively. Dendrimers 1−6 were dissolved in water, dialyzed against water, and subsequently lyophilized. *N*-diazeniumdiolate-functionalized PPI dendrimers 1a−6a were prepared by adding 5.4 M sodium methoxide solution in MeOH (1 equivalent with respect to the molar amount of primary amine functionalities in PPI-NH2 used to synthesize dendrimers 1−6) to a vial containing dendrimers 1−6 in methanol (2 mL). Vials of the dendrimer solutions were then placed in the Parr hydrogenation vessel, purged with Ar, exposed to NO, and stored following the aforementioned protocol.

2.2.3 Synthesis of nitric oxide-releasing chitosan oligosaccharides

Chitosan oligosaccharides of varied molecular weights were prepared by oxidative degradation using hydrogen peroxide. Medium molecular weight chitosan (2.5 g) was suspended in a hydrogen peroxide solution (15 or 30 wt%) under stirring for 1 h at 65–85 ^{o}C. After removal of undissolved chitosan via filtration, the chitosan oligosaccharides were precipitated with acetone, collected by centrifugation, washed twice with ethanol, and dried under vacuum.

The chitosan oligosaccharides were then grafted with 2-methyl aziridine (MAz) based on a previously reported procedure.[47] Briefly, a mixture of concentrated HCl (11 μL), water (100 μL) and MAz with a 1:1 (Chitosan 1) or 2:1 (Chitosan 2) molar ratio to primary amines on the chitosan oligosaccharides was added dropwise to a solution of chitosan oligosaccharides (100 mg) in deionized water (5 mL). The resulting solution was stirred at room temperature for 5 d, and then 75 ^{o}C for 24 h. The MAz-grafted chitosan oligosaccharides were then purified by dialysis and collected by lyophilization. The chitosan oligosaccharides were further functionalized with PEG by adding poly(ethylene glycol) methyl ether acrylate (Chitosan 3) to tune hydrophobicity. The resulting PEG-functionalized chitosan oligosaccharides were purified by dialysis and collected by lyophilization. The chitosan oligosaccharides were characterized by nuclear magnetic resonance (NMR) spectroscopy (data not shown).

N-diazeniumdiolation of the secondary amine-functionalized chitosan oligosaccharides (Chitosan 1, Chitosan 2, and Chitosan 3) was achieved by adding the chitosan and 5.4 M sodium methoxide (75 μL) to a water/methanol mixture (2 mL). The suspensions were then placed in a Parr hydrogenation vessel, purged with Ar, exposed to NO, and stored following the aforementioned protocol.

2.2.4 Fluorescently-labeled scaffolds

Fluorescently-labeled silica nanoparticles,[44] dendrimers,[46] and chitosan oligosaccharides[48] were achieved via covalent modification with rhodamine B isothiocyanate (RITC) based on a previously published procedures. The silica particles

(50 mg) were suspended in EtOH (100 mL) with RITC (5 mg) and stirred in the dark for 48 h. Following fluorescent modification, the particles were collected and washed copiously with EtOH using the collection/centrifugation protocol described above. After a clear supernatant was achieved, the particles were dried under vacuum, *N*-diazeniumdiolated, and stored until use. Fluorescently-labeled dendrimers were prepared by dissolving G2-PPI-NH_2 7(100 mg) and RITC (7.5 mg) in methanol (2 mL). The solution was stirred for 24 h, dialyzed, and lyophilized to yield RITC-labeled dendrimers that were then modified with PO (1 equivalent) and further reacted with NO. To obtain fluorescently-labeled chitosan, chitosan oligosaccharides (50 mg) were dissolved in water (2 mL) at pH 9.0 and RITC was added to the solution in a 1:100 molar ratio to the primary amine of the chitosan oligosaccharides prior to the grafting of 2-methyl aziridine. The solution was then stirred at room temperature for 3 d, dialyzed, lyophilized, and further reacted with NO to achieve fluorescently-labeled NO-releasing chitosan oligosaccharides.

2.2.5 Scaffold characterization and nitric oxide release

Size and shape (i.e., aspect ratio) of the silica particles were determined using transmission electron microscopy (TEM) and scanning electron microscopy (SEM). Transmission electron micrographs of the 50, 100, and 200 nm silica particles were obtained on a JEOL 100 CX II transmission electron microscope (Tokyo, Japan). Scanning electron micrographs of the AR1, AR4, and AR8 silica particles were recorded using a Hitachi S-4700 scanning electron microscope (Tokyo, Japan). Real-time NO-release from the silica particles, dendrimers, and chitosan oligosaccharides was measured

using a Sievers 280i Chemiluminesence Nitric Oxide Analyzer (NOA; Boulder, CO). The NO-releasing silica particles (1 mg), dendrimers (1 mg), or chitosan oligosaccharides (aliquot in water/methanol mixture) were added to a sample vessel containing 30 mL deoxygenated PBS (pH 7.4, 37 °C). Liberated NO was carried from the sample vessel to the NOA at a flow rate of 70 mL/min. To match the collection rate of the NOA (200 mL/min), additional nitrogen flow was supplied to the sample vessel. Nitric oxide-release measurements were terminated when the levels fell below 10 ppb NO/mg scaffold. The real-time NO-release data was used to determine the total NO-release duration and half-life ($t_{1/2}$). Total NO storage (t[NO]) was also characterized using the Griess assay.[49, 50]

2.2.6 Planktonic bactericidal assays

Pseudomonas aeruginosa and *Staphylococcus aureus* bacterial cultures were grown from frozen stock (-80 °C) in TSB overnight at 37 °C. An aliquot of the suspension (0.5 mL) was added to fresh TSB (50 mL) and incubated at 37 °C until the bacteria reached mid-exponential phase (~1×10^8 colony forming units (cfu)/mL) as determined by the optical density at 600 nm (OD_{600}). The relationship between the concentration of the bacteria in suspension and the OD_{600} was calibrated for each strain using an Eppendorf BioPhotometer Plus Spectrophotometer (Hamburg, Germany); the colony forming units were enumerated from culture dilutions grown on TSA plates. The bacterial suspension was then centrifuged (3645 *g* for 10 min, 25 °C), resuspended in PBS, and diluted to ~1×10^6 cfu/mL in PBS.

The minimum bactericidal concentration (MBC) of the NO-releasing 50, 100, and 200 nm silica particles for planktonic *P*. *aeruginosa* was defined as the concentration that resulted in a 3-log reduction in viability versus untreated cells after 2 or 24 h. The MBC of the NO-releasing AR1, AR4, and AR8 silica particles and dendrimers for planktonic *P*. *aeruginosa* and *S*. *aureus* was defined as the concentration that resulted in a 3-log reduction in viability versus untreated cells after 4 and 2 h, respectively. The MBC of the NO-releasing chitosan oligosaccharides for planktonic *P*. *aeruginosa* was defined as the concentration that resulted in a 3-log reduction in viability versus untreated cells after 4 h. The bacterial suspensions (10^6 cfu/mL) were incubated with the NO-releasing scaffolds over a range of concentrations for the duration noted. After exposure, the samples were nanomaterial–bacteria suspensions were diluted and plated on TSA, with counting of resulting colonies to determine viability.

2.2.7 Confocal microscopy

To observe association of the silica particles with the bacteria, *P*. *aeruginosa* (10^6 cfu/mL) was first incubated in a glass bottom confocal dish and allowed to adhere for 45 min at 37 °C. The slide was rinsed with fresh PBS to remove loosely or unadhered bacteria. A suspension of the RITC-modified silica nanoparticles (500 μL of 10 μg/mL in PBS) was then added to the bacteria on the glass slide. To observe association of NO-releasing particles with bacteria over time, fluorescence images were taken immediately following the addition of the 50 nm particles at 20 s intervals for 40min. To compare the influence of particle size on the extent of particle–bacteria association, fluorescence

images were obtained of bacteria treated with the 50, 100, and 200 nanoparticles (10 μg/mL) for 10 min. After the 10 min incubation period, the suspension was removed, and the bacteria were copiously washed with fresh PBS to remove unassociated particles. Fresh PBS was then added, and the bacteria were imaged.

Intracellular NO levels and subsequent cell death were evaluated for the AR1 and AR8 NO-releasing silica particles using confocal microscopy. Bacteria (*P*. *aeruginosa* and *S*. *aureus*) were cultured in TSB to a concentration of 1×10^8 CFU/mL, collected via centrifugation (3645 *g* for 10 min), resuspended in sterile PBS, and adjusted to 1×10^6 CFU/mL in PBS supplemented with 10 μ M DAF-2 DA and 30 μ M PI. The bacteria solution (2.5 mL) was incubated in a glass bottom confocal dish for 45 min at 37 ° C. Suspensions (1.5 mL) of AR1 or AR8 NO-releasing silica particles (44 μ g/mL) in PBS (supplemented with 10 μ M DAF-2 DA and 30 μ M PI) were added to the bacteria solution (1.5 mL) in the glass confocal dish. Images were collected every 5 min to observe intracellular NO concentrations and cell death.

Similarly, intracellular NO, cell death, and scaffold-bacteria association were observed for the NO-releasing PPI dendrimers. *P*. *aeruginosa* was cultured in TSB to a concentration of 1×10^8 CFU/mL, collected via centrifugation (3645 × g for 10 min), resuspended in sterile PBS, and adjusted to 1×10^6 CFU/mL in PBS supplemented with 10 μM DAF-2 DA and 30 μM PI. Aliquots of the bacteria solution were incubated in a glass bottom confocal dish for 45 min at 37 °C. Suspensions (1.5 mL) of G2 (17.4 μg/mL) or G5 (20.0 μg/mL) PPI-SO NO-releasing dendrimers (5a and 6a) or 50 nm NO-releasing AHAP3/TEOS nanoparticles[44] (44.0 μg/mL) in PBS supplemented with 10 μM

DAF-2 DA and 30 μM PI were added to the bacteria solution (1.5 mL) in the glass confocal dish. Images were collected every 2 min to observe intracellular NO concentrations and bacteria cell death temporally. For association experiments, *S*. *aureus* was cultured in TSB to a concentration of 1×10^8 CFU/mL, collected via centrifugation (3645 × g for 10 min), resuspended in sterile PBS, and adjusted to 1×10^6 CFU/mL. Aliquots of the bacteria solution were incubated in a glass bottom confocal dish for 45 min at 37 °C. Solutions of RITC-labeled control (400 μg/mL) or NO-releasing (400 μg/mL) G2-PPI-PO dendrimers in PBS (1.5 mL) were added to the bacteria solution (1.5 mL) in the glass confocal dish to achieve a final concentration of 200 μg/mL. Images were collected every 2 min to monitor association of the dendrimers with *S*. *aureus* temporally.

Prior to examining association of the chitosan oligosaccharides with the bacteria, *P*. *aeruginosa* was cultured in TSB to a concentration of ~1×10^8 CFU/mL, collected *via* centrifugation (3645 × *g* for 10 min), resuspended in sterile PBS, and adjusted to ~1×10^6 CFU/mL. Aliquots of the bacteria solution were incubated in a glass bottom confocal dish for 1.5 h at 37 °C. Solutions of RITC-labeled NO-releasing chitosan oligosaccharides in PBS (1.5 mL) were added to the bacteria solution (1.5 mL) in the glass confocal dish to achieve a final concentration of 150 μg/mL. Images were collected every 2 min to characterize the association, if any, of the chitosan oligosaccharides with *P*. *aeruginosa* temporally.

A Zeiss 510 Meta inverted laser scanning confocal microscope (Carl Zeiss, Thornwood, NY) with a 488 nm Ar excitation laser (2.0% intensity) and a BP 505–530

nm filter was used to obtain DAF-2 (green) fluorescence images. A 543 nm HeNe excitation laser (25.3% intensity) with a BP 560–615 nm filter was used to obtain PI and RITC (red) fluorescence images. The images were collected using a Zeiss C-apochromat lens (20 or 40x, 1.2 numerical aperture).

2.2.8 In vitro cytotoxicity

L929 mouse fibroblasts were cultured in DMEM supplemented with 10% (v/v) FBS and 1 wt% Pen Strep solution, and incubated in 5% (v/v) CO_2 under humidified conditions at 37 ^{o}C. After reaching 80% confluency, the cells were trypsinized, seeded onto tissue culture-treated polystyrene 96-well plates at a density of 3×10^4 cells/mL and incubated at 37 ^{o}C for 48 h. The supernatant was then aspirated prior to adding fresh DMEM (200 μL) with control (i.e., non-NO-releasing) or NO-releasing scaffolds to each well. After incubation at 37 ^{o}C for 24 h, the supernatant was aspirated and the cells rinsed 3x with PBS. A mixture of DMEM/MTS/PMS (105/20/1, v/v/v) (120 μL) was then added to each well. The absorbance of the resulting colored solution after 1.5 h incubation at 37 ^{o}C was quantified at 490 nm using a Thermo Scientific Multiskan EX plate reader (Thermo Fisher Scientific, Inc., Waltham, MA). The mixture of DMEM/MTS/PMS and untreated cells were used as the blank and control, respectively. Cell viability was calculated by taking the ratio of the absorbance of treated to untreated cells after subtracting the absorbance of the blank from each.

2.3 Results and Discussion

2.3.1 Nitric oxide-releasing silica particles

Three distinct silica particle sizes (56 ± 7, 93 ± 14, and 199 ± 27 nm for the 50, 100, and 200 nm particles, respectively) were synthesized via reverse microemulsion for evaluation of *P. aeruginosa* eradication as a function of particle size.[44] Following *N*-diazeniumdiolation, the NO-releasing particles were characterized for NO storage and release at 2 and 24 h to mimic bactericidal assays. At 2 h, the total NO storage was similar for the three sizes of particles (0.47 ± 0.02, 0.38 ± 0.01, and 0.42 ± 0.01 μmol/mg for the NO-releasing 50, 100, and 200 nm particles, respectively). Likewise, the total NO released within the 24 h bactericidal assay was similar for all three systems (1.49 ± 0.29, 1.26 ± 0.17, and 1.01 ±0.08 μmol/mg , for the NO-releasing 50, 100, and 200 nm particles, respectively), confirming their utility for evaluation of efficacy as a function of size.

The role of nanoparticle shape (i.e., aspect ratio) on antibacterial activity was evaluated using silica particles of three varied aspect ratios (i.e., 1, 4, and 8), but identical particle volume. Nitric oxide released over the 4 h planktonic killing assay was 0.63 ± 0.07, 0.59 ± 0.07, and 0.64 ± 0.09 μmol/mg for the AR1, AR4, and AR8 particles, respectively. Given their identical NO storage, the NO-releasing AR1, AR4, and AR8 particles allowed for examination of the influence of nanoparticle shape on bactericidal efficacy against both *P. aeruginosa* and *S. aureus*.

2.3.1.1 Bactericidal efficacy against planktonic bacteria as a function of size and shape

As expected, the smaller NO-releasing 50 nm particles exhibited the greatest biocidal action against *P. aeruginosa*. For the 2 h MBC assay, the 50, 100, and 200 nm

particles had MBC values of 0.8, 1.5, and 1.5 mg/mL, respectively. However, the increased treatment time of 24 h reduced the necessary dose further, resulting in 24 h MBC values of 0.2, 0.2, and 0.4 mg/mL for the 50, 100, and 200 nm particles, respectively. Of note, no reduction in *P*. *aeruginosa* viability was observed for control (i.e., non-NO-releasing) particles at the MBC concentrations.

Assays for evaluating the influence of particle shape on bacterial killing were conducted over 4 h. Increased antibacterial activity was observed for the NO-releasing AR8 particles over the AR4 and AR1 particles for both *P*. *aeruginosa* and *S*. *aureus*. The MBC values for the NO-releasing AR8, AR4, and AR1 particles against *P*. *aeruginosa* were 150, 250, and 500 μg/mL, respectively. However, increased NO doses were necessary for killing of *S*. *aureus*, with MBCs of 300, 1000, and 2000 μg/mL for the AR8, AR4, and AR1 particles, respectively. No reduction in viability of *P*. *aeruginosa* or *S*. *aureus* was noted when exposed to control scaffolds at the maximum MBC concentration of the NO-releasing particles.

2.3.1.2 Confocal microscopy

The bactericidal assays confirmed the enhanced efficacy of the smaller NO-releasing 50 nm particles over the 100 and 200 nm particles. However, it was unclear how nanoparticle–bacteria interactions played a role in the NO-induced bacterial killing. Thus, confocal microscopy was used to evaluate association between the *P*. *aeruginosa* cells and the 50, 100, and 200 nm silica particles. The RITC-labeled 50, 100, and 200 nm particles (10 μg/mL) were incubated with *P*. *aeruginosa* cells for 10 min, and after

washing, increased nanoparticle–bacteria association was observed for the 50 nm particles as expected (Figure 2.1). Although interactions between the 100 and 200 nm particles and the bacteria were visible, the degree of association was significantly less as particle size was increased. Particle–bacteria association was further examined by incubating *P*. *aeruginosa* cells with RITC-modified 50 nm particles and imaging the cells every 20 s over 40 min (Figure 2.2). This time-based experiment revealed that the 50 nm particles associate rapidly (~2 min post-addition) with the *P*. *aeruginosa* cells, even at low concentrations (10 μg/mL). Given the improved association of the 50 nm particles with the *P*. *aeruginosa* cells, it is likely that they exhibited more efficient NO delivery, and thus better antibacterial activity.

Confocal microscopy was also utilized to evaluate intracellular NO levels in *P*. *aeruginosa* and *S*. *aureus* cells exposed to NO-releasing AR1 and AR8 particles. Since *S*. *aureus* required greater NO doses for eradication, it was hypothesized that the improved killing of *P*. *aeruginosa* may result from more efficient NO delivery. The bacteria were exposed to NO-releasing AR1 or AR8 particles (22 μg/mL) and intracellular NO concentrations were subsequently monitored with the DAF-2 (green) fluorescent probe. As shown in Figure 2.3, *P*. *aeruginosa* cells exhibited increased DAF-2 fluorescence upon exposure to the higher aspect ratio (i.e., AR8) particles, thus confirming the increased efficiency in NO delivery for the rod-like particles. Of note, minimal DAF-2 fluorescence was observed in *S*. *aureus* cells exposed to the same NO-releasing particle

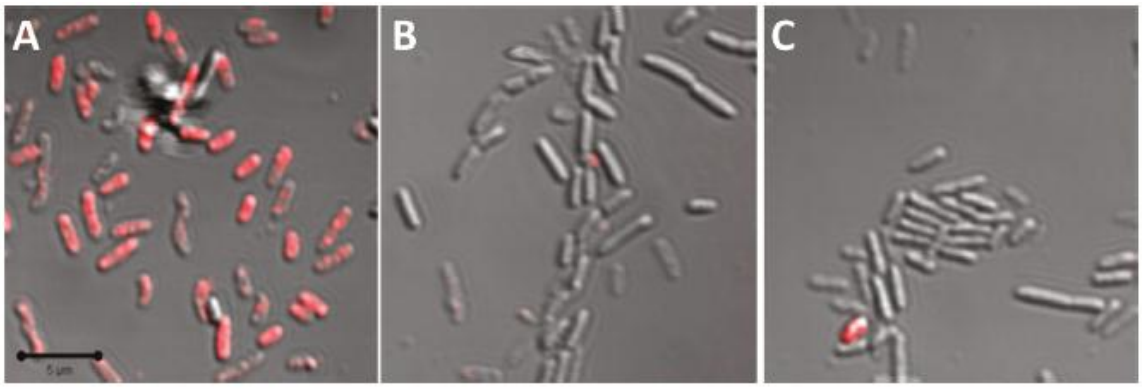

Figure 2.1 Confocal microscopy images of RITC-modified (A) 50, (B) 100, and (C) 200 nm silica nanoparticle (10 μg/mL) association with planktonic *P. aeruginosa* after 10 min incubation. Scale bar is 5 μm.

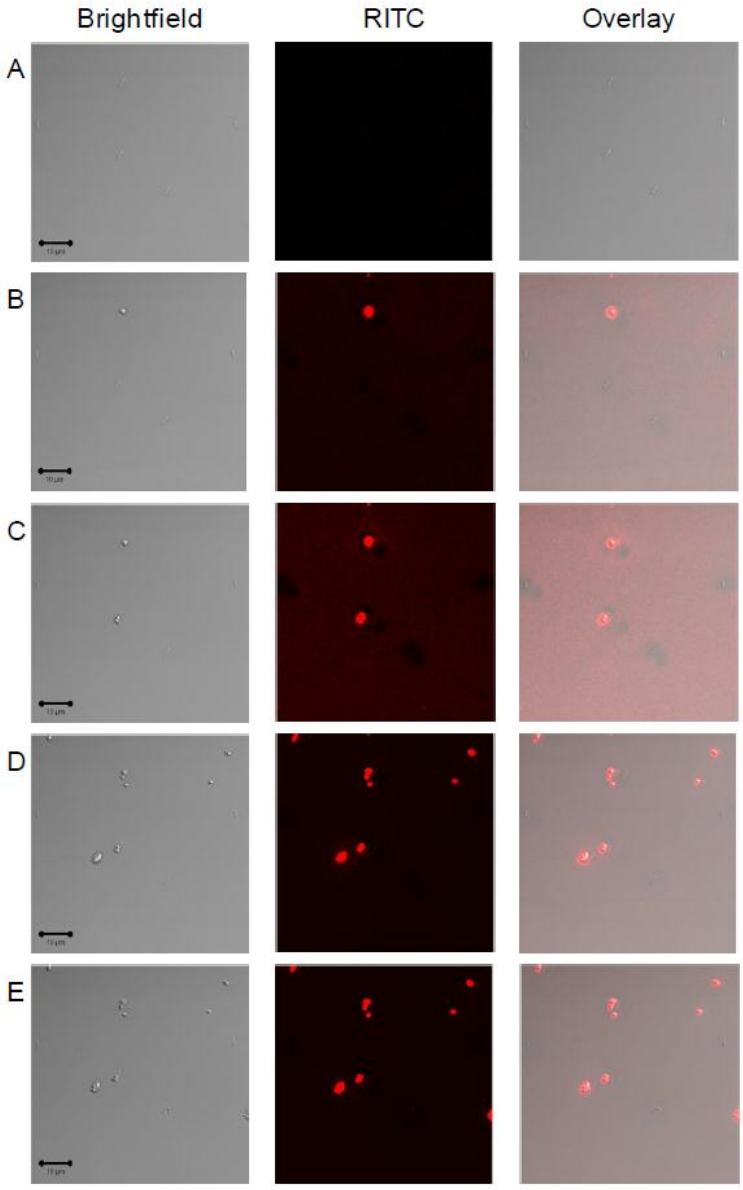

Figure 2.2 Confocal images of 50 nm RITC-modified NO-releasing silica particle association with planktonic *P. aeruginosa*. Images were acquired (A) 0 (addition of particles), (B) 2.4, (C), 6.4, (D) 19.5, and (E) 39 min after addition of nanoparticles at 10 μg/mL. Scale bar is 10 μm.

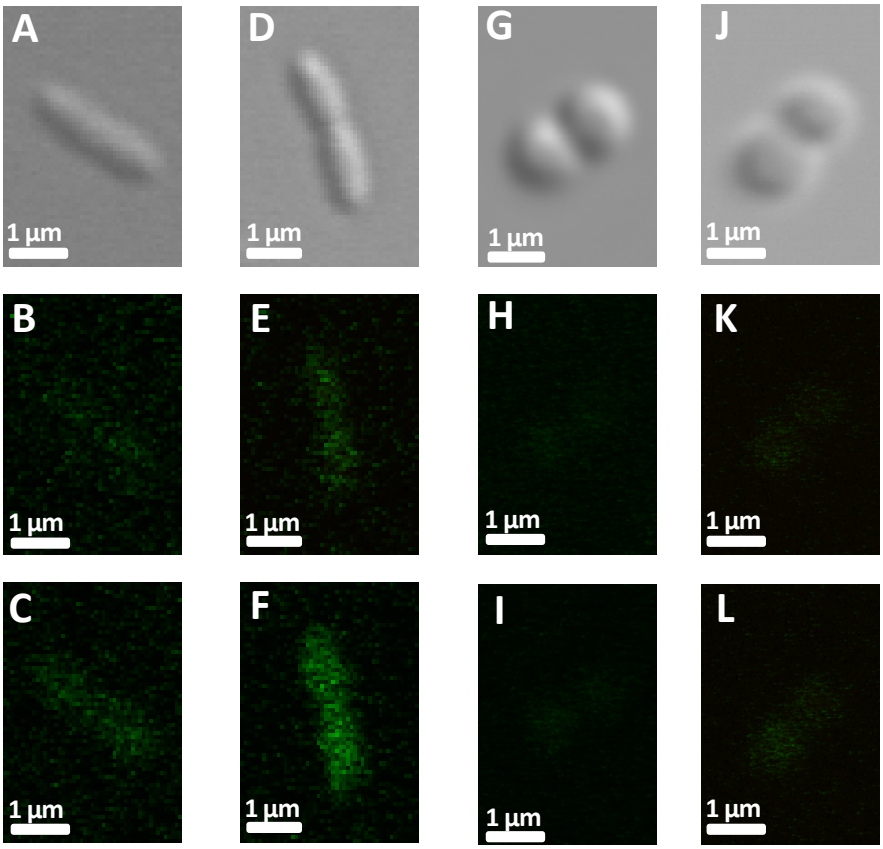

Figure 2.3 Intracellular DAF-2 fluorescence from *P. aeruginosa* bacterial cells incubated with 22 µg/mL AR1(Bright field (A), 120 min (B), 125 min (C)) and AR8(Bright field (D), 95 min (E), 100 min (F)) and from *S. aureus* bacterial cells incubated with AR1 (Bright field (G), 135 min (H), 155 min (I)) AR8 (Bright field (J), 100 min (K), 130 min (L)). Intensity of DAF-2 (green) fluorescence indicates intracellular NO levels.

concentration (22 μg/mL). This corroborates the higher MBC values for *S*. *aureus* compared to *P*. *aeruginosa*. The greater bactericidal NO doses necessary to kill *S*. *aureus* vs. *P*. *aeruginosa* are attributed to several possible factors including differential thickness of the peptidoglycan layer in the cell membrane,[51] varied production of antioxidant enzymes (e.g., superoxide dismutase) to mitigate the effects of NO,[52] and *S*. *aureus*' use of NO as a cytoprotection agent.[53]

2.3.1.3 In vitro cytotoxicity

To ensure the therapeutic utility of the silica scaffolds, the 50, 100, and 200 nm particles as well as the AR1, AR4, and AR8 particles were tested for in vitro cytotoxicity against L929 mouse fibroblasts. The fibroblasts were selected as a model host cell due to their ubiquitous presence in connective tissue.[54] Cytotoxicity of the control and NO-releasing 50, 100, and 200 nm silica particles was evaluated at 2 and 24 h to mimic bacteria assays. All three particles sizes were non-toxic to mammalian cells at the highest concentrations necessary for planktonic killing of *P*. *aeruginosa* (i.e., 1.6 and 0.4 mg/mL for the 2 and 24 h exposures, respectively). Likewise, the control and NO-releasing AR1, AR4, and AR8 particles were non-toxic at MBCs for *P*. *aeruginosa* eradication. However, some reduction in fibroblast was noted for particle concentrations necessary to kill *S*. *aureus*.

2.3.1.4 Conclusions

Both NO-releasing nanoparticle size and shape played a role in bactericidal efficacy against Gram-negative *P*. *aeruginosa* and Gram-positive *S*. *aureus*. As expected,

particles with decreased size and increased aspect ratio exhibited greater biocidal action. Bacterial killing was shown to improve with longer treatment times (i.e., 2 vs 24 h) and thus future work should evaluate assay duration to achieve the lowest therapeutic dose. Additionally, the NO-releasing 50, 100, and 200 nm and AR1, AR4, and AR8 silica scaffolds were effective against bacteria with minimal cytotoxicity and should be investigated as anti-biofilm agents.

2.3.2 Nitric oxide-releasing dendrimers

Nitric oxide-releasing dendrimers were synthesized with varied size (i.e., G2 and G5) and exterior functionalities (i.e., PO, SO, and PEG) (Figure 2.4).[46] Total nitric oxide release from the scaffolds ranged from 0.65 to 2.61 μmol/mg over the 2 h planktonic killing assays. In addition to varied hydrophobicity and total NO storage, the PO, SO, and PEG scaffolds had a range of NO-release kinetics, with $t_{1/}2$ ranging from 0.67 to 1.70 h. The varied NO-release characteristics of the NO-releasing PPI dendrimers allowed from evaluation of bactericidal efficacy against planktonic *P. aeruginosa* and *S. aureus* as a function of size (i.e., G2 versus G5) and exterior modification.

2.3.2.1 Bactericidal efficacy against planktonic bacteria as a function of exterior functionality

Details on the planktonic MBCs for the control (i.e., non-NO-releasing) and NO-releasing PPI dendrimers has been reported by Sun et al.[46] In general, the SO-modified dendrimers exhibited greater antibacterial activity to both *P. aeruginosa* and *S. aureus* due to the improved association with the cell membrane. Likewise, the hydrophilic PEG-modified dendrimers were less effective. For example, ~600x the bactericidal NO dose

(1254 versus 2 μmol NO/L) was required for *P*. *aeruginosa* eradication for the G2-PEG-NO dendrimers compared to the G2-SO-NO dendrimers. Size effects were also noted, with greater biocidal action for the larger dendrimers (i.e., G5-SO-NO versus G2-SO-NO).

2.3.2.2 Confocal microscopy

Confocal microscopy was used to determine if larger size dendrimers exhibited improved bacterial killing due to more localized NO delivery to the cell. As shown in Figure 2.5, larger intracellular NO concentrations (DAF-2 fluorescence) were observed for *P*. *aeruginosa* cells exposed to G5-SO-NO dendrimers compared to G2-SO-NO, thus confirming improved NO delivery efficiency for the larger dendrimer. Additionally, dendrimer–bacteria interactions were evaluated for *S*. *aureus* to explain the improved killing of the control G2-PO dendrimers compared to the NO-releasing G2-PO dendrimers (MBC of 484.0 versus 967.9 μg/mL). *S*. *aureus* cells were exposed to the RITC-modified dendrimers and imaged over time to evaluate association (Figure 2.6). Indeed, the control G2-PO dendrimers exhibited more rapid association with *S*. *aureus* cells compared to their NO-releasing counterparts, likely due to more favorable electrostratic interactions with the negatively-charged cell membrane (zeta potentials were +7.1 ± 0.6 and -14.0 ± 5.4 mV for the control and NO-releasing G2-PO dendrimers, respectively.

2.3.2.3 In vitro cytotoxicity

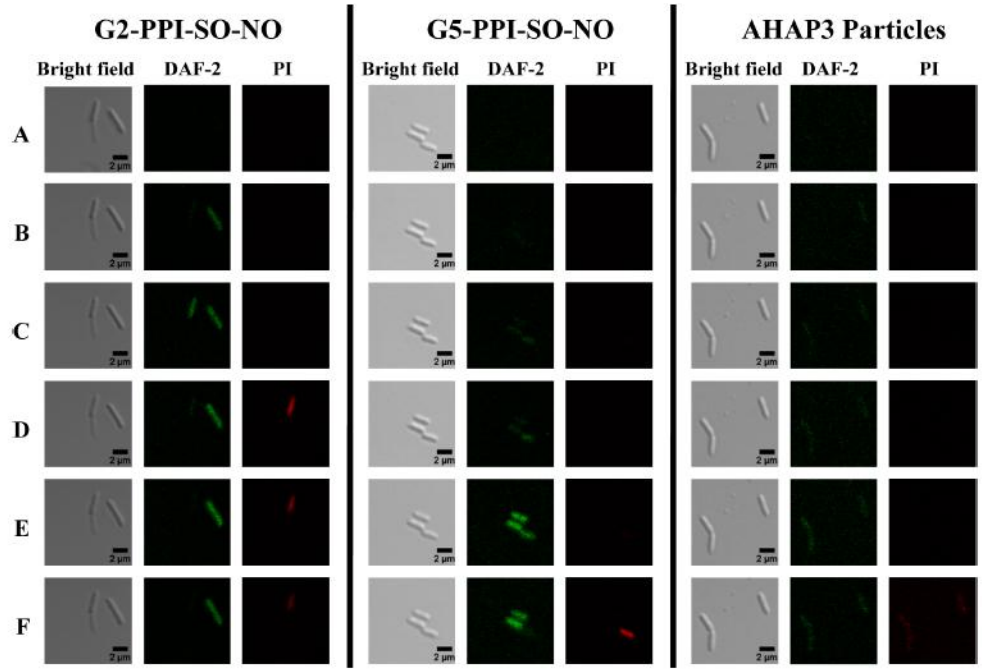

Figure 2.4 Confocal microscopy images of *P. aeruginosa* cells exposed to the same NO dosage (10 μmol/L) via incubation with NO-releasing G2- and G5-PPI-SO (8.7 and 10 μg/mL, respectively) and 50 nm AHAP3/TEOS nanoparticles (22 μg/mL). Intracellular NO is indicated by the appearance of DAF-2 green fluorescence, while PI red fluorescence indicates compromised membranes (cell death). Images were acquired (A) 30, (B) 46, (C) 60, (D) 64, (E) 86, and (F) 94 min after dendrimer/nanoparticle addition.

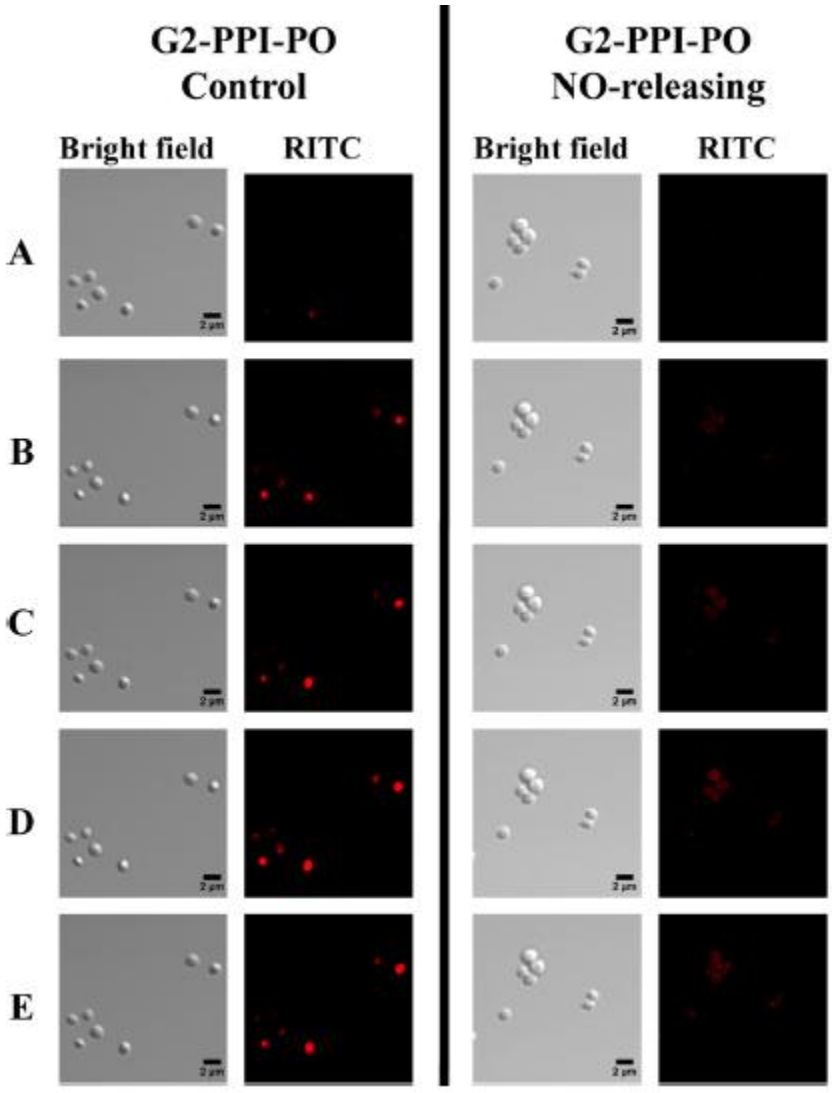

Figure 2.5 Confocal microscopy images of RITC-modified control and NO-releasing G2 PPI-PO dendrimer (400 μg/mL) association with *S. aureus* cells. Images were acquired (A) 4, (B) 12, (C) 18, (D) 30, and (E) 45 min following dendrimer addition.

In vitro cytotoxicity to L929 mouse fibroblasts was evaluated for the control and NO-releasing PPI dendrimers to determine their potential for therapeutic use. Although many of the PPI dendrimer scaffolds exhibited potent antibacterial activity against both *P. aeruginosa* and *S. aureus*, significant reductions in fibroblast viability (>80%) were observed for many control and NO-releasing scaffolds at the corresponding MBC.

2.3.2.4 Conclusions

The planktonic killing of *P. aeruginosa* and *S. aureus* was dependent on both NO-releasing PPI dendrimer size and hydrophobicity. Larger, hydrophobic dendrimers (i.e., G5-SO-NO) were most effective. Despite the low scaffold does necessary for bacterial eradication, these scaffolds were significantly toxic to healthy host cells, thus limiting their widespread utility. Further tailoring of the exterior modification or use of a less toxic dendritic scaffold (e.g., poly(amidoamine)) is thus warranted to maintain biocidal action while reducing unwanted cytotoxic effects.

2.3.3 Nitric oxide-releasing chitosan oligosaccharides

Nitric oxide-releasing chitosan oligosaccharides with varied exterior functionality and molecular weight were synthesized (Figure 2.7). The chitosan oligosaccharides were modified with different ratios of 2-methyl aziridine to tune the exterior functionality (Chitosan 1 and 2). Chitosan 2 was further modified with PEG (Chitosan 3) to evaluate a wider range of functionalities. Additionally, three different molecular weights of Chitosan 2 (2.5k, 5k, and 10k)were synthesized to study the influence of molecular weight on chitosan antibacterial activity.

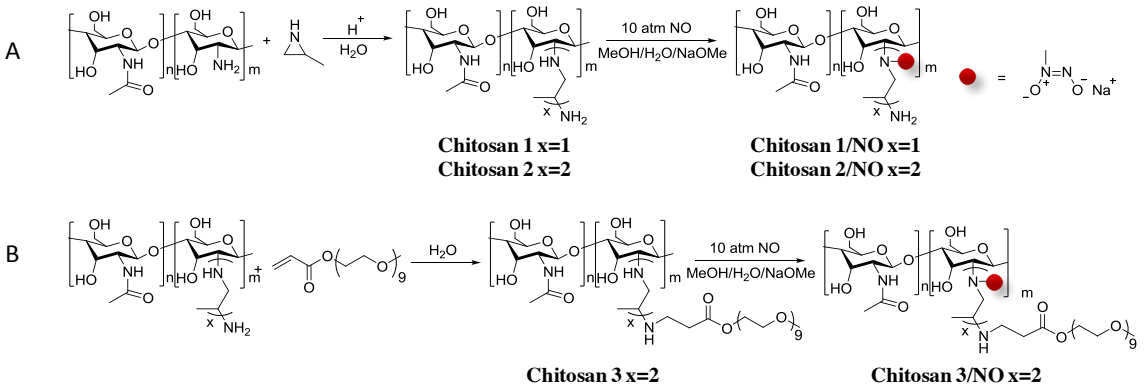

Figure 2.6 Synthesis of secondary amine- and *N*-diazeniumdiolate-functionalized chitosan oligosaccharide derivatives. A) Chitosan 1 and Chitosan 2) and subsequent *N*-diazeniumdiolate formation of the resulting materials (Chitosan 1/NO and Chitosan 2/NO); B) Modification of secondary amine-functionalized chitosan oligosaccharides with PEG (Chitosan 3 and Chitosan 3/NO).

2.3.3.1 Bactericidal efficacy against planktonic bacteria as a function of exterior functionality and molecular weight

The NO-releasing chitosan oligosaccharides (Chitosan 1–3) were evaluated for planktonic killing against *P. aeruginosa*. Minimum bactericidal concetrations for the NO-releasing Chitosan 2-2.5k, Chitosan 2-5k, and Chitosan2-10k were 0.12, 0.12, and 0.12, μmol NO/mL respectively. Thus chitosan molecular weight did not significantly impact *P. aeruginosa* killing. Exterior functionality did influence antibacterial activity, with MBCs of 0.32, 0.10, and 0.45 for Chitosan 1/NO, Chitosan 2/NO, and Chitosan 3/NO, respectively. Based on previous work published with dendrimers,[46] it was expected that the PEG-modified chitosan would be the least biocidal, likely due to decreased interaction with the bacteria membrane.

2.3.3.2 Confocal microscopy

Confocal microscopy was used to evaluate the association of both Chitosan 2/NO and Chitosan 3/NO with P. aeruginosa to gain insight into the mechanism by which the PEG-modified chitosan exhibited reduced bactericidal efficacy (Figure 2.8). Planktonic P. aeruginosa cells were incubated with either RITC-labeled Chitosan 2/NO or Chitosan 3/NO (150 μg/mL) and imaged over time. Significant red fluorescence was noted for the cells exposed to Chitosan 2/NO within ~24 min. However, even at 82 min, minimal red fluorescence was observed in cells exposed to Chitosan 3/NO, likely due to less association between the neutral PEG functionality and the bacterial membrane.

2.3.3.3 In vitro cytotoxicity

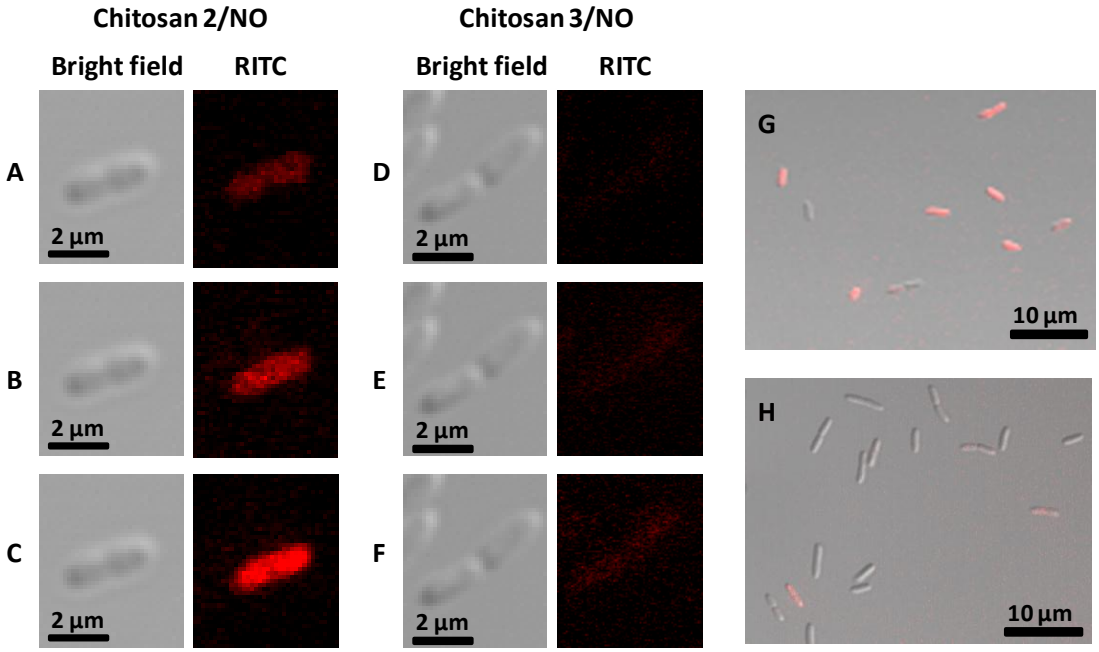

Figure 2.7 Confocal microscopy images of RITC-modified Chitosan 2/NO-5k; (A) 24 min, (B) 28 min, (C) 42 min and Chitosan 3/NO-5k; (D) 82 min, (E) 86 min, (F) 110 min, (H) 120 min association with *P. aeruginosa* cells (150 µg/ mL). Overlay images of *P. aeruginosa* cells incubated with (G) Chitosan 2/NO-5k at 44 min and (H) Chitosan 3/NO-5k at 120 min.

Control and NO-releasing chitosan oligosaccharides were evaluated for their influence on L929 mouse fibroblast viability. As expected for the natural biopolymer, the chitosan oligosaccharides were not toxic at concentrations necessary for planktonic killing of *P. aeruginosa*. Fibroblast proliferation was observed for the NO-releasing chitosans in some cases,[55] which may further the potential for use of these scaffolds as anti-biofilm agents.

2.3.3.4 Conclusions

The evaluation of NO-releasing chitosan oligosaccharides in the killing of planktonic *P.aeruginosa* showed the importance of exterior functionality. Molecular weight of the chitosan oligosaccharides was not observed to influence planktonic bacteria killing. However, it is likely that some molecular-weight dependent effects would be noted for these scaffolds against bacterial biofilms.

REFERENCES

1. Neal, A. L., What can be inferred from bacterium-nanoparticle interactions about the potential consequences of environmental exposure to nanoparticles? *Ecotoxicol*. **2008,** *17*, 362-371.

2. Bryers, J. D., Medical biofilms. *Biotechnol*. *Bioeng*. **2008,** *100*, 1-18.

3. D'Avignon, L. C.; Hogan, B. K.; Murray, C. K.; Loo, F. L.; Hospenthal, D. R.; Cancio, L. C.; Kim, S. H.; Renz, E. M.; Barillo, D.; Holcomb, J. B.; Wade, C. E.; Wolf, S. E., Contribution of bacterial and viral infections to attributable mortality in patients with severe burns: An autopsy series. *Burns* **2010,** *36*, 773-779.

4. Goswami, A. P.; Goswami, N.; Patel, T.; Tripathi, C.; Trivedi, H., Antibiotic sensitivity profile of bacterial pathogens in postoperative wound infections at a tertiary care hospital in Gujarat, India. *J*. *Pharmacol*. *Pharmacother*. **2011,** *2*, 158-164.

5. Nablo, B. J.; Prichard, H. L.; Butler, R. D.; Klitzman, B.; Schoenfisch, M. H., Inhibition of implant-associated infections via nitric oxide release. *Biomaterials* **2005,** *26*, 6984-6990.

6. Rutala, W. A.; Weber, D. J., Infection control: the role of disinfection and sterilization. *J*. *Hosp*. *Infect*. **1999,** *43, Supplement 1*, S43-S55.

7. Cerca, N.; Martins, S.; Cerca, F.; Jefferson, K. K.; Pier, G. B.; Oliveira, R.; Azeredo, J., Comparative assessment of antibiotic susceptibility of coagulase-negative staphylococci in biofilm versus planktonic culture as assessed by bacterial enumeration or rapid XTT colorimetry. *J*. *Antimicrob*. *Chemother*. **2005,** *56*, 331-336.

8. Anderl, J. N.; Franklin, M. J.; Stewart, P. S., Role of antibiotic penetration limitation in *Klebsiella pneumoniae* biofilm resistance to ampicillin and ciprofloxacin. *J*. *Antimicrob*. *Chemother*. **2000,** *44*, 1818-1824.

9. Nickel, J. C.; Ruseska, I.; Wright, J. B.; Costerton, J. W., Tobramycin resistance of *Pseudomonas aeruginosa* cells growing as a biofilm on urinary catheter material. *J*. *Antimicrob*. *Chemother*. **1985,** *27*, 619-624.

10. Lindsay, D.; von Holy, A., Bacterial biofilms within the clinical setting: what healthcare professionals should know. *J*. *Hosp*. *Infect*. **2006,** *64*, 313-325.

11. Stewart, P. S.; William Costerton, J., Antibiotic resistance of bacteria in biofilms. *The Lancet* **2001,** *358*, 135-138.

12. Costerton, J. W.; Stewart, P. S.; Greenberg, E. P., Bacterial biofilms: A common cause of persistent infections. *Science* **1999,** *284*, 1318-1322.

13. Lyczak, J. B.; Cannon, C. L.; Pier, G. B., Lung infections associated with cystic fibrosis. *Clin*. *Microbiol*. *Rev*. **2002,** *15*, 194-222.

14. Dowd, S. E.; Wolcott, R. D.; Sun, Y.; McKeehan, T.; Smith, E.; Rhoads, D., Polymicrobial nature of chronic diabetic foot ulcer biofilm infections determined using bacterial tag encoded FLX amplicon pyrosequencing (bTEFAP). *PloS one* **2008,** *3*, e3326.

15. Smith, A. W., Biofilms and antibiotic therapy: Is there a role for combating bacterial resistance by the use of novel drug delivery systems? . *Adv*. *Drug Deliv*. *Rev*. **2005,** *57*, 1539-1550.

16. Ignarro, L. J.; Buga, G. M.; Wood, K. S.; Byrns, R. E.; Chaudhuri, G., Endothelium-derived relaxing factor produced and released from artery and vein is nitric oxide. *Proc*. *Natl*. *Acad*. *Sci*. *U*.*S*.*A*. **1987,** *84*, 9265-9269.

17. Ignarro, L. J.; Napoli, C.; Loscalzo, J., Nitric oxide donors and cardiovascular agents modulating the bioactivity of nitric oxide: an overview. *Circulation Research* **2002,** *90*, 21-28.

18. Carpenter, A. W.; Schoenfisch, M. H., Nitric oxide release: Part II. Therapeutic applications. *Chem*. *Soc*. *Rev*. **2012,** *41*, 3742-3752.

19. Fang, F. C., Perspectives series: host/pathogen interactions. Mechanisms of nitric oxide-related antimicrobial activity. *J*. *Clin*. *Invest*. **1997,** *99*, 2818-2825.

20. Hetrick, E. M.; Shin, J. H.; Stasko, N. A.; Johnson, C. B.; Wespe, D. A.; Holmuhamedov, E.; Schoenfisch, M. H., Bactericidal efficacy of nitric oxide-releasing silica nanoparticles. *ACS Nano* **2008,** *2*, 235-246.

21. Hetrick, E. M. S., J.-H.; Paul, H.S.; Schoenfisch, M.H., Anti-biofilm efficacy of nitric oxide-releasing silica nanoparticles. *Biomaterials* **2009,** *30*, 2782-2789.

22. De Groote, M. A.; Fang, F. C., NO inhibitions: antimicrobial properties of nitric oxide. *Clinical infectious diseases* **1995,** *21*, S162-S165.

23. Privett, B. J.; Deupree, S. M.; Backlund, C. J.; Rao, K. S.; Johnson, C. B.; Coneski, P. N.; Schoenfisch, M. H., Synergy of nitric oxide and silver

sulfadiazine against gram-negative, gram-positive, and antibiotic-resistant pathogens. *Mol*. *Pharm*. **2010,** *7*, 2289-2296.

24. Stasko, N. A.; Schoenfisch, M. H., Dendrimers as a scaffold for nitric oxide release. *J*. *Am*. *Chem*. *Soc*. **2006,** *128*, 8265-8271.

25. Diwan, A. D.; Wang, M. X.; Jang, D.; Zhu, W.; Murrell, G. A., Nitric oxide modulates fracture healing. *J*. *Bone Miner*. *Res*. **2000,** *15*, 342-351.

26. Brinker, C. J.; Scherer, G. W., *Sol-gel science: the physics and chemistry of sol-gel processing*. Elsevier: 1990.

27. Morones, J. R.; Elechiguerra, J. L.; Camacho, A.; Holt, K.; Kouri, J. B.; Ramirez, J. T.; Yacaman, M. J., The bactericidal effect of silver nanoparticles. *Nanotechnology* **2005,** *16*, 2346-2353.

28. Nair, S.; Sasidharan, A.; Rani, V. D.; Menon, D.; Nair, S.; Manzoor, K.; Raina, S., Role of size scale of ZnO nanoparticles and microparticles on toxicity toward bacteria and osteoblast cancer cells. *J*. *Mater*. *Sci*.*: Mater*. *Med*. **2009,** *20*, 235-241.

29. Pal, S.; Tak, Y.-K.; Song, J.-M., Does the antibacterial activity of silver nanoparticles depend on the shape of the nanoparticle? A study of the Gram-negative bacterium Escherichia coli. *Appl*. *Environ*. *Microbiol*. **2007,** *73*, 1712-1720.

30. Tomalia, D. A.; Naylor, A. M.; Goddard, W. A., Starburst dendrimers: molecular-level control of size, shape, surface chemistry, topology, and flexibility from atoms to macroscopic matter. *Angew*. *Chem*., *Int*. *Ed*. *Engl*. **1990,** *29*, 138-175.

31. Patri, A. K.; Kukowska-Latallo, J. F.; Baker Jr, J. R., Targeted drug delivery with dendrimers: comparison of the release kinetics of covalently conjugated drug and non-covalent drug inclusion complex. *Adv*. *Drug Deliv*. *Rev*. **2005,** *57*, 2203-2214.

32. Patil, M. L.; Zhang, M.; Taratula, O.; Garbuzenko, O. B.; He, H.; Minko, T., Internally cationic polyamidoamine PAMAM-OH dendrimers for siRNA delivery: effect of the degree of quaternization and cancer targeting. *Biomacromolecules* **2009,** *10*, 258-266.

33. Taratula, O.; Garbuzenko, O. B.; Kirkpatrick, P.; Pandya, I.; Savla, R.; Pozharov, V. P.; Minko, T., Surface-engineered targeted PPI dendrimer for efficient intracellular and intratumoral siRNA delivery. *J*. *Controlled Release* **2009,** *140*, 284-293.

34. Wathier, M.; Jung, P. J.; Carnahan, M. A.; Kim, T.; Grinstaff, M. W., Dendritic macromers as in situ polymerizing biomaterials for securing cataract incisions. *J*. *Am*. *Chem*. *Soc*. **2004,** *126*, 12744-12745.

35. Chen, C. Z.; Beck-Tan, N. C.; Dhurjati, P.; van Dyk, T. K.; LaRossa, R. A.; Cooper, S. L., Quaternary ammonium functionalized poly (propylene imine) dendrimers as effective antimicrobials: structure-activity studies. *Biomacromolecules* **2000,** *1*, 473-480.

36. Calabretta, M. K.; Kumar, A.; McDermott, A. M.; Cai, C., Antibacterial activities of poly(amidoamine) dendrimers terminated with amino and poly(ethylene glycol) groups. *Biomacromolecules* **2007,** *8*, 1807-1811.

37. Lu, Y.; Sun, B.; Li, C.; Schoenfisch, M. H., Structurally diverse nitric oxide-releasing poly(propylene imine) dendrimers. *Chem*. *Mater*. **2011,** *23*, 4227-4233.

38. Stasko, N. A.; Fischer, T. H.; Schoenfisch, M. H., S-Nitrosothiol-modified dendrimers as nitric oxide delivery vehicles. *Biomacromolecules* **2008,** *9*, 834-841.

39. Yang, Y.; Bajaj, N.; Xu, P.; Ohn, K.; Tsifansky, M. D.; Yeo, Y., Development of highly porous large PLGA microparticles for pulmonary drug delivery. *Biomaterials* **2009,** *30*, 1947-1953.

40. Jameela, S. R.; Jayakrishnan, A., Glutaraldehyde cross-linked chitosan microspheres as a long acting biodegradable drug delivery vehicle: studies on the in vitro release of mitoxantrone and in vivo degradation of microspheres in rat muscle. *Biomaterials* **1995,** *16*, 769-775.

41. Agrawal, C. M.; Ray, R. B., Biodegradable polymeric scaffolds for musculoskeletal tissue engineering. *J*. *Biomed*. *Mater*. *Res*., *Part A* **2001,** *55*, 141-150.

42. Rabea, E. I.; Badawy, M. E. T.; Stevens, C. V.; Smagghe, G.; Steurbaut, W., Chitosan as antimicrobial agent: Applications and mode of action. *Biomacromolecules* **2003,** *4*, 1457-1465.

43. Chang, K. L. B.; Tai, M.-C.; Cheng, F.-H., Kinetics and products of the degradation of chitosan by hydrogen peroxide. *Journal of Agric*. *and Food Chem*. **2001,** *49*, 4845-4851.

44. Carpenter, A. W. S., D.L.; Rao, K.S.; Schoenfisch, M.H., Influence of scaffold size on bactericidal activity of nitric oxide-releasing silica nanoparticles. *ACS Nano* **2011,** *5*, 7235-7244.

45. Lu, Y.; Slomberg, D. L.; Sun, B.; Schoenfisch, M. H., Shape- and nitric oxide flux-dependent bactericidal activity of nitric oxide-releasing silica nanorods. *Small* **2013,** *9*, 2189-2198.

46. Sun, B.; Slomberg, D. L.; Chudasama, S. L.; Lu, Y.; Schoenfisch, M. H., Nitric oxide-releasing dendrimers as antibacterial agents. *Biomacromolecules* **2012,** *13*, 3343-3354.

47. Wong, K.; Sun, G. B.; Zhang, X. Q.; Dai, H.; Liu, Y.; He, C. B.; Leong, K. W., PEI-g-chitosan, a novel gene delivery system with transfection efficiency comparable to polyethylenimine in vitro and after liver administration in vivo. *Bioconjugate Chemistry* **2006,** *17* (1), 152-158.

48. Tokura, S.; Ueno, K.; Miyazaki, S.; Nishi, N., Molecular weight dependent antimicrobial activity by chitosan. *Macromolecular Symposia* **1997,** *120*, 1-9.

49. Coneski, P. N.; Schoenfisch, M. H., Nitric oxide release: Part III. Measurement and reporting. *Chem*. *Soc*. *Rev*. **2012,** *41*, 3753-3758.

50. Hunter, R. A.; Storm, W. L.; Coneski, P. N.; Schoenfisch, M. H., Inaccuracies of nitric oxide measurement methods in biological media. *Anal*. *Chem*. **2013,** *85*, 1957-1963.

51. Silhavy, T. J.; Kahne, D.; Walker, S., The bacterial cell envelope. *Cold Spring Harb*. *Perspect*. *Biol*. **2010**, 1-16.

52. Mandell, G., Catalase, superoxide dismutase, and virulence of *Staphylococcus aureus*. In vitro and in vivo studies with emphasis on staphylococcal--leukocyte interaction. *J*. *Clin*. *Invest*. **1975,** *55*, 561-566.

53. Gusarov, I.; Nudler, E., NO-mediated cytoprotection: Instant adaptation to oxidative stress in bacteria. *Proc*. *Natl*. *Acad*. *Sci*. *U*.*S*.*A*. **2005,** *102*, 13855-13860.

54. Alberts, B.; Johnson, A.; Lewis, J., *Molecular Biology of the Cell*. 4th ed.; Garland Science: New York, 2002.

55. Cooke, J. P.; Losordo, D. W., Nitric oxide and angiogenesis. *Circulation* **2002,** *105*, 2133-2135.

CHAPTER 3: ROLE OF NITRIC OXIDE-RELEASING SCAFFOLD PROPERTIES ON ANTIBACTERIAL EFFICACY AGAINST BIOFILM-BASED BACTERIA

3.1 Introduction

The prevalence of bacteria in clinical settings continues to pose a great challenge in treating and eradicating nosocomial (hospital-acquired) infections, with an estimated 1.7 million infections resulting in ~99,000 deaths in the United States alone each year.[1, 2] Most infections are the result of biofilm-based bacteria that irreversibly adhere to a surface and secrete an exopolysaccharide (EPS) matrix.[3] Bacteria utilize the EPS matrix to retain nutrients and impede the diffusion of antibacterial agents.[2, 4] Antibiotic-inactivating enzymes, anoxic regions, and the differentiation of cell subpopulations into a more resistant, dormant metabolic state[4] are also employed by the biofilm bacteria to further prevent eradication. As a result, biofilm-based bacteria exhibit increased resistance to treatment and are less susceptible to antibacterial agents compared to planktonic suspensions.[2, 5-7] In turn, complete eradication of bacterial biofilms is complex and often not feasible.[1, 8, 9]

Ideally, implant-associated infections would be controlled by eliminating initial bacteria attachment to a surface and thus preventing biofilm formation of adherent cells.[3] However, superhydrophobic,[10] heparin-coated,[11] and antibacterial-doped substrates[12, 13] have not proven effective clinically in reducing infection rates.[3] Researchers have thus

turned to more aggressive strategies involving the active release of antibacterial agents.[14] Nitric oxide (NO), a diatomic free radical, serves a number of roles in the body, including the immune response to pathogens, with antibacterial properties via oxidative and nitrosative stresses when sustained at mid-pM or higher concentrations.[15-17] The effects of NO release on bacterial biofilms are generally concentration dependent, with biofilm dispersal occurring at low NO concentrations (~nM) and killing of the embedded bacteria at higher concentrations (~μM).[18-20] Barraud et al. reported NO-mediated dispersal of *Pseudomonas aeruginosa* biofilms with exposure to 25–500 nM sodium nitroprusside, after which the bacteria were more susceptible to antibacterials (i.e., tobramycin, hydrogen peroxide, and sodium dodecyl sulfate).[18] At greater NO-release levels (total release ~10 μmol NO) using an enzymatic gaseous NO-releasing dressing, Sulemankhil et al. reported the eradication of *Acinetobacter baumannii*, methicillin-resistant *Staphylococcus aureus*, and *Pseudomonas aeruginosa* biofilms (6 h exposure).[19]

Due to enhanced delivery of NO compared to small molecule NO donors, our lab and others have focused on the synthesis of macromolecular NO donors including silica, metallic nanoparticles, and dendrimers.[21] For example, *N*-diazeniumdiolate-modified silica nanoparticles were developed to deliver large NO payloads and kill planktonic bacteria.[21, 22] Using such scaffolds, Hetrick et al. reported the bacterial killing property of *N*-diazeniumdiolate-modified silica nanoparticles (~100 nm) against *Pseudomonas aeruginosa*, *Escherichia coli*, *Staphylococcus aureus*, *Staphylococcus epidermidis*, and *Candida albicans* biofilms.[20] Nitric oxide released from the particles (~61 μmol/mL) eradicated >99% of the biofilm-embedded bacteria. Selective tuning of the

physicochemical properties of NO-releasing scaffolds to enhance killing of bacterial biofilms has not been investigated, although initial work with planktonic bacteria indicates that scaffold size,[23] shape,[24] and exterior functionality[25] are important.

3.1.1 Nitric oxide-releasing silica particles

As discussed in Chapter 2, silica nanoparticle size and shape proved influential in planktonic bacterial killing. Carpenter et al. reported improved killing of *Pseudomonas aeruginosa* with smaller (50 nm) silica particles.[23] Lu et al. observed improved biocidal efficacy for rod-like particles vs. silica spheres.[24] Herein, the role of NO-releasing silica nanoparticle size (i.e., 14, 50, 150 nm) and shape (i.e., aspect ratio 1, 4, and 8) on the eradication of established Gram-negative *Pseudomonas aeruginosa* and Gram-positive *Staphylococcus aureus* biofilms was investigated. Such studies are important since >99% of all bacteria exist in a biofilm state and such communities are increasingly difficult to treat.[2]

3.1.2 Nitric oxide-releasing dendrimers

Nitric oxide-releasing dendrimers have also demonstrated biocidal action against planktonic bacteria as a function of physicochemical properties. Sun et al. reported the efficacy of NO-releasing PPI dendrimers against both *P. aeruginosa* and *S. aureus* as a function of size (i.e., generation) and exterior functionality.[25] Enhanced bacterial killing was observed for the higher generation (i.e., G5), hydrophobic SO-modified dendrimers, however, the control PPI dendrimers were also toxic to mammalian cells (i.e., >80% viability reduction) at bactericidal concentrations. As such, NO-releasing amphiphilic

PAMAM dendrimers with varied exterior hydrophobicity were evaluated for maximum bactericidal efficacy against *P.aeruginosa* biofilms and minimal toxicity to healthy host cells.

3.1.3 Nitric oxide-releasing chitosan oligosaccharides

Similar to NO-releasing silica and dendrimer scaffolds, the exterior functionality of NO-releasing chitosan oligosaccharides (as detailed in Chapter 2) played a role in planktonic bacterial killing. However, significant differences in efficacy against *P. aeruginosa* were not observed for chitosan oligosaccharides of varied molecular weight (i.e., 2.5k, 5k, and 10k). Both NO-releasing and control chitosan scaffolds were non-toxic to L929 mouse fibroblasts at concentrations necessary to eradicate planktonic bacteria, thus necessitating their evaluation against more clinically-relevant bacterial biofilms.

3.2 Materials and Methods

Note: Silica nanorod, dendrimer, and chitosan synthesis, characterization, and evaluation of cytotoxicity were supported by other members of the Schoenfisch lab

Tetraethylorthosilicate (TEOS), *N*-(6-aminohexyl)aminopropyltrimethoxysilane (AHAP), and *N*-(2-aminoethyl)-3-amino-isobutyl-dimethyl-methoxysilane (AEAI) were purchased from Gelest (Morrisville, PA). Cetyltrimethylammonium bromide (CTAB), propylene oxide (PO), and 1,2-epoxy-9-decene (ED) were obtained from Acros Organics (Geel, Belgium). Ethanol (EtOH), ammonium hydroxide (28 wt%), Tris base, and Tris hydrochloride were purchased from Fisher Scientific (Fair Lawn, NJ). Organosilicasol

MT-ST silica particles (14 nm) in methanol were obtained from Nissan Chemical Corporation (Houston, TX). Tetramethylorthosilicate (TMOS), sodium methoxide (5.4 M in methanol), sulfanilamide, *N*-1-napthylethylenediamine dihydrochloride, rhodamine B isothiocyanate (RITC), propidium iodide (PI), fetal bovine serum (FBS), Dulbecco's Modified Eagle's Medium (DMEM), phenazine methosulfate (PMS), 3-(4,5-dimethylthiazol-2-yl)-5-(3-carboxymethoxyphenyl)-2-(4-sulfophenyl)-2H-tetrazolium inner salt (MTS), trypsin, phosphate buffered saline (PBS) used for cell culture, and Pen Strep solution (10,000 u/mL penicillin, 10,000 μg/mL streptomycin), medium molecular weight chitosan, 2-methyl aziridine (MAz), and poly(ethylene glycol) methyl ether acrylate (average Mn = 480) (PEG) were purchased from the Sigma Aldrich Corp. (St. Louis, MO). Tryptic soy broth (TSB) and tryptic soy agar (TSA) were obtained from Becton, Dickinson, and Company (Franklin Lakes, NJ). *Pseudomonas aeruginosa* (ATCC #19143) and *Staphylococcus aureus* (ATCC# 29231) were obtained from the American Type Culture Collection (Manassas, VA). The Centers for Disease Control and Prevention (CDC) bioreactor was purchased from BioSurface Technologies Corporation (Bozeman, Montana). Medical grade silicone rubber (1.45 mm thick) was purchased from McMaster Carr (Atlanta, GA) and doubled in thickness using Superflex Clear RTV silicone adhesive sealant (Loctite, Westlake, OH) to fabricate coupons to fit the CDC reactor (thickness ~4 mm and diameter ~12.7 mm). L929 mouse fibroblasts (ATCC #CCL-1) were purchased from the University of North Carolina Tissue Culture Facility (Chapel Hill, NC). Spectra/Por Float-A-Lyzers for dialysis of the dendrimers were purchased from Spectrum Laboratories, Inc. (Rancho Dominguez, CA). Syto 9 green

fluorescent nucleic acid stain was purchased from Life Technologies (Grand Island, NY).4,5-Diaminofluorescein diacetate (DAF-2 DA) was purchased from Calbiochem (San Diego, CA). Glass bottom microscopy dishes were received from MatTek Corporation (Ashland, MA). Nitric oxide (NO) was purchased from Praxair (Bethlehem, PA). Argon (Ar) gas was obtained from Airgas National Welders (Raleigh, NC). A Millipore Milli-Q UV Gradient A10 System (Bedford, MA) was used to purify distilled water to a final resistivity of 18.2 MΩ·cm and a total organic content of ≤6 parts per billion (ppb). Other solvents and chemicals were analytical-reagent grade and used as received. Nuclear magnetic resonance (NMR) spectra were recorded on a 400 MHz Bruker instrument. Elemental (carbon, hydrogen, nitrogen or CHN) analysis was performed using a PerkinElmer Elemental Analyzer Series 2400 instrument (Waltham, MA).

3.2.1 Synthesis of nitric oxide-releasing silica particles

Three silica nanoparticle systems (i.e., 14, 50, and 150 nm) were utilized to evaluate anti-biofilm efficacy over a range of sizes. Secondary amine-functionalized 14 nm silica particles were prepared via surface grafting according to a modified previously reported procedure.[26] Briefly, 600 μL of 14 nm Organosilicasol MT-ST particles in methanol (225 mg/mL) and 1 mL *N*-(6-aminohexyl)aminopropyltrimethoxysilane (AHAP) were added to a stirred solution of EtOH (100 mL) and allowed to react overnight (~18 h) with heating (48 °C). The particles were collected by adding water to the solution in a 2:1 ratio (v/v) and centrifugation (4696 *g* for 15 min, 4 °C). Following

collection, the particles were resuspended in EtOH via sonication and collected again by centrifugation. This washing procedure was performed twice. The particles were then dried under vacuum. The 50 nm silica particles were synthesized by adding TEOS (2.28 mL) to a stirred solution of EtOH (110 mL), ammonium hydroxide (4.05 mL), and water (1.74 mL). After 5 h, the 50 nm silica particles were surface-grafted with AHAP by adding an aliquot of the silane (5.02 mL) to the reaction flask and allowing the reaction to proceed overnight (~18 h). The particles were then collected by adding hexane to the solution in a 2:1 ratio (v/v) and centrifugation (4696 *g* for 15 min, 4 °C). Following collection, the 50 nm particles were resuspended in EtOH via sonication and collected again by centrifugation. This washing procedure was carried out twice. The particles were then dried under vacuum. Secondary amine-functionalized 150 nm silica particles were synthesized by adding TMOS (0.71 mL) and AHAP (1.17 mL) to a stirred solution of EtOH (59.16 mL), ammonium hydroxide (9.8 mL), and water (27.84 mL). After 2 h, the 150 nm particles were collected via centrifugation (4696 *g* for 15 min, 4 °C), washed with EtOH, and dried according to the aforementioned procedure.

Silica particles of three distinct aspect ratios (AR1, AR4, and AR8) were synthesized via a surfactant-templated approach as previously described by varying reaction temperature and ammonia concentration.[24] Elevated temperature (30 vs. 20 °C) was used to increase the aspect ratio of the particles (AR8), while a greater ammonia concentration (1.0 vs. 0.5 M) allowed for the synthesis of a more spherical particle (AR1). Of note, cetyltrimethylammonium bromide (CTAB) removal was confirmed via CHN analysis prior to surface grafting. Monoalkoxysilane, *N*-(2-aminoethyl)-3-amino-

isobutyl-dimethyl-methoxysilane (AEAI) was then surface grafted onto the particle/rods to impart secondary amine functionality for *N*-diazeniumdiolation as described below.

The 14, 50, and 150 nm silica particles were functionalized with *N*-diazeniumdiolate NO donors by suspending the particles (20 mg) in a 9:1 (v/v) solution of *N*,*N*-dimethylformamide (DMF) and methanol (MeOH) and adding 37, 25, and 50 μL of 5.4 M sodium methoxide in MeOH for the 14, 50, and 150 nm particles, respectively. Vials of the solution suspensions were then placed in a Parr hydrogenation vessel and stirred. Residual oxygen in the suspensions was removed by purging the vessel with argon (Ar) three times quickly, followed by three longer (10 min) Ar purges. The vessel was then pressurized to 10 atm with purified gaseous NO. The hydrogenation vessel was maintained at 10 atm throughout a 3 d period after which the Ar purging procedure was repeated to remove unreacted NO prior to removal of the vials from the vessel. The *N*-diazeniumdiolated particles were recollected by centrifugation (4696 *g* for 15 min, 25 °C), washed three times with EtOH, dried under vacuum, and stored at -20 °C until use. Similarly, *N*-diazeniumdiolate-functionalized AR1, AR4, and AR8 silica particles were prepared by suspending the AEAI-functionalized particles (15 mg) in a 9:1 (v/v) solution of DMF and MeOH, and adding 50 μL sodium methoxide (5.4 M in MeOH). Vials of the suspensions were placed in the Parr hydrogenation vessel, purged with Ar, exposed to NO, and the resulting particles were recollected and stored following the same protocol.

3.2.2 Synthesis of nitric-oxide releasing amphiphilic dendrimers

Secondary amine-functionalized PAMAM dendrimers (generation 1 or G1 and generation 3 or G3) were synthesized as described previously.[27] Briefly, primary amine-functionalized G1-PAMAM dendrimer (100 mg) was dissolved in methanol (2 mL). One molar equivalent of PO, ED, or a mixture of PO and ED relative to the primary amines was subsequently added to the G1-PAMAM-NH_2 solution under constant stirring at room temperature for 4 d to yield secondary amine-functionalized G1-PAMAM conjugates. Secondary amine-functionalized G3-PAMAM conjugates were synthesized in a similar manner. The resulting G1- and G3-secondary amine-functionalized dendrimers were characterized by nuclear magnetic resonance (NMR) spectroscopy (data not shown).

The PAMAM dendrimers were subsequently *N*-diazeiumdiolated by adding one equivalent of sodium methoxide (5.4 M in methanol) (with respect to the molar amount of primary amine functionality in PAMAM-NH_2 used to synthesize dendrimers) to a vial containing dendrimers (100 mg) in methanol (1 mL). The glass vials were then inserted in a Parr hydrogenation vessel and exposed to gaseous NO following the aforementioned procedure for *N*-diazeniumdiolation of silica particles.

3.2.3 Synthesis of nitric oxide-releasing chitosan oligosaccharides

Chitosan oligosaccharides of varied molecular weights were prepared by oxidative degradation using hydrogen peroxide. Medium molecular weight chitosan (2.5 g) was suspended in a hydrogen peroxide solution (15 or 30 wt%) under stirring for 1 h at 65–85 ^{o}C. After removal of undissolved chitosan via filtration, the chitosan

oligosaccharides were precipitated with acetone, collected by centrifugation, washed twice with ethanol, and dried under vacuum.

The chitosan oligosaccharides were then grafted with 2-methyl aziridine (MAz) based on a previously reported procedure.[28] Briefly, a mixture of concentrated HCl (11 μL), water (100 μL) and MAz with a 1:1 (Chitosan 1) or 2:1 (Chitosan 2) molar ratio to primary amines on the chitosan oligosaccharides was added dropwise to a solution of chitosan oligosaccharides (100 mg) in deionized water (5 mL). The resulting solution was stirred at room temperature for 5 d, and then 75 ^{o}C for 24 h. The MAz-grafted chitosan oligosaccharides were then purified by dialysis and collected by lyophilization. The chitosan oligosaccharides were further functionalized with PEG by adding poly(ethylene glycol) methyl ether acrylate (Chitosan 3) to tune hydrophobicity. The resulting PEG-functionalized chitosan oligosaccharides were purified by dialysis and collected by lyophilization. The chitosan oligosaccharides were characterized by nuclear magnetic resonance (NMR) spectroscopy (data not shown).

N-diazeniumdiolation of the secondary amine-functionalized chitosan oligosaccharides (Chitosan 1, Chitosan 2, and Chitosan 3) was achieved by adding the chitosan and 5.4 M sodium methoxide (75 μL) to a water/methanol mixture (2 mL). The suspension was added to vials in a Parr hydrogenation vessel and exposed to gaseous NO as previously discussed.

3.2.4 Fluorescently-labeled scaffolds

Fluorescently-labeled silica nanoparticles,[23] dendrimers,[25] and chitosan oligosaccharides[29] were achieved via covalent modification with rhodamine B isothiocyanate (RITC) based on a previously published procedures. The 14, 50, or 150 nm silica particles (50 mg) were suspended in EtOH (100 mL) with RITC (5 mg) and stirred in the dark for 48 h. Following fluorescent modification, the particles were collected and washed copiously with EtOH using the collection/centrifugation protocol described above. After a clear supernatant was achieved, the particles were dried under vacuum and stored until use. Fluorescently-labeled dendrimers were prepared by dissolving G1 or G3-PAMAM-NH_2 (100 mg) and RITC (3 mg) in methanol (2 mL). The solution was stirred for 3 d, dialyzed, and lyophilized to yield RITC-labeled dendrimers that were then modified with PO or ED alone, or a PO/ED mixture, and further reacted with NO. Chitosan oligosaccharides (50 mg) were dissolved in water (2 mL) at pH 9.0 and RITC was added to the solution in a 1:100 molar ratio to the primary amine of the chitosan oligosaccharides prior to the grafting of 2-methyl aziridine. The solution was then stirred at room temperature for 3 d, dialyzed, and lyophilized to collect the RITC-labeled chitosan oligosaccharides.

3.2.5 Scaffold characterization and nitric oxide release

Size and shape (i.e., aspect ratio) of the silica particles were determined using transmission electron microscopy (TEM) and scanning electron microscopy (SEM). Transmission electron micrographs of the 14, 50, and 150 nm silica particles were obtained on a JEOL 100 CX II transmission electron microscope (Tokyo, Japan).

Scanning electron micrographs of the AR1, AR4, and AR8 silica particles were recorded using a Hitachi S-4700 scanning electron microscope (Tokyo, Japan). Real-time NO-release from the silica particles, dendrimers, and chitosan oligosaccharides was measured using a Sievers 280i Chemiluminesence Nitric Oxide Analyzer (NOA; Boulder, CO). The NO-releasing silica particles (1 mg), dendrimers (1 mg), or chitosan oligosaccharides (aliquot in water/methanol mixture) were added to a sample vessel containing 30 mL deoxygenated PBS (pH 7.4, 37 °C). Liberated NO was carried from the sample vessel to the NOA at a flow rate of 70 mL/min. To match the collection rate of the NOA (200 mL/min), additional nitrogen flow was supplied to the sample vessel. Nitric oxide-release measurements were terminated when the levels fell below 10 ppb NO/mg scaffold. The real-time NO-release data was used to determine the total NO-release duration and half-life ($t_{1/2}$). Total NO storage (t[NO]) was also characterized using the Griess assay.[30, 31]

3.2.6 Planktonic bactericidal assays

Pseudomonas aeruginosa and *Staphylococcus aureus* bacterial cultures were grown from frozen stock (-80 °C) in TSB overnight at 37 °C. An aliquot of the suspension (0.5 mL) was added to fresh TSB (50 mL) and incubated at 37 °C until the bacteria reached mid-exponential phase (~1×10^8 colony forming units (cfu)/mL) as determined by the optical density at 600 nm (OD_{600}). The relationship between the concentration of the bacteria in suspension and the OD_{600} was calibrated for each strain using an Eppendorf BioPhotometer Plus Spectrophotometer (Hamburg, Germany); the colony forming units were enumerated from culture dilutions grown on TSA plates. The

bacterial suspension was then centrifuged (3645 *g* for 10 min, 25 °C), resuspended in PBS, and diluted to ~1 × 10^6 cfu/mL in PBS (dendrimer and chitosan oligosaccharide exposures) or PBS supplemented with 1% (w/w) glucose, 0.5% (v/v) TSB, and 100 mM Tris (silica nanoparticle exposures) for planktonic bactericidal assays.

The minimum bactericidal concentration (MBC) of the NO-releasing silica particles for planktonic *P. aeruginosa* and *S. aureus* was defined as the concentration that resulted in a 3-log reduction in viability versus untreated cells after 24 h. The MBC of the NO-releasing dendrimers and chitosan oligosaccharides for planktonic *P. aeruginosa* was defined as the concentration that resulted in a 3-log reduction in viability versus untreated cells after 4 h. The bacterial suspensions (10^6 cfu/mL) were incubated with the NO-releasing scaffolds over a range of particle concentrations for the duration noted. After exposure, the samples were nanomaterial–bacteria suspensions were diluted and plated on TSA, with counting of resulting colonies to determine viability.

3.2.7 Bacterial biofilm assays

A CDC bioreactor was used to grow *P. aeruginosa* and *S. aureus* biofilms over 48 h.[32] Growth conditions (e.g., nutrient concentrations, additives, flow rate) were optimized for both the *P. aeruginosa* and *S. aureus* biofilms. Briefly, medical grade silicone rubber substrates were mounted in the coupon holders within the CDC reactor. After autoclaving, the reactor effluent line was clamped and 500 mL sterile 1% (w/v) TSB (*P. aeruginosa* growth) or 10% (w/v) TSB and 0.1% (w/v) glucose (*S. aureus* growth) was added aseptically. Similar to planktonic experiments, *P. aeruginosa* and *S. aureus*

bacterial cultures were grown from frozen stock (-80 °C) overnight in TSB at 37 °C, reinoculated, and grown to mid-exponential phase. The reactor was then inoculated with an aliquot (1 mL) of the resulting 1×10^8 cfu/mL bacterial suspension (final concentration ~2×10^5 cfu/mL). The completed assembly was incubated at 37 °C for 24 h with stirring (150 rpm). Following this "batch phase" growth, the effluent line was opened and the reactor media was refreshed continuously with 0.33% (v/v) TSB at 6 mL/min (*P. aeruginosa* growth) or 1% (v/v) TSB at 2.7 mL/min (*S. aureus* growth) for another 24 h to complete growth of the biofilms.

The MBCs for biofilm eradication were determined as the concentrations of NO-releasing silica particles, dendrimers, or chitosan oligosaccharides that resulted in bacterial viability below the limit of detection for the plate counting method (2.5×10^3 cfu/mL).[23] Each scaffold was tested in triplicate over an optimized concentration range. For determination of NO-releasing silica nanoparticle anti-biofilm efficacy, *P. aeruginosa* and *S. aureus* biofilms grown on silicone rubber substrates were exposed to several particle concentrations in 3 mL PBS supplemented with 1% (w/w) glucose, 0.5% (v/v) TSB, and 100 mM Tris at 37 °C with slight agitation for 24 h. Nitric oxide-releasing dendrimer and chitosan oligosaccharide anti-biofilm assays were conducted by exposing *P. aeruginosa* biofilms to several scaffold concentrations in PBS (static conditions) at 37 °C with slight agitation for 24 h. After 24 h of incubation, the samples were sonicated and vortexed to disrupt the biofilm. Aliquots of the cell/nanoparticle suspensions were diluted in PBS, plated on TSA, and incubated at 37 °C overnight. Bacterial viability was then determined by counting the observed colonies.

3.2.8 Confocal microscopy

P. aeruginosa biofilms were grown on glass substrates (Biosurface Technologies) and subsequently exposed to NO-releasing silica nanoparticles or dendrimers to evaluate intracellular NO levels and cell death. *P. aeruginosa* biofilms were incubated with NO-releasing silica nanoparticles (1 mg/mL) in PBS supplemented with DAF-2 DA (10 μM) and PI (30 μM) for 15–60 min or RITC-labeled 14 or 150 nm control (i.e., non-NO-releasing) silica nanoparticles (0.1 mg/mL) in PBS supplemented with Syto 9 (10 μM) for 30 min. Similarly, the efficiency of NO delivery was also evaluated as a function of dendrimer composition by incubating *P. aeruginosa* biofilms with NO-releasing dendrimers (20 μg/mL) in PBS supplemented with 10 μM DAF-2 DA and 30 μM PI for 60 min. For examination of dendrimer diffusion within the biofilm, *P. aeruginosa* biofilms were incubated with RITC-labeled NO-releasing dendrimers (50 μg/mL) for 60 min and stained with Syto 9 (10 μM) before imaging Likewise, RITC-labeled chitosan oligosaccharides (0.15 mg/mL in PBS) were incubated with *P. aeruginosa* biofilms for 150 min. Before imaging, the substrates were dipped in PBS to remove excess dye and loosely adhered cells. A Zeiss 510 Meta inverted laser scanning confocal microscope (Carl Zeiss, Thornwood, NY) with a 488 nm Ar excitation laser (2.0% intensity) and a BP 505–530 nm filter was used to obtain DAF-2 and Syto 9 (green) fluorescence images. A 543 nm HeNe excitation laser (25.3% intensity) with a BP 560–615 nm filter was used to obtain PI and RITC (red) fluorescence images. The images were collected using a Zeiss C-apochromat lens (20x, 1.2 numerical aperture).

3.2.9 In vitro cytotoxicity

L929 mouse fibroblasts were cultured in DMEM supplemented with 10% (v/v) FBS and 1 wt% Pen Strep solution, and incubated in 5% (v/v) CO_2 under humidified conditions at 37 ^{o}C. After reaching 80% confluency, the cells were trypsinized, seeded onto tissue culture-treated polystyrene 96-well plates at a density of 3×10^4 cells/mL and incubated at 37 ^{o}C for 48 h. The supernatant was then aspirated prior to adding fresh DMEM (200 μL) with control (i.e., non-NO-releasing) or NO-releasing nanoparticles to each well. After incubation at 37 ^{o}C for 24 h, the supernatant was aspirated and the cells rinsed 3x with PBS. A mixture of DMEM/MTS/PMS (105/20/1, v/v/v) (120 μL) was then added to each well. The absorbance of the resulting colored solution after 1.5 h incubation at 37 ^{o}C was quantified at 490 nm using a Thermo Scientific Multiskan EX plate reader (Thermo Fisher Scientific, Inc., Waltham, MA). The mixture of DMEM/MTS/PMS and untreated cells were used as the blank and control, respectively. Cell viability was calculated by taking the ratio of the absorbance of treated to untreated cells after subtracting the absorbance of the blank from each.

3.3 Results and Discussion

3.3.1 Nitric oxide-releasing silica particles

Although several studies have evaluated the effects of metal and metal oxide nanoparticle physicochemical properties on planktonic bacteria killing, [23, 24, 33-35] most bacteria exist in a biofilm state where the secreted EPS matrix impedes antibacterial agent diffusion and prevents eradication. In turn, the results of such studies must be

considered carefully, particularly with respect to antibacterial efficacy. The potential to realize an effective bacterial biofilm killing scaffold using NO-releasing silica nanoparticles warrants a detailed study of particle size and shape on bacterial biofilm eradication.

Since smaller (<200 nm) NO-releasing silica nanoparticles were previously reported to be more bactericidal than larger scaffolds,[23] experiments using particles spanning 14–150 nm were initiated to enable a thorough evaluation of anti-biofilm efficacy as a function of particle size.[36, 37] The sizes of the as obtained/prepared particles measured by electron microscopy are provided in Table 3.1. Nitric oxide release was achieved by modifying the particles with *N*-(6-aminohexyl)aminopropyltrimethoxysilane (AHAP), and reacting the amines with NO. As expected based on the amount of sodium methoxide used in the *N*-diazeniumdiolation process, the three particle systems exhibited similar NO-release kinetics with total NO-release durations of ~5–6 h.

To study the role of nanoparticle shape on NO-mediated bactericidal action, silica particles of varied aspect ratio (AR1, AR4, and AR8) were synthesized via a surfactant-templating method in which aspect ratio (1.1 ± 0.2, 4.3 ± 0.5, and 8.2 ± 0.6 for the AR1, AR4, and AR8 particles, respectively) was controlled by tuning temperature and ammonia concentration.[24] Similar to the spherical particles, the rod-like scaffolds were surface modified with *N*-(2-aminoethyl)-3-amino-isobutyl-dimethyl-methoxysilane (AEAI), and reacted with NO to obtain NO-releasing AR1, AR4, and AR8 silica particles. To ensure any differences in bactericidal action were the result of shape (i.e.,

aspect ratio) alone, the overall particle volume (~0.02 μm^3) and total NO release (~0.7 μmol/mg) were tuned to be identical for each particle system (Table 3.2).[24]

Table 3.1 Particle size as determined by transmission electron microscopy (TEM) and total micromoles NO released per mg of particle as measured by the Griess assay. Size measurements are n≥20 and total NO release is n≥3 syntheses.

Scaffold	Size (nm)	Total NO release (μmol/mg)
14 nm	14.8 ± 2	0.24 ± 0.01
50 nm	56.1 ± 5	0.26 ± 0.02
150 nm	139.9 ± 13	0.25 ± 0.03

Table 3.2 Size and aspect ratio of silica nanorods as determined by scanning electron microscopy (SEM) and total micromoles NO released per mg of particle as measured by the Griess assay. Size measurements are n≥50 and total NO release is n≥3 syntheses.

Scaffold	Aspect Ratio	Length (nm)	Width (nm)	Total NO release (μmol/mg)
AR1	1.1 ± 0.2	312 ± 26	285 ± 31	0.66 ± 0.14
AR4	4.3 ± 0.5	736 ± 49	170 ± 42	0.65 ± 0.04
AR8	8.2 ± 0.6	1115 ± 62	137 ± 45	0.68 ± 0.14

The three rod-like NO-releasing silica particles (i.e., AR1, AR4, and AR8) exhibited similar NO-release kinetics with NO-release half-lives of ~0.7 h.

3.3.1.1 Bactericidal efficacy against planktonic bacteria as a function of size and shape

Prior to evaluating the biofilm eradication ability of NO-releasing silica particles as a function of size, the bactericidal activity of 14, 50, and 150 nm NO-releasing silica was evaluated against planktonic *P. aeruginosa* and *S. aureus* suspensions. Minimum bactericidal concentration (MBC) assays were carried out over a 24 h period in bacteria solutions containing nutrients (i.e., PBS supplemented with 1% (w/w) glucose, 0.5% (v/v) TSB, and 100 mM Tris) to ensure survival of the bacteria and mimic conditions for the anti-biofilm assays. As expected, the smaller 14 and 50 nm particles were more effective against planktonic *P. aeruginosa* compared to the 150 nm silica particles (MBC_{24h} of 0.5 mg/mL for the 14 and 50 nm versus 1 mg/mL for 150 nm) (Table 3.3). Likewise, the 14 nm particles were more effective against planktonic *S. aureus* compared to the larger particles, with an MBC_{24h} of 2 versus 4 mg/mL for the 50 and 150 nm particles. As discussed in Chapter 2, the greater bactericidal NO doses necessary to kill *S. aureus* vs. *P. aeruginosa* (0.48–1.0 vs. 0.12–0.25 μmol NO/mL) are attributed to several factors including differential thickness of the peptidoglycan layer in the cell membrane,[38] varied production of antioxidant enzymes (e.g., superoxide dismutase) to mitigate the effects of NO,[39] and *S. aureus*' use of NO as a cytoprotection agent.[40]

The planktonic bactericidal efficacy of the NO-releasing nanorods was evaluated similarly against *P. aeruginosa* and *S. aureus* suspensions. As reported previously in a 4

h assay,[24] the higher aspect ratio AR8 particles were more effective at killing *P. aeruginosa* after 24 h than the AR4 and AR1 scaffolds (MBC_{24h} values of 0.125, 0.250,

Table 3.3 Determination of planktonic and biofilm MBCs and bactericidal NO doses for NO-releasing 14, 50, and 150 nm silica particles against *P. aeruginosa* and *S. aureus* biofilms.

Scaffold	*P. aeruginosa*				*S. aureus*			
	MBC_{24h} (mg/mL)		Bactericidal NO Dose (μmol/mL)		MBC_{24h} (mg/mL)		Bactericidal NO Dose (μmol/mL)	
	Planktonic[a]	Biofilm[b]	Planktonic	Biofilm	Planktonic[a]	Biofilm[b]	Planktonic	Biofilm
14 nm	0.5	6	$0.12 \pm 5.0 \times 10^{-3}$	1.44 ± 0.06	2	10	$0.48 \pm 2.0 \times 10^{-2}$	2.40 ± 0.10
50 nm	0.5	6	$0.13 \pm 1.0 \times 10^{-2}$	1.56 ± 0.12	4	12	$1.0 \pm 8.0 \times 10^{-2}$	3.12 ± 0.24
150 nm	1	10	$0.25 \pm 3.0 \times 10^{-2}$	2.50 ± 0.30	4	14	$1.0 \pm 1.2 \times 10^{-2}$	3.50 ± 0.42

[a]MBC: Minimum Bactericidal Concentration resulting in 3-log reduction in bacterial viability.
[b]MBC: Minimum Bactericidal Concentration resulting in bacterial viability below the limit of detection for the plating method (2.5×10^3 cfu/mL).

Table 3.4 Determination of planktonic and biofilm MBCs and bactericidal NO doses for NO-releasing AR1, AR4, and AR8 silica particles against *P. aeruginosa* and *S. aureus* biofilms.

Scaffold	*P. aeruginosa*				*S. aureus*			
	MBC_{24h} (mg/mL)		Bactericidal NO Dose (μmol/mL)		MBC_{24h} (mg/mL)		Bactericidal NO Dose (μmol/mL)	
	Planktonic[a]	Biofilm[b]	Planktonic	Biofilm	Planktonic[a]	Biofilm[b]	Planktonic	Biofilm
AR1	0.250	8	$0.17 \pm 3.2 \times 10^{-2}$	5.28 ± 1.12	0.500	12	$0.33 \pm 7.0 \times 10^{-2}$	7.92 ± 1.68
AR4	0.250	1	$0.16 \pm 1.0 \times 10^{-2}$	$0.65 \pm 4.0 \times 10^{-2}$	0.500	4	$0.33 \pm 2.0 \times 10^{-2}$	2.60 ± 0.16
AR8	0.125	1	$0.09 \pm 1.8 \times 10^{-2}$	0.68 ± 0.14	0.125	4	$0.09 \pm 1.8 \times 10^{-2}$	2.72 ± 0.56

[a]MBC: Minimum Bactericidal Concentration resulting in 3-log reduction in bacterial viability.
[b]MBC: Minimum Bactericidal Concentration resulting in bacterial viability below the limit of detection for the plating method (2.5×10^3 cfu/mL).

and 0.250 mg/mL for the AR8, AR4, and AR1 particles, respectively) (Table 3.4).[24] An identical trend in bactericidal action was noted against planktonic *S*. *aureus* with an MBC_{24h} of 0.125 versus 0.500 mg/mL for the AR4 and AR1 particles. Slightly greater NO doses (0.09–0.33 μmol NO/mL) were also required for *S*. *aureus* killing compared to those for Gram-negative *P*. *aeruginosa* (0.09–0.17 μmol NO/mL).

3.3.1.2 Biofilm killing assays as a function of size and shape

The anti-biofilm efficacy of the particles/rods was evaluated next to assess their utility in eradicating bacteria under more clinically relevant conditions. *P*. *aeruginosa* (~3 x 10^8 cfu per substrate) and *S*. *aureus* (~3 x 10^7 cfu per substrate) biofilms were exposed to NO-releasing 14, 50, and 150 nm silica particles for 24 h in PBS supplemented with 1% (w/w) glucose, 0.5% (v/v) TSB, and 100 mM Tris buffer. Based on the size-dependent efficacy against planktonic bacteria, we hypothesized that the smaller NO-releasing particles would show enhanced biofilm killing compared to the larger particles. As shown in Table 3.3, the NO-releasing 14 and 50 nm particles proved more effective than the 150 nm particles, with concentrations as low as 6 mg/mL killing *P*. *aeruginosa* biofilms compared to 10 mg/mL for the 150 nm particles. As in the planktonic assays, the Gram-positive *S*. *aureus* biofilms required a greater NO dose for eradication compared to the Gram-negative *P*. *aeruginosa* biofilms, with MBC_{24h} values of 10, 12, and 14 mg/mL for the 14, 50, and 150 nm particles, respectively. Overall, the smaller (i.e., 14 nm) silica particles were characterized by more effective killing of both *P*. *aeruginosa* and *S*. *aureus* biofilms compared to the 50 and 150 nm particles. The biofilm bactericidal NO doses

were ~10–12x those required for planktonic killing of *P*. *aeruginosa*, but only ~3–5x the NO levels required for planktonic killing of *S*. *aureus*. The increased NO dose necessary for *P*. *aeruginosa* biofilm eradication compared to *S*. *aureus* may arise from general differences in biofilm formation, cell density, and the biofilm's propensity to disperse.[18, 41, 42] Control (i.e., non-NO-releasing) 14, 50, and 150 nm particles did not significantly reduce *P*. *aeruginosa* biofilm viability (<1 log killing at their respective MBC concentrations). Control 50 and 150 nm particles slightly reduced *S*. *aureus* biofilm viability at their respective MBCs (~1.5 log), while the 14 nm control particles did not affect *S*. *aureus* cells (<1 log killing) at 10 mg/mL.

Determination of the role of nanoparticle shape on *P*. *aeruginosa* and *S*. *aureus* biofilm killing showed a dependence on aspect ratio similar to that observed in planktonic studies. We hypothesized that higher particle aspect ratios (i.e., AR4 and AR8) would improve NO delivery to bacteria within the biofilm based on the planktonic assays. As shown in Table 3.4, the 24 h MBCs for the NO-releasing AR8 and AR4 rod-like particles were 1 and 4 mg/mL for *P*. *aeruginosa* and *S*. *aureus* biofilms, respectively. The more spherical, NO-releasing AR1 particles were significantly less effective, with biofilm MBCs of 8 and 12 mg/mL for *P*. *aeruginosa* and *S*. *aureus*. The biofilm bactericidal NO doses were ~4–31x those required for planktonic killing of *P*. *aeruginosa* and ~8–30x the NO levels required for planktonic killing of *S*. *aureus*. As mentioned above, these differences may arise from a variety of biological factors.[18, 41, 42] Control AR1, AR4, and AR8 particles at their respective biofilm MBCs resulted in negligible reduction in *P*. *aeruginosa* biofilm viability (<1 log killing). However, the control

scaffolds resulted in a greater reduction in *S. aureus* biofilm viability at their respective biofilm MBCs (~2.5, 2, and 1.5 log killing for the AR1, AR4, and AR8 particles, respectively) due to the increased scaffold concentration required for eradication. Of note, the MBC values for the NO-releasing 14, 50, and 150 nm silica particles and the AR1, AR4, and AR8 nanorods must be evaluated independently due to differences in NO loading capacity between the particles synthesized via the Stöber method (14, 50, 150 nm) and surfactant-templated approach (AR1, AR4, AR8).[23]

3.3.1.3 Confocal microscopy

To determine whether the enhanced anti-biofilm efficacy observed for smaller particles (i.e., 14 and 50 nm) and higher aspect ratio nanorods (i.e., AR4 and AR8) was due to improved NO delivery, confocal microscopy was used to visualize intracellular NO concentrations and subsequent cell death. Intracellular NO levels were monitored by using 4,5-diaminofluorescein diacetate (DAF-2 DA), a membrane permeable dye that enters the cell and is then hydrolyzed to an impermeable form, DAF-2, via intracellular esterases.[22] Once in the cell, DAF-2 will react with NO to form a green fluorescent derivative, triazolofluorescein, resulting in fluorescence that scales with NO concentration. Cell death was visualized using propidium iodide (PI), a dye that only permeates cells with compromised membranes; red fluorescence is produced upon binding with nucleic acids (i.e., DNA and RNA).[43] The build-up of intracellular NO has previously been shown to precede PI signal at sub-MBC particle exposures.[22, 44] Intracellular NO levels and cell death were visualized for *P. aeruginosa* biofilms exposed to NO-releasing 14, 50, or 150 nm particles (1 mg/mL in a solution of PBS supplemented

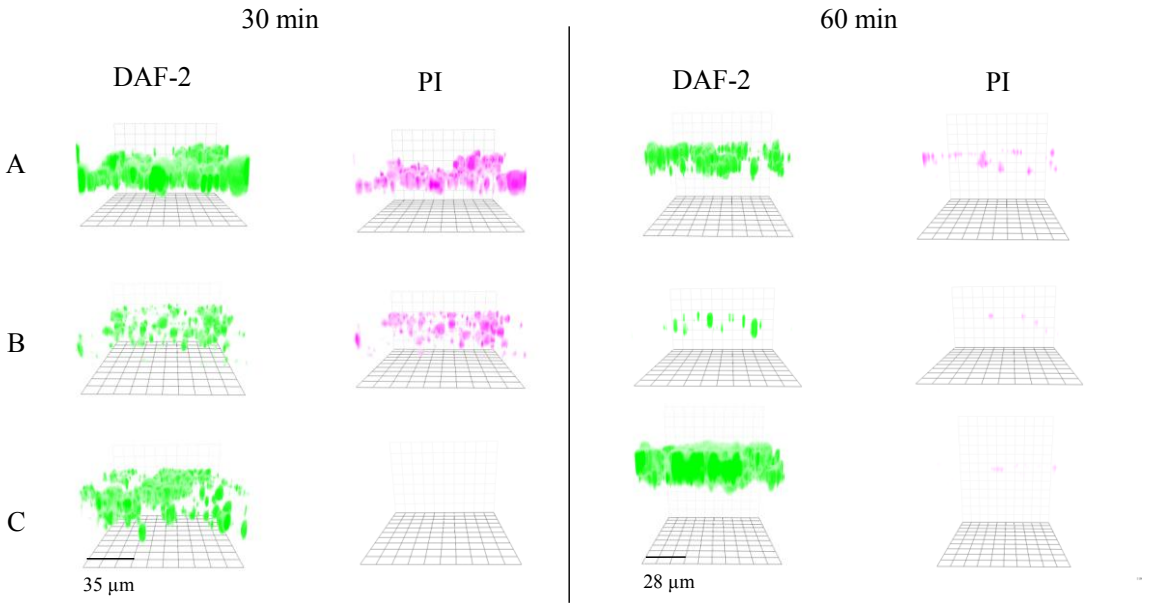

Figure 3.1 Fluorescent images of *P. aeruginosa* biofilm exposed to the same particle concentration (1 mg/mL) and NO dosage (~250 µmol/L) of NO-releasing (A) 14, (B) 50, or (C) 150 nm particles for 30 or 60 min. DAF-2 green fluorescence indicates increased intracellular NO and PI red fluorescence indicates compromised cell membranes (i.e., cell death).

with DAF-2 DA and PI) for 30 or 60 min. Of note, intracellular NO levels, cell death, and particle diffusion were not evaluated for *S. aureus* biofilms as killing trends were identical to *P. aeruginosa*. As shown in Figure 3.1, the DAF-2 (green) signal was greatest for the 14 nm scaffold after incubation with the NO-releasing particles. Such efficient delivery of NO also lead to more rapid cell death for the smallest silica particle NO-release vehicle. Greater intracellular NO (i.e., green fluorescence) was ultimately observed within the *P. aeruginosa* biofilm after 60 min when using 150 nm NO-releasing particles, despite no visible cell death (red fluorescence). Conversely, the 14 and 50 nm NO-releasing particles effectively dispersed the *P. aeruginosa* biofilm at 60 min,[18] resulting in decreased DAF-2 and PI fluorescence from the few biofilm cells remaining on the substrate (Figure 3.1).

Intracellular NO levels and cell death were also measured for *P. aeruginosa* biofilms exposed to NO-releasing particles of varied aspect ratio (AR1–AR8). Based on confocal experiments with planktonic bacterial suspensions,[24] we hypothesized that increased DAF-2 and PI fluorescence would also be observed for biofilms exposed to higher aspect ratio scaffolds due to improved efficiency of NO delivery. As shown in Figure 3.2, significant DAF-2 and PI fluorescence were observed throughout the entire *P. aeruginosa* biofilm after exposure to NO-releasing AR4 or AR8 particles at 1 mg/mL for 15 min. Although intracellular NO and cell death were detected for the biofilm exposed to the NO-releasing AR1 particles (1 mg/mL), the fluorescence was localized to small regions of the biofilm (Figure 3.2). Furthermore, bacteria killing was not observed until 60 min. Conversely, the visibility of the DAF-2 and PI fluorescence decreased for the

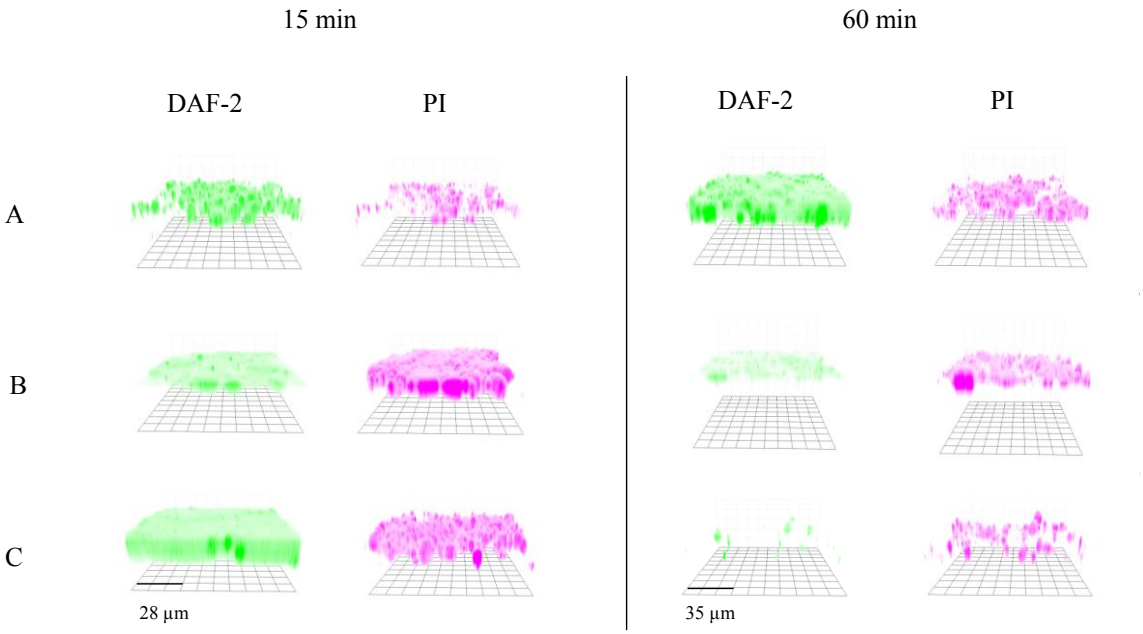

Figure 3.2 Fluorescent images of *P. aeruginosa* biofilm exposed to the same particle concentration (1 mg/mL) and NO dosage (~700 µmol/L) of NO-releasing (A) AR1, (B) AR4, or (C) AR8 particles for 15 or 60 min. DAF-2 green fluorescence indicates increased intracellular NO and PI red fluorescence indicates compromised cell membranes (i.e., cell death).

NO-releasing AR4 and AR8 nanorods at the 60 min timepoint due to effective *P. aeruginosa* biofilm dispersal.[18]

The role of particle diffusion into the biofilm on bacteria killing was evaluated next to understand if the vehicle or just NO penetrated the biofilms. To carry out this study, the biofilm was stained with a membrane-permeable dye, Syto 9, to enable visualization of the biofilm bacteria.[45] *P. aeruginosa* biofilms were incubated with RITC-labeled 14 and 150 nm control particles (0.1 mg/mL) for 30 min, and then rinsed with PBS to determine whether the particles could penetrate and diffuse into the biofilm. Although particle diffusion into the *P. aeruginosa* biofilm was observed for both the 14 and 150 nm RITC-labeled particles, more significant RITC (red) fluorescence was noted for the 14 nm particles, indicating faster diffusion for the smaller vs. larger particles at 30 min (Figure 3.3). Comparison of the biofilm regions stained with Syto 9 to those with RITC fluorescence also confirmed that the 150 nm particles did not adequately penetrate the *P. aeruginosa* biofilm. Of note, the rod-like particles were too large (e.g., AR1 ~300 nm)[46] to readily diffuse into the biofilm, and thus particle–biofilm associations for the nanorods were not visualized.

3.3.1.4 In vitro cytotoxicity

The utility of NO-release scaffolds for eradicating biofilms will be governed by both their ability to kill bacteria and not impact healthy host cells or tissue. To assess cytotoxicity, we exposed L929 mouse fibroblasts to NO-releasing and control silica particles. L929 mouse fibroblasts were selected as a model host cell due to their ubiquitous presence in connective tissue.[47] Normalized cell viability was determined after

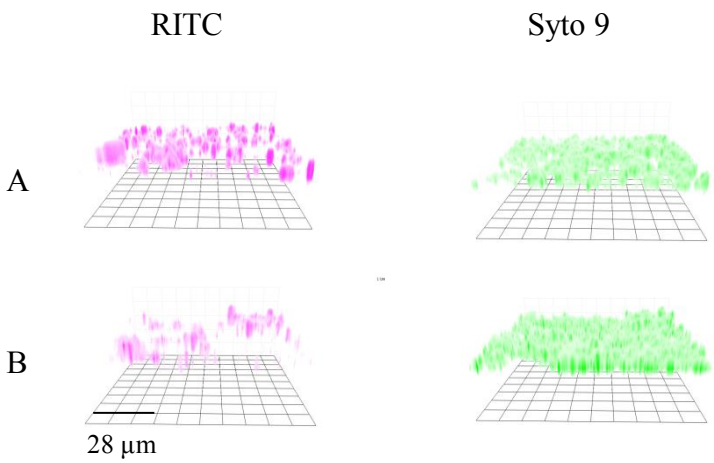

Figure 3.3 Fluorescent images of RITC-modified (A) 14 and (B) 150 nm control particle (0.1 mg/mL) diffusion in *P. aeruginosa* biofilm 30 min after particle addition. Green Syto 9 fluorescence shows biofilm cells. Increased RITC red fluorescence indicates more efficient particle diffusion within biofilm.

a 24 h exposure using the MBCs for *P*. *aeruginosa* and *S*. *aureus* biofilm eradication. As shown in Figure 3.4, the NO-releasing 50 nm, AR4, and AR8 particles were non-toxic to the L929 fibroblasts at the MBCs necessary to eradicate *P*. *aeruginosa* biofilms, with ~30, 22, and 15% reduction in fibroblast viability, respectively. Likewise, control 50 nm, AR4, and AR8 particles did not greatly impact the L929 cells at these concentrations. The cytotoxicity of both control and NO-releasing scaffolds was significantly greater for all other particle systems (e.g., 14 and 150 nm and AR1 particles) at the concentrations (≥6 mg/mL) necessary to kill *P*. *aeruginosa* biofilms. Similarly, Hetrick et al. reported significantly reduced fibroblast viability for both control and NO-releasing silica particles at 8 mg/mL (50 and 70% reductions, respectively).[20] At concentrations necessary to eradicate *S*. *aureus* biofilms, all particle systems proved cytotoxic (36–71% viability reduction). Overall, the NO-releasing particles decreased fibroblast viability to a greater extent than control systems at the MBCs for *S*. *aureus* killing, which might be expected given the increased concentration of both scaffold and NO required to eradicate *S*. *aureus* biofilms. Despite the greater scaffold concentration required to eradicate *S*. *aureus* biofilms, the fibroblast viabilities for control particles at MBCs for *P*. *aeruginosa* and *S*. *aureus* were identical, indicating that the greater NO-release levels play a significant role in the observed toxicity.

3.3.1.5 Conclusions

Despite the moderate cytotoxicity observed for the NO-releasing silica scaffolds at concentrations necessary for biofilm eradication, this work successfully demonstrates the benefits of NO as an anti-biofilm agent. Both particle size and shape clearly play

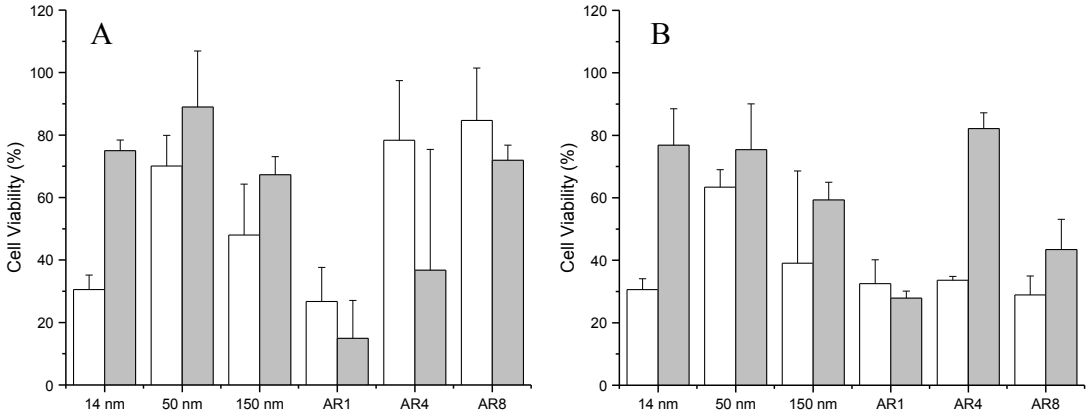

Figure 3.4 Cytotoxicity of NO-releasing (white) and control (gray) silica particles against L929 mouse fibroblasts at MBC concentrations required for biofilm killing listed in Tables 3 and 4; (A) *P. aeruginosa* and (B) *S. aureus*.

important roles in biofilm eradication, with smaller sizes and higher aspect ratios being most effective. The use of NO can effectively eradicate *P. aeruginosa* and *S. aureus* biofilms at concentrations only 3–31x those required for planktonic killing with minimal concern about antibacterial resistance.[48] In contrast, other anti-biofilm agents (e.g., antibiotics) exhibit significantly decreased efficacy toward biofilm bacteria and often promote resistance upon repeated exposure.[2] Future work should focus on reducing the toxicity of the NO-release scaffolds to healthy cells and tissue. Additionally, the combination of NO with other antibacterial agents (e.g., antibiotics, silver) should be explored, as biofilm dispersal by low, non-toxic levels of NO is likely to make the action of current antibiotics more effective.

3.3.2 Nitric oxide-releasing amphiphilic dendrimers

The bactericidal efficacy of NO-releasing dendrimers as a function of exterior functionality has previously been demonstrated.[49] Functionalization with hydrophobic groups (e.g., SO) at the dendrimer exterior improved bactericidal efficacy, but also resulted in significant toxicity towards mammalian cells (~80% reduction in viability) even at low concentrations (< 50 μg/mL). Thus, NO-releasing amphiphilic dendrimers with tunable exterior hydrophobicity were synthesized to evaluate the impact of dendrimer structure on both bactericidal action and cytotoxicity.

In addition to PO and ED-modified dendrimers, the feed molar ratio of PO and ED was tuned to yield PO/ED ratios of 7:3 (i.e., G1-PE 73, G3-PE 73), 5:5 (i.e., G1-PE 55), and 3:7 (i.e., G1-PE 37) to study the effects of relative hydrophobicity on biofilm

eradication and cytotoxicity. As noted in Chapter 2, dendrimer size (i.e., dendrimer generation) plays a significant role in antibacterial activity, with higher generation (e.g., G5 versus G2) NO-releasing dendrimers being more effective due to the greater concentration of *N*-diazeniumdiolates at the dendrimer surface.[49] Thus, two sizes of amphiphilic dendrimers (i.e., G1 and G3) were utilized to understand the influence of dendrimer size on the eradication of *P. aeruginosa* biofilms. Of note, the dendrimers exhibited similar NO storage (~1 μmol/mg) and NO-release kinetics (i.e., half -life ~1 h) regardless of modification. Prior to evaluating the NO-releasing amphiphilic dendrimers against bacterial biofilms, the dendrimers were first tested against planktonic bacteria to confirm efficacy.

3.3.2.1 Bactericidal efficacy against planktonic bacteria as a function of exterior functionality

Planktonic *P. aeruginosa* was exposed to control and NO-releasing dendrimers over 4 h (static conditions) to evaluate the effects of the varied hydrophobicity (i.e., PO/ED ratio) on bacterial killing. Amphiphilic control dendrimers functionalized with ED alone or a PO/ED mixture (e.g., G1-ED, G1-PE 37, G1-PE 55, G1-PE 73) exhibited enhanced biocidal activity against planktonic *P. aeruginosa* compared to the more hydrophilic PO-modified dendrimers (Table 3.5).

3.3.2.2 Biofilm killing assays as a function of function of exterior functionality

Table 3.5. Bactericidal doses (3-log reduction in bacterial viability) for NO-releasing dendrimers against planktonic Gram-negative *P. aeruginosa* after 4 h exposure.

Dendrimer	Bactericidal NO Doses (nmol/mL)
G1-ED	3.55
G1-PE 37	3.72
G1-PE 55	7.70
G1-PE 73	17.6
G1-PO	182
G3-PE 73	13.4

While planktonic killing assays are important in evaluating potential antibacterial agents, most medically-relevant infections arise from biofilm-based bacteria.[50] Thus, *P. aeruginosa* biofilms were exposed to a range of NO-releasing dendrimer concentrations (10–800 μg/mL) for 24 h. Similar to the planktonic *P. aeruginosa* bactericidal assays, the amphiphilic control dendrimers (G1-PE 73, G1-PE 55, G1-PE 37, and G1-ED) proved more effective in eradicating the biofilm compared to the hydrophilic dendrimer (G1-PO). The MBCs for the NO-releasing dendrimers were 800, 80, 20, 10, and 15 μg/mL for the G1-PO-NO, G1-PE 73-NO, G1-PE 55-NO, G1-PE 37-NO, and G1-ED-NO dendrimers, respectively. Of the dendrimers evaluated, G1-PE 37-NO exhibited the greatest anti-biofilm efficacy (i.e., lowest MBC). To determine if the enhanced G1-PE-37-NO antibacterial activity was due to more thorough diffusion within the biofilm, the association of G1-PE 73-NO, G1-PE 37-NO, and G1-ED-NO dendrimers and *P. aeruginosa* biofilms was characterized using confocal microscopy. As shown in Figure 3.5, a greater number of bacteria in the biofilms exhibited red fluorescence upon incubation with RITC-labeled G1-PE 37-NO compared to the biofilm incubated with G1-PE 73-NO. Hydrophobic dendrimers generally exhibit improved bacteria association due to favorable electrostatic effects. However, the more hydrophobic G1-ED-NO dendrimer was not as effective in associating with the bacterial biofilm, likely due to less efficient penetration through the EPS.[51]

The G1-PE 37-NO dendrimer proved to be the most effective in eradicating the *P. aeruginosa* biofilm due to its improved association with bacterial cells and diffusion within the biofilm. Of note, dendrimer size did not appear to significantly impact

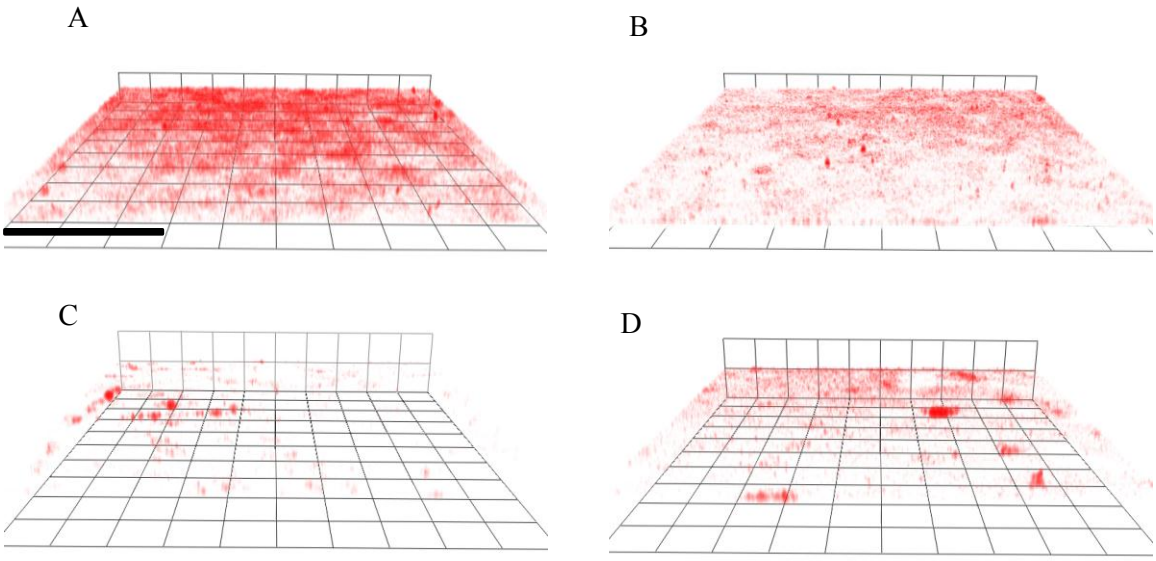

Figure 3.5 Confocal microscopy images of *P. aeruginosa* biofilms incubated with (A) G1-PE-37-NO, (B) G1-ED-NO, (C) G1-PE 73-NO, and (D) G3-PE 73-NO RITC-labeled dendrimers for 1 h (50 μg/mL). Increased red fluorescence indicates more efficient dendrimer–bacteria association and improved diffusion. Scale bar is 300 μm.

bacterial association with the *P*. *aeruginosa* biofilm. Although G3-PE 73-NO exhibited similar association with the biofilm compared to G1-PE 73-NO, greater intracellular NO levels (DAF-2 fluorescence) were observed for biofilms incubated with the larger G3 dendrimers, indicating enhanced NO delivery efficiency (Figure 3.6). The increased concentration of *N*-diazeniumdiolates at the G3 dendrimer surface may facilitate more localized NO delivery, thus improving bactericidal efficacy even if the dendrimer–bacteria association is similar to the smaller G1 systems.

3.3.2.3 In vitro cytotoxicity

Both control and NO-releasing dendrimers were evaluated for cytotoxicity toward L929 mouse fibroblasts at concentrations necessary for *P*. *aeruginosa* biofilm eradication. As expected, the more hydrophobic dendrimers (e.g., G1-ED-NO and G1-PE 37-NO) exhibited greater cytotoxicity (i.e., ~70% cell viability reduction) after 24 h. Dendrimers with intermediate ratios of PO/ED (e.g., G1-PE 55-NO and G1-PE 73-NO) were non-cytotoxic at the biofilm MBCs, supporting their potential future therapeutic use compared to other scaffolds.

3.3.2.4 Conclusions

The bactericidal efficacy of NO-releasing amphiphilic dendrimers was demonstrated to be a function of dendrimer exterior functionality (i.e., hydrophobicity) and dendrimer size (i.e., generation). The dendrimer hydrophobicity significantly influenced association and diffusion within the biofilm, as well as the efficiency of intracellular NO delivery. Dendrimers modified with approximately equal ratios of the

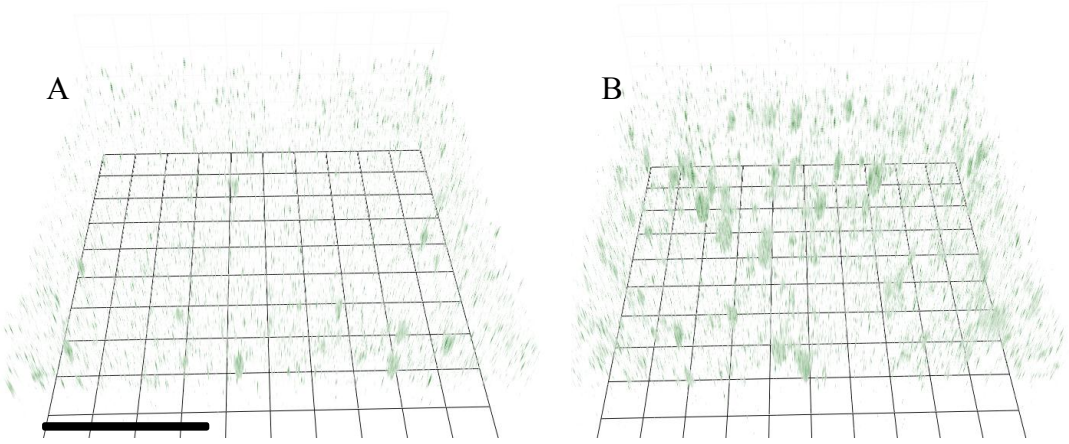

Figure 3.6 Confocal microscopy images of intracellular DAF-2 fluorescence in *P. aeruginosa* biofilms incubated with (A) G1- and (B) G3-PE 73-NO for 1 h (20 μg/mL) Green DAF-2 fluorescence indicates increased intracellular NO levels. Scale bar is 50 μm.

hydrophilic PO and hydrophobic ED groups were found to successfully eradicate the *P. aeruginosa* biofilms at concentrations that were also non-toxic to healthy host cells.

3.3.3 Nitric oxide-releasing chitosan oligosaccharides

Chitosan has been widely used in antibacterial and wound healing applications due to its non-toxic, biodegradable scaffold.[52-55] In Chapter 2, the synthesis of NO-releasing chitosan oligosaccharides for use as antibacterial agents was presented. The Chitosan 1/NO, Chitosan 2/NO, and Chitosan 3/NO scaffolds were evaluated for any molecular weight and exterior functionality dependence on killing of *P. aeruginosa* biofilms in addition to the previous results obtained for planktonic cells.

3.3.3.1 Bactericidal efficacy against planktonic bacteria as a function of exterior functionality and molecular weight

As discussed in Chapter 2, planktonic *P. aeruginosa* cells were exposed to a range of concentrations of NO-releasing chitosan oligosaccharides (e.g., Chitosan 1/NO -5k, Chitosan 2/NO-5k, Chitosan 3/NO -5k) to evaluate their ability to kill bacteria. The neutral PEG-modified chitosans were less effective in killing due to poor association with the bacteria. Molecular weight did not play a role in the bactericidal efficacy of Chitosan 2-2.5k, 5k, or 10k, however it was hypothesized that a greater dependence may be observed against biofilms.

3.3.3.2 Biofilm killing assays as a function of nitric oxide-releasing chitosan exterior functionality and molecular weight

Pseudomonas aeruginosa biofilms were exposed to a range of concentrations of NO-releasing chitosan oligosaccharides (0.2–1.3 mg/mL) for 24 h. After 24 h, the

biofilms were disrupted and cell/chitosan suspensions were diluted and plated to determine bacterial viability.[56565656] The biofilm MBC (5-log reduction) was 400, 700, and 1000 μg/mL for Chitosan 2/NO-5k, Chitosan 1/NO-5k, and Chitosan 3/NO-5k, respectively. Chitosan 2/NO-5k exhibited the greatest anti-biofilm efficacy, attributed to its increased NO storage and rapid association with the negatively-charged bacteria (Chapter 2, Figure 2.8). Chitosan 1/NO-5k and Chitosan 3/NO-5k stored similar amounts of NO (~0.3 μmol/mg); however, less Chitosan 1/NO-5k was necessary (700 μg/mL) to completely eradicate the biofilm compared to Chitosan 3/NO-5k (1000 μg/mL). Reduced efficacy of Chitosan 3/NO-5k was likely due to less association between the neutral PEG chains and the bacterial membrane. To confirm this hypothesis, the association of RITC-Chitosan 2/NO-5k and RITC-Chitosan 3/NO-5k with the *P. aeruginosa* biofilm was evaluated using confocal microscopy. As shown in Figure 3.8, biofilms incubated with RITC-Chitosan 2/NO-5k exhibited more intense red fluorescence compared to RITC-Chitosan 3/NO-5k, thus confirming the lessened association of the chitosan modified with the neutral PEG chain.

Although chitosan molecular weight did not play a significant role in planktonic killing of *P. aeruginosa*, reduced bactericidal efficacy was observed for Chitosan 2/NO-10k compared to Chitosan 2/NO-2.5k (600 μg/mL vs. 400 μg/mL for Chitosan 2/NO-10k and Chitosan 2/NO-2.5k, respectively) against biofilms. The exopolysaccharide (EPS) matrix of the bacterial biofilm likely slows the diffusion of the Chitosan 2/NO-10k into

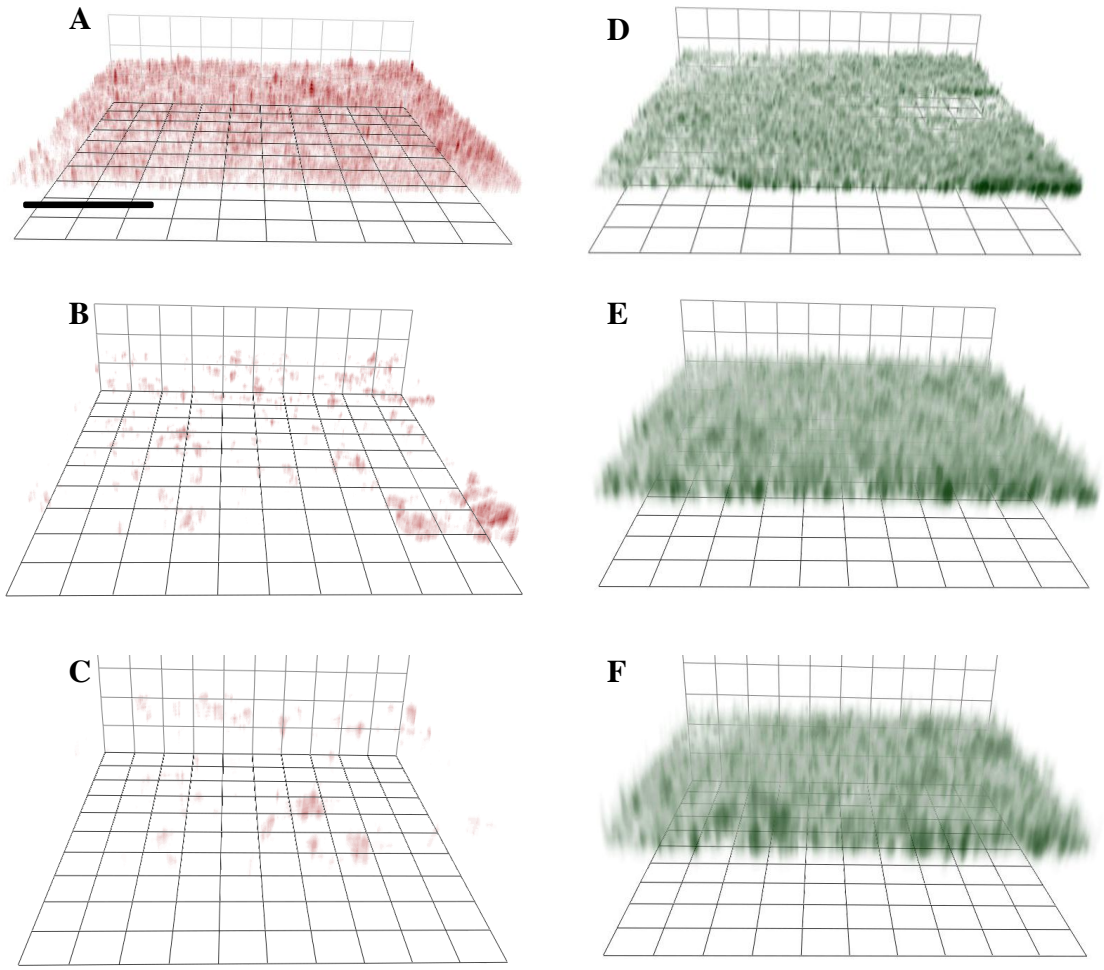

Figure 3.7 Confocal fluorescence images of RITC-labeled chitosan oligosaccharide association with *P. aeruginosa* biofilms: A) Chitosan 2/NO-5k, B) Chitosan 3/NO-5k, C) Chitosan 2-10k) and images of Syto 9 labeled biofilms incubated with D) Chitosan 2/NO-5k, E) Chitosan 3/NO-5k and F) Chitosan 2/NO-10k. Scale bar is 40 μm. The Syto 9 (green) fluorescence shows biofilm cells. Increased RITC (red) fluorescence indicates more efficient chitosan diffusion within the biofilm.

the biofilm, thus reducing antibacterial activity. Previous studies have observed less efficient EPS penetration of high-molecular weight dextran compared to the low-molecular weight polymer.[57] This hypothesis was further confirmed with confocal microscopy by comparing chitosan–bacteria association as a function of molecular weight. Indeed, when *P. aeruginosa* biofilms were exposed to both RITC-Chitosan 2/NO-2.5k and RITC-Chitosan 2/NO-10k, increased red fluorescence and diffusion within the biofilm was observed for the lower molecular weight scaffold (Figure 3.8).

3.3.3.3 In vitro cytotoxicity

Control and NO-releasing chitosan oligosaccharides were evaluated for cytotoxicity using L929 mouse fibroblasts and found to be non-toxic, even at the MBCs necessary for biofilm eradication. Similar to cytotoxicity results evaluated at the planktonic MBC concentrations, fibroblast proliferation was observed for some NO-releasing chitosans.[58] The potent antibacterial activity and minimal toxicity of the NO-releasing chitosan oligosaccharides warrants further examination into their use as antibacterial therapeutics.

3.3.3.4 Conclusions

The NO-releasing chitosan oligosaccharides presented herein allowed for diffusion into *P. aeruginosa* biofilms and association with bacteria cells, resulting in complete biofilm eradication at concentrations eliciting no significant toxicity against healthy host cells. This study demonstrated the great potential of NO-releasing chitosan oligosaccharides as future therapeutics.

REFERENCES

1. Bryers, J. D., Medical biofilms. *Biotechnol*. *Bioeng*. **2008**, *100*, 1-18.

2. Smith, A. W., Biofilms and antibiotic therapy: is there a role for combating bacterial resistance by the use of novel drug delivery systems? *Adv*. *Drug Delivery Rev*. **2005**, *57*, 1539-1550.

3. Lindsay, D.; von Holy, A., Bacterial biofilms within the clinical setting: what healthcare professionals should know. *J*. *Hospital Infection* **2006**, *64*, 313-325.

4. Costerton, J. W.; Stewart, P. S.; Greenberg, E. P., Bacterial biofilms: A common cause of persistent infections. *Science* **1999**, *284*, 1318-1322.

5. Anderl, J. N.; Franklin, M. J.; Stewart, P. S., Role of antibiotic penetration limitation in *Klebsiella pneumoniae* biofilm resistance to ampicillin and ciprofloxacin. *J*. *Antimicrob*. *Chemother*. **2000**, *44*, 1818-1824.

6. Nickel, J. C.; Ruseska, I.; Wright, J. B.; Costerton, J. W., Tobramycin resistance of *Pseudomonas aeruginosa* cells growing as a biofilm on urinary catheter material. *J*. *Antimicrob*. *Chemother*. **1985**, *27*, 619-624.

7. Cerca, N.; Martins, S.; Cerca, F.; Jefferson, K. K.; Pier, G. B.; Oliveira, R.; Azeredo, J., Comparative assessment of antibiotic susceptibility of coagulase-negative staphylococci in biofilm versus planktonic culture as assessed by bacterial enumeration or rapid XTT colorimetry. *J*. *Antimicrob*. *Chemother*. **2005**, *56*, 331-336.

8. James, G. A.; Swogger, E.; Wolcott, R.; Pulcini, E. d.; Secor, P.; Sestrich, J.; Costerton, J. W.; Stewart, P. S., Biofilms in chronic wounds. *Wound Rep*. *Regen*. **2008**, *16*, 37-44.

9. Singh, P. K.; Schaefer, A. L.; Parsek, M. R.; Moninger, T. O.; Welsh, M. J.; Greenberg, E. P., Quorum-sensing signals indicate that cystic fibrosis lungs are infected with bacterial biofilms. *Nature* **2000**, *407*, 762-764.

10. Fadeeva, E.; Truong, V. K.; Stiesch, M.; Chichkov, B. N.; Crawford, R. J.; Wang, J.; Ivanova, E. P., Bacterial retention on superhydrophobic titanium surfaces fabricated by femtosecond laser ablation. *Langmuir* **2011**, *27*, 3012-3019.

11. Appelgren, P.; Ransjo, U.; Bindslev, L.; Larm, O., Does surface heparinisation reduce bacterial colonisation of central venous catheters? *The Lancet* **1995**, *345*, 130.

12. Chilukuri, D. M.; Shah, J. C., Local delivery of vancomycin for the prophylaxis of prosthetic device-related infections. *Pharm*. *Res*. **2005**, *22*, 563-572.

13. Morris, N. S.; Stickler, D. J., Encrustation of indwelling urethral catheters by *Proteus mirabilis* biofilms growing in human urine. *J*. *Hosp*. *Infect*. **1998**, *39*, 227-234.

14. Hetrick, E. M.; Schoenfisch, M. H., Reducing implant related infections:active release strategies. *Chem*. *Soc*. *Rev*. **2006**, *35*, 780-789.

15. Ignarro, L. J., *Nitric Oxide: Biology and Pathobiology*. Academic Press: San Diego, CA, 2000.

16. Fang, F. C., Mechanisms of nitric oxide-related antimicrobial activity. *J*. *Clin*. *Invest*. **1997**, *99*, 2818-2825.

17. Carpenter, A. W.; Schoenfisch, M. H., Nitric oxide release: Part II. Therapeutic applications. *Chem*. *Soc*. *Rev*. **2012**, *41*, 3742-3752.

18. Barraud, N.; Hassett, D. J.; Hwang, S.-H.; Rice, S. A.; Kjelleberg, S.; Webb, J. S., Involvement of nitric oxide in biofilm dispersal of *Pseudomonas aeruginosa*. *J*. *Bacteriol*. **2006**, *188*, 7344-7353.

19. Sulemankhil, I.; Ganopolsky, J. G.; Dieni, C. A.; Dan, A. F.; Jones, M. L.; Prakash, S., Prevention and treatment of virulent bacterial biofilms with an enzymatic nitric oxide-releasing dressing. *Antimicrob*. *Agents Chemother*. **2012**, *56*, 6095-6103

.

20. Hetrick, E. M. S., J.-H.; Paul, H.S.; Schoenfisch, M.H., Anti-biofilm efficacy of nitric oxide-releasing silica nanoparticles. *Biomaterials* **2009**, *30*, 2782-2789.

21. Riccio, D. A.; Schoenfisch, M. H., Nitric oxide release: Part I. Macromolecular scaffolds. *Chem*. *Soc*. *Rev*. **2012**, *41*, 3731-3741.

22. Hetrick, E. M.; Shin, J.-H.; Stasko, N. A.; Johnson, C. B.; Wespe, D. A.; Holmuhamedov, E.; Schoenfisch, M. H., Bactericidal efficacy of nitric oxide-releasing silica nanoparticles. *ACS Nano* **2008**, *2*, 235-246.

23. Carpenter, A. W. S., D.L.; Rao, K.S.; Schoenfisch, M.H., Influence of scaffold size on bactericidal activity of nitric oxide-releasing silica nanoparticles. *ACS Nano* **2011**, *5*, 7235-7244.

24. Lu, Y.; Slomberg, D. L.; Sun, B.; Schoenfisch, M. H., Shape- and nitric oxide flux-dependent bactericidal activity of nitric oxide-releasing silica nanorods. *Small* **2013**, *9*, 2189-2198.

25. Sun, B.; Slomberg, D. L.; Chudasama, S. L.; Lu, Y.; Schoenfisch, M. H., Nitric oxide-releasing dendrimers as antibacterial agents. *Biomacromolecules* **2012**, *13*, 3343-3354.

26. Zhang, H.; Annich, G. M.; Miskulin, J.; Stankiewicz, K.; Osterholzer, K.; Merz, S. I.; Bartlett, R. H.; Meyerhoff, M. E., Nitric oxide-releasing fumed silica particles: Synthesis, characterization, and biomedical Application. *J*. *Am*. *Chem*. *Soc*. **2003**, *125*, 5015-5024.

27. Privett, B. J.; Deupree, S. M.; Backlund, C. J.; Rao, K. S.; Johnson, C. B.; Coneski, P. N.; Schoenfisch, M. H., Synergy of nitric oxide and silver sulfadiazine against gram-negative, gram-positive, and antibiotic-resistant pathogens. *Mol*. *Pharm*. **2010**, *7*, 2289-2296.

28. Wong, K.; Sun, G. B.; Zhang, X. Q.; Dai, H.; Liu, Y.; He, C. B.; Leong, K. W., PEI-g-chitosan, a novel gene delivery system with transfection efficiency comparable to polyethylenimine in vitro and after liver administration in vivo. *Bioconj*. *Chem*. **2006**, *17*, 152-158.

29. Tokura, S.; Ueno, K.; Miyazaki, S.; Nishi, N., Molecular weight dependent antimicrobial activity by chitosan. *Macromol*. *Symposia* **1997**, *120*, 1-9.

30. Coneski, P. N.; Schoenfisch, M. H., Nitric oxide release: Part III. Measurement and reporting. *Chem*. *Soc*. *Rev*. **2012**, *41*, 3753-3758.

31. Hunter, R. A.; Storm, W. L.; Coneski, P. N.; Schoenfisch, M. H., Inaccuracies of nitric oxide measurement methods in biological media. *Anal*. *Chem*. **2013**, *85*, 1957-1963.

32. Goeres, D. M. L., L.R.; Hamilton, M.A.; Murga, R.; Kirby, D.W.; Donlan, R., A statistical assessment of a laboratory method for growing biofilms. *Microbiology* **2005**, *151*, 757-762.

33. Lu, Z.; Rong, K.; Li, J.; Yang, H.; Chen, R., Size-dependent antibacterial activities of silver nanoparticles against oral anaerobic pathogenic bacteria. *J*. *Mater*. *Sci*.*: Mater*. *Med*. **2013**, *24*, 1465-1471.

34. Pal, S.; Tak, Y.-K.; Song, J.-M., Does the antibacterial activity of silver nanoparticles depend on the shape of the nanoparticle? A study of the Gram-

negative bacterium Eschericia coli. *Appl*. *Environ*. *Microbiol*. **2007**, *73*, 1712-1720.

35. Aminedi, R.; Wadwha, G.; Das, N.; Pal, B., Shape-dependent bactericidal activity of TiO_2 for the killing of Gram-negative bacteria *Agrobacterium tumefaciens* under UV torch irradiation. *Environ*. *Sci*. *Pollut*. *Res*. **2013**, *20*, 6521-6530.

36. Stober, W.; Fink, A., Controlled growth of monodisperse spheres in the micron size range. *J*. *Colloid Interface Sci*. **1968**, *26*, 62-69.

37. Bogush, G. H.; Tracy, M. A.; Zukoski IV, C. F., Preparation of monodisperse silica particles:Control of size and mass fraction. *J*. *Non-Cryst*. *Solids* **1988**, *104*, 95-106.

38. Silhavy, T. J.; Kahne, D.; Walker, S., The bacterial cell envelope. *Cold Spring Harb*. *Perspect*. *Biol*. **2010**, 1-16.

39. Mandell, G., Catalase, superoxide dismutase, and virulence of *Staphylococcus aureus*. In vitro and in vivo studies with emphasis on staphylococcal--leukocyte interaction. *J*. *Clin*. *Invest*. **1975**, *55*, 561-566.

40. Gusarov, I.; Nudler, E., NO-mediated cytoprotection: Instant adaptation to oxidative stress in bacteria. *Proc*. *Natl*. *Acad*. *Sci*. *U.S.A*. **2005**, *102*, 13855-13860.

41. Boyd, A.; Chakrabarty, A. M., Role of alginate lyase in cell detachment of *Pseudomonas aeruginosa*. *Appl*. *Environ*. *Microbiol*. **1994**, *60*, 2355-2359.

42. Boles, B. R.; Horswill, A. R., Agr-mediated dispersal of *Staphylococcus aureus* biofilms. *PLoS Pathog*. **2008**, *4*.

43. Boulos, L.; Prevost, M.; Barbeau, B.; Coallier, J.; Desjardins, R., LIVE/DEAD BacLight: application of a new rapid staining method for direct enumeration of viable and total bacteria in drinking water. *Journal of Microbiol*. *Methods* **1999**, *37*, 77-86.

44. Lu, Y.; Sun, B.; Li, C.; Schoenfisch, M. H., Structurally diverse nitric oxide-releasing poly(propylene imine) dendrimers. *Chem*. *Mater*. **2011**, *23*, 4227-4233.

45. Boulos, L.; Prevost, M.; Barbeau, B.; Coallier, J.; Desjardins, R., LIVE/DEAD BacLight application of a new rapid staining method for direct enumeration of viable and total bacteria in drinking water. *Journal of Microbiological Methods* **1999**, *37*, 77-86.

46. Peulen, T.-O.; Wilkinson, K. J., Diffusion of nanoparticles in a biofilm. *Environ*. *Sci*. *Technol*. **2011**, *45*, 3367-3373.

47. Alberts, B.; Johnson, A.; Lewis, J., *Molecular Biology of the Cell*. 4th ed.; Garland Science: New York, 2002.

48. Privett, B. J.; Broadnax, A. D.; Bauman, S. J.; Riccio, D. A.; Schoenfisch, M. H., Examination of bacterial resistance to nitric oxide. *Nitric Oxide* **2012**, *26*, 169-173.

49. Sun, B.; Slomberg, D. L.; Chudasama, S. L.; Lu, Y.; Schoenfisch, M. H., Nitric oxide-releasing dendrimers as antibacterial agents. *Biomacromolecules* **2012**, *13*, 3343-54.

50. Costerton, J. W.; Stewart, P. S.; Greenberg, E. P., Bacterial biofilms: A common cause of persistent infections. *Science* **1999**, *284*, 1318-1322.

51. Wicke, D.; Bockelmann, U.; Reemtsma, T., Environmental influences on the partitioning and diffusion of hydrophobic organic contaminants in microbial Biofilms. *Environ*. *Sci*. *Technol*. **2008**, *42*, 1990-1996.

52. Tokoro, A.; Tatewaki, N.; Suzuki, K.; Mikami, T.; Suzuki, S.; Suzuki, M., Growth-Inhibitory Effect of hexa-*N*-acetylchitohexaose and chitohexaose against meth-a solid tumor. *Chemical & Pharmaceutical Bulletin* **1988**, *36*, 784-790.

53. Pae, H. O.; Seo, W. G.; Kim, N. Y.; Oh, G. S.; Kim, G. E.; Kim, Y. H.; Kwak, H. J.; Yun, Y. G.; Jun, C. D.; Chung, H. T., Induction of granulocytic differentiation in acute promyelocytic leukemia cells (HL-60) by water-soluble chitosan oligomer. *Leukemia Res*. **2001**, *25*, 339-346.

54. Porporatto, C.; Bianco, I. D.; Riera, C. M.; Correa, S. G., Chitosan induces different L-arginine metabolic pathways in resting and inflammatory macrophages. *Biochemical and Biophysical Research Communications* **2003**, *304*, 266-272.

55. Hirano, S., Chitin biotechnology applications. *Biotechnol Annu Rev* **1996**, *2*, 237-258.

56. Barraud, N.; Hassett, D. J.; Hwang, S. H.; Rice, S. A.; Kjelleberg, S.; Webb, J. S., Involvement of nitric oxide in biofilm dispersal of Pseudomonas aeruginosa. *J*. *Bacteriol*. **2006**, *188*, 7344-7353.

57. Takenaka, S.; Pitts, B.; Trivedi, H. M.; Stewart, P. S., Diffusion of macromolecules in model oral biofilms. *Appl*. *Environ*. *Microbiol*. **2009**, *75*, 1750-1753.

58. Cooke, J. P.; Losordo, D. W., Nitric oxide and angiogenesis. *Circulation* **2002**, *105*, 2133-2135.

CHAPTER 4: ROLE OF DENDRIMER NITRIC OXIDE-RELEASE KINETICS IN ERADICATION OF PLANKTONIC BACTERIA AND BIOFILMS

4.1 Introduction

The ubiquitous presence of bacteria in clinical settings has necessitated the development of antibacterial agents to combat infections associated with open wounds and implanted medical devices,[1-3] as well as infections resulting from persistent conditions such as diabetes mellitus[4] and cystic fibrosis.[1, 5-7] Although many antibacterial agents have proven effective against planktonic (i.e., free-floating) bacteria, medically-relevant infections generally arise from the formation of complex bacterial biofilm communities.[6] Several factors contribute to the observed antibacterial resistance of biofilms compared to planktonic suspensions, including slow antibacterial penetration through the layers of self-secreted extracellular polymeric substances (EPS), differentiation of biofilm cells into a resistant phenotype, and reduced antibacterial action in altered microenvironments (e.g., regions of nutrient depletion).[7-12] Strategies for preventing bacterial biofilm formation and eradicating established biofilms while minimizing the development of resistance are thus warranted.

While antibiotics (e.g., vancomycin and ciprofloxacin),[13] antimicrobial peptides,[14] silver ions,[15, 16] and dendrimers[17] have proven effective against biofilms, recent research has focused on the importance of tailoring antibacterial

pharmacodynamics for maximum eradication and prevention of bacteria re-growth.[18-23] As such, several labs have evaluated bacterial biofilm formation and eradication as a function of antibacterial-release kinetics.[23-28] For example, Cheow et al. studied the influence of levofloxacin-release rate from nanoparticles against *E. coli* biofilms.[19] The antibiotic-release profile was deemed to be equally as important as total dosage in biofilm eradication, suggesting that a biphasic release profile is optimal for maximum killing and prevention of biofilm re-growth while minimizing the potential for antibiotic tolerance. Similarly, antimicrobial peptide (i.e., ponericin G1) release from polyelectrolyte multilayer films with both burst- and linear-release profiles was investigated against *S. aureus* biofilms.[27] Biphasic release was again preferential where a large initial bolus rapidly eradicated cells, and subsequent smaller doses eliminated any residual bacteria. Despite the demonstrated killing potential of these antibacterials, continued concerns over resistance preclude their long-term therapeutic utility.[29] Bacteria have developed resistance to antibiotics and antimicrobial peptides through a myriad of mutations[29] and modification of cell surface charge.[30, 31] Therefore, even if antibacterial pharmacodynamics can be controlled, complete eradication of planktonic bacteria and biofilms is complex and new antibacterials that do not foster resistance are urgently needed.[1, 32, 33]

Nitric oxide (NO), an endogenously-produced radical, is a broad-spectrum antibacterial generated by the immune system to exert bacterial membrane damage through both oxidative and nitrosative stresses.[34-36] Bacterial resistance to NO is unlikely given its dual-mechanistic action and small structure. Privett et al. observed no increase

in resistance to exogenous NO treatment for *S*. *aureus*, methicillin-resistant *S*. *aureus*, *S*. *epidermidis*, *E*. *coli*, or *P*. *aeruginosa* cells after exposure to sub-inhibitory concentrations through 20 d.[37] As noted in Chapter 3, the effects of NO release on bacterial biofilms are concentration dependent, with low NO concentrations (~nM) resulting in biofilm dispersal and higher concentrations (~μM) killing the embedded bacteria.[38-40] Due to the reactive nature of NO, macromolecular NO donors including silica, metallic nanoparticles, and dendrimers have been designed to enhance localized delivery to the site of infection.[41] For example, *N*-diazeniumdiolate-modified silica nanoparticles and dendrimers that store large NO payloads have demonstrated efficacy against both planktonic bacteria and biofilms.[40, 42, 43] Selective tuning of NO-release kinetics for bacterial eradication has not yet been investigated, although initial work indicates the importance of NO-release profiles in bactericidal efficacy.[40] Hetrick et al. observed increased efficacy of NO-releasing *N*-methylaminopropyltrimethoxysilane (MAP3) silica particles (~6 min half-life) against *P*. *aeruginosa* biofilms compared to *N*-(6-aminohexyl)aminopropyltrimethoxysilane (AHAP3) particles (~18 min half-life). The increased anti-biofilm efficacy for the more rapid NO-releasing MAP3 particles may suggest that large initial bursts of NO are preferred; however, the MAP3 and AHAP3 systems exhibited varied total NO storage (~7.6 and 3.8 μmol/mg, respectively), and thus bacterial killing as a function of NO-release kinetics cannot be directly determined using these systems.

Ideal systems for determining the effects of NO-release kinetics on bactericidal efficacy would exhibit a range of half-lives while maintaining similar total NO storage.

As such, four NO-releasing poly(amidoamine) (PAMAM) dendrimer scaffolds with varied half-lives (~0.9–3.5 h) and similar 24 h NO storage (~1.8 μmol/mg) were utilized to evaluate the role of NO-release kinetics on bacterial killing. The goal was to evaluate the optimal NO-release profile (i.e., burst or sustained release) for eradication of planktonic and biofilm-based Gram-negative *Pseudomonas aeruginosa* and Gram-positive *Staphylococcus aureus* bacteria.

4.2 Materials and Methods

Note: Dendrimer synthesis, characterization, and cytotoxicity evaluation were supported by other members of the Schoenfisch lab

Sodium methoxide (5.4 M in methanol), rhodamine B isothiocyanate (RITC), propidium iodide (PI), fetal bovine serum (FBS), Dulbecco's Modified Eagle's Medium (DMEM), phenazine methosulfate (PMS), 3-(4,5-dimethylthiazol-2-yl)-5-(3-carboxymethoxyphenyl)-2-(4-sulfophenyl)-2H-tetrazolium inner salt (MTS), trypsin, phosphate buffered saline (PBS) used for cell culture, and Pen Strep solution (10,000 u/mL penicillin, 10,000 μg/mL streptomycin) were purchased from the Sigma Aldrich Corp. (St. Louis, MO). Propylene oxide (PO) and acrylonitrile (ACN) were obtained from Acros Organics (Geel, Belgium). Spectra/Por Float-A-Lyzers for dialysis of the dendrimers were purchased from Spectrum Laboratories, Inc. (Rancho Dominguez, CA). Tryptic soy broth (TSB) and tryptic soy agar (TSA) were obtained from Becton, Dickinson, and Company (Franklin Lakes, NJ). *Pseudomonas aeruginosa* (ATCC #19143) and *Staphylococcus aureus* (ATCC# 29231) were obtained from the American

Type Culture Collection (Manassas, VA). The Centers for Disease Control and Prevention (CDC) bioreactor was purchased from BioSurface Technologies Corporation (Bozeman, Montana). Medical grade silicone rubber (1.45 mm thick) was purchased from McMaster-Carr (Atlanta, GA) and doubled in thickness using Superflex Clear RTV silicone adhesive sealant (Loctite, Westlake, OH) to fabricate coupons to fit the CDC reactor (thickness ~4 mm and diameter ~12.7 mm). L929 mouse fibroblasts (ATCC #CCL-1) were purchased from the University of North Carolina Tissue Culture Facility (Chapel Hill, NC). Syto 9 green fluorescent nucleic acid stain was purchased from Life Technologies (Grand Island, NY). 4,5-Diaminofluorescein diacetate (DAF-2 DA) was purchased from Calbiochem (San Diego, CA). Nitric oxide (NO) was purchased from Praxair (Bethlehem, PA). Argon (Ar) gas was obtained from Airgas National Welders (Raleigh, NC). A Millipore Milli-Q UV Gradient A10 System (Bedford, MA) was used to purify distilled water to a final resistivity of 18.2 MΩ·cm and a total organic content of ≤6 parts per billion (ppb). Other solvents and chemicals were analytical-reagent grade and used as received.

4.2.1 Synthesis of secondary amine-functionalized PAMAM dendrimers

Secondary amine-functionalized PAMAM dendrimers (generation 3 or G3) were synthesized as described previously.[44] Briefly, primary amine-functionalized G3-PAMAM dendrimers (100 mg) were dissolved in methanol (1 mL). One molar equivalent of PO, ACN, or a mixture of PO and ACN relative to the primary amines was then added to the G3-PAMAM-NH_2 solution under constant stirring at room temperature for 3 d to

yield the secondary amine-functionalized G3-PAMAM conjugates. Solvent and unreacted PO or ACN were removed under reduced pressure. The resulting secondary amine-functionalized dendrimers were characterized by nuclear magnetic resonance (NMR) spectroscopy in deuterated methanol (data not shown).

4.2.2 N-diazeniumdiolation of secondary-amine functionalized PAMAM dendrimers

N-diazeniumdiolate-functionalized PAMAM dendrimers were synthesized by adding one equivalent of 5.4 M sodium methoxide solution in methanol (with respect to the molar amount of primary amine functionality in PAMAM-NH_2 used to synthesize dendrimers) to a vial containing dendrimers (100 mg) in methanol (1 mL). The glass vials were then inserted into a stainless steel reactor, and the headspace of the reactor was subsequently flushed with Ar three times followed by three longer purges with Ar (3 x 10 min) to remove oxygen from the stirred solution. The reactor was filled with purified gaseous NO to 10 atm for 3 d. Unreacted NO was then removed using the same Ar flushing procedure described above prior to removing the vials from the vessel. The resulting *N*-diazeniumdiolate-modified PAMAM dendrimers were stored at -20 °C until use.

4.2.3 NO-release measurements

Real-time NO-release from the dendrimers was measured using a Sievers 280i Chemiluminesence Nitric Oxide Analyzer (NOA; Boulder, CO). The NO-releasing dendrimers (1 mg) were added to a sample vessel containing 30 mL deoxygenated PBS (pH 7.4, 37 °C). Liberated NO was carried from the sample vessel to the NOA at a flow

rate of 70 mL/min. Additional nitrogen flow was supplied to the sample vessel to match the collection rate of the NOA (200 mL/min). Nitric oxide-release measurements were terminated when the levels fell below 10 ppb NO/mg dendrimer. The real-time NO-release measurements were used to determine the total NO-release duration (t[NO]), total NO-release after 24 h ($t[NO]_{24h}$, maximum NO flux ($[NO]_{max}$), and half-life ($t_{1/2}$).

4.2.4 Planktonic bactericidal assays

Pseudomonas aeruginosa and *Staphylococcus aureus* bacterial cultures were grown from frozen stock (-80 °C) in TSB overnight at 37 °C. An aliquot of the suspension (0.5 mL) was added to fresh TSB (50 mL) and incubated at 37 °C until the bacteria reached mid-exponential phase (~1×10^8 colony forming units (cfu)/mL) as determined by the optical density at 600 nm (OD_{600}). The relationship between the concentration of the bacteria in suspension and the OD_{600} was calibrated for each strain using an Eppendorf BioPhotometer Plus Spectrophotometer (Hamburg, Germany). Colony forming units were enumerated from culture dilutions grown on TSA plates. The bacterial suspension was then centrifuged (3645 *g* for 10 min, 25 °C), resuspended in PBS, and diluted to ~1×10^6 cfu/mL in PBS supplemented with 1% (w/w) glucose and 0.5% (v/v) TSB for planktonic bactericidal assays.

The minimum bactericidal concentration (MBC) of the NO-releasing PAMAM dendrimers for planktonic *P. aeruginosa* and *S. aureus* was defined as the concentration that resulted in a 3-log reduction in viability versus untreated cells after 24 h. The bacterial suspensions (10^6 cfu/mL) were incubated with the NO-releasing dendrimers for

24 h over a range of dendrimer concentrations that were tested in triplicate. After exposure, the samples were diluted, plated on TSA, with counting of resulting colonies to determine viability.

4.2.5 Biofilm bacterial assays

A CDC bioreactor was used to grow *P. aeruginosa* and *S. aureus* biofilms over 48 h. Growth conditions (e.g., nutrient concentrations, additives, flow rate) were optimized for both the *P. aeruginosa* and *S. aureus* biofilms. Briefly, medical grade silicone rubber substrates were mounted in the coupon holders within the CDC reactor. After autoclaving, the reactor effluent line was clamped and 500 mL sterile 1% (w/v) TSB (*P. aeruginosa* growth) or 10% (w/v) TSB and 0.1% (w/v) glucose (*S. aureus* growth) was added aseptically. Similar to planktonic experiments, *P. aeruginosa* and *S. aureus* bacterial cultures were grown from frozen stock (-80 °C) overnight in TSB at 37 °C, reinoculated, and grown to mid-exponential phase. The reactor was then inoculated with an aliquot (1 mL) of the resulting 1×10^8 cfu/mL bacterial suspension (final concentration $\sim 2 \times 10^5$ cfu/mL). The completed assembly was incubated at 37 °C for 24 h with stirring (150 rpm). Following this "batch phase" growth, the effluent line was opened and the reactor media was refreshed continuously with 0.33% (v/v) TSB at 6 mL/min (*P. aeruginosa* growth) or 1% (v/v) TSB at 2.7 mL/min (*S. aureus* growth) for another 24 h to complete growth of the biofilms.

The MBC for biofilm eradication was determined as the concentration of NO-releasing PAMAM dendrimers that resulted in bacterial viability below the limit of

detection for the plate counting method (2.5 x 10^3 cfu/mL).[45] Each strain of bacteria was tested in triplicate over an optimized concentration range. *P. aeruginosa* and *S. aureus* biofilms grown on silicone rubber substrates were exposed to different concentrations of NO-releasing dendrimers in 3 mL PBS supplemented with 1% (w/w) glucose and 0.5% (v/v) TSB at 37 °C with slight agitation for 24 h. After 24 h of incubation, the samples were sonicated and vortexed to disrupt the biofilm. Aliquots of the cell/nanoparticle suspensions were diluted in PBS, plated on TSA, and incubated at 37 °C overnight. Bacterial viability was then determined by counting the observed colonies.

4.2.6 Confocal microscopy

Fluorescently-labeled control (i.e., non-NO-releasing) PAMAM dendrimers were prepared following a previously reported procedure.[43] Briefly, G3-PAMAM-NH_2 (100 mg) and rhodamine B isothiocyanate (RITC) (3 mg) were dissolved in methanol (2 mL). The solution was stirred for 3 d in the dark and the resulting product solution was dialyzed against 0.1 M NaCl (2 L) for 24 h, and ultrapure Milli-Q water for 3 d (3 × 2 L). Subsequent lyophilization yielded RITC-labeled G3-PAMAM-NH_2. The fluorescently-labeled G3-PAMAM-NH_2 dendrimers were then modified with one molar equivalent of PO, ACN, or a PO/ACN mixture to yield the RITC-labeled secondary-amine-functionalized dendrimers for dendrimer–bacteria association studies.

P. aeruginosa biofilms were grown on glass substrates (Biosurface Technologies) and subsequently exposed to NO-releasing dendrimers (200 μg/mL) in PBS supplemented with DAF-2 DA (10 μM) and PI (30 μM) for 1 and 4 h or RITC-labeled

control dendrimers (200 μg/mL) in PBS for 1 h followed by staining with PBS supplemented with Syto 9 (10 μM) for 20 min. Before imaging, the substrates were dipped in PBS to remove excess dye and loosely adhered cells. A Zeiss 510 Meta inverted laser scanning confocal microscope (Carl Zeiss, Thornwood, NY) with a 488 nm Ar excitation laser (2.0% intensity) and a BP 505–530 nm filter was used to obtain DAF-2 and Syto 9 (green) fluorescence images. A 543 nm HeNe excitation laser (25.3% intensity) with a BP 560–615 nm filter was used to obtain PI and RITC (red) fluorescence images. The images were collected using a Zeiss C-apochromat lens (10x, 1.2 numerical aperture).

4.2.7 In vitro cytotoxicity

L929 mouse fibroblasts were cultured in DMEM supplemented with 10% (v/v) FBS and 1 wt% Pen Strep solution, and incubated in 5% (v/v) CO_2 under humidified conditions at 37 ^{o}C. After reaching 80% confluency, the cells were trypsinized, seeded onto tissue culture-treated polystyrene 96-well plates at a density of 3×10^4 cells/mL and further incubated at 37 ^{o}C for 48 h. The supernatant was subsequently aspirated prior to adding fresh DMEM (200 μL) with control (i.e., non-NO-releasing) or NO-releasing dendrimers to each well. After incubation at 37 ^{o}C for 24 h, the supernatant was aspirated and the cells rinsed 3x with PBS. A mixture of DMEM/MTS/PMS (105/20/1, v/v/v) (120 μL) was then added to each well. The absorbance of the resulting colored solution after 1.5 h incubation at 37 ^{o}C was quantified at 490 nm using a Thermo Scientific Multiskan EX plate reader (Thermo Fisher Scientific, Inc., Waltham, MA). The mixture of

DMEM/MTS/PMS and untreated cells were used as the blank and control, respectively. Cell viability was calculated by taking the ratio of the absorbance of treated to untreated cells after subtracting the absorbance of the blank from each.

4.3 Results and Discussion

Although many reports on the bactericidal action of NO have appeared in the literature,[42, 46] the effects of NO-release kinetics on planktonic bacteria and biofilm eradication, and how these release profiles impact healthy cells have not yet been investigated. Thus, the goal of this study was to evaluate NO-induced killing of planktonic and biofilm-based *P. aeruginosa* and *S. aureus* bacteria as a function of NO-release kinetics (i.e., burst versus sustained release). Poly(amidoamine) dendrimers were functionalized with PO, ACN, or a PO/ACN mixture (i.e., 1:1 or 1:7 PO/ACN) to vary the maximum NO flux and half-life while maintaining the same total NO storage over 24 h. As shown in Table 4.1, the dendrimers exhibited a range of NO-release kinetics with half –lives ranging from 0.9 to 3.5 h. Importantly, the four scaffolds had similar total NO storage over 24 h (1.89 ± 0.11, 1.70 ± 0.16, 1.56 ± 0.08, and 1.89 ± 0.10 μmol/mg for the PO, 1:1, 1:7, and ACN NO-releasing dendrimers, respectively). The PO-modified dendrimer exhibited an initial burst of NO release ($[NO]_{max}$ = 6500 ± 675 ppb/mg), while a lower maximum flux and more sustained release was observed for the ACN-modified dendrimer ($(NO]_{max}$ = 3815 ± 875 ppb/mg). Hydrophobic ACN functional groups likely slow the proton-initiated *N*-diazeniumdiolate decomposition compared to hydrophilic PO functional groups, thus delaying NO release. As expected, the NO-release profiles for the

1:1 and 1:7 PO/ACN-modified dendrimers exhibited a combination of the PO and ACN release profiles ($[NO]_{max}$ = 5150 ± 890 and 4800 ± 1065 ppb/mg, respectively).

Table 4.1 Nitric oxide release properties of *N*-diazeniumdiolate-modified PAMAM dendrimers as measured by NOA. All values are n≥3 measurements.

Dendrimer	Feed Ratio	t[NO] (μmol/mg)	$t[NO]_{24h}$ (μmol/mg)	$[NO]_{max}$ (ppb/mg)	$t_{1/2}$ (h)
PO	–	1.89 ± 0.11	1.89 ± 0.11	6500 ± 675	0.9 ± 0.3
PO/ACN 1:1	70:30	1.90 ± 0.20	1.70 ± 0.16	5150 ± 890	1.8 ± 0.4
PO/ACN 1:7	30:70	1.75 ± 0.12	1.56 ± 0.08	4800 ± 1065	2.4 ± 0.3
ACN	–	2.06 ± 0.19	1.89 ± 0.10	3815 ± 875	3.5 ± 0.4

4.3.1 Bactericidal efficacy against planktonic bacteria

Prior to evaluating the effects of NO-release kinetics on clinically-relevant bacterial biofilms, we sought to determine any relation between NO-release profile and eradication of planktonic bacteria. Indeed, the bactericidal efficacy of the NO-releasing dendrimers against *P*. *aeruginosa* was dependent on the NO-release kinetics, with the PO-modified dendrimers proving the most effective (MBC_{24h} = 0.05 mg/mL), followed by the 1:1 PO/ACN, 1:7 PO/ACN, and ACN-modified dendrimers with 24 h MBCs of 0.10, 0.20, and 0.20 mg/mL, respectively (Table 4.2). The killing of planktonic *S*. *aureus* followed a similar trend (MBC values of 0.20, 0.60, 0.60, and 0.60 mg/mL for the PO, 1:1 PO/ACN, 1:7 PO/ACN, and ACN-modified dendrimers, respectively), although increased doses of NO (~3–4x) were required to exhibit 3-log viability reductions. The increased NO dose required for Gram-positive *S*. *aureus* killing compared to Gram-negative *P*. *aeruginosa* has been observed previously.[43, 47] Such disparity is likely the result of multiple factors including differential peptidoglycan thicknesses,[48] varied production of antioxidant enzymes (e.g., superoxide dismutase) to mitigate the effects of NO,[49] and *S*. *aureus*' use of NO as a cytoprotection agent.[50]

The NO-release profiles of the dendrimer scaffolds influenced planktonic bacterial killing, with the PO-modified dendrimer (i.e., burst release) being the most effective (~0.09 μmol NO/mL) and the ACN-modified dendrimer (i.e., lower, sustained release) being the least effective (~0.38 μmol NO/mL). The large initial burst of NO from the PO-modified dendrimers is sufficient to quickly kill the planktonic bacteria, releasing

Table 4.2 Determination of planktonic and biofilm MBCs and bactericidal NO doses for NO-releasing PAMAM dendrimers against *P. aeruginosa* and *S. aureus* bacteria.

	P. aeruginosa				*S. aureus*			
Dendrimer	Planktonic MBC_{24h} (mg/mL)[a]	Biofilm MBC_{24h} (mg/mL)[b]	Planktonic NO Dose (μmol/mL)	Biofilm NO Dose (μmol/mL)	Planktonic MBC_{24h} (mg/mL)[a]	Biofilm MBC_{24h} (mg/mL)[b]	Planktonic NO Dose (μmol/mL)	Biofilm NO Dose (μmol/mL)
PO	0.05	5.0	0.09 ± 0.01	9.45 ± 0.55	0.2	5.0	0.38 ± 0.02	9.45 ± 0.55
PO/ACN 1:1	0.10	3.0	0.17 ± 0.02	5.10 ± 0.50	0.6	3.0	1.02 ± 0.10	5.10 ± 0.50
PO/ACN 1:7	0.20	3.0	0.31 ± 0.02	4.68 ± 0.24	0.6	3.0	0.94 ± 0.05	4.68 ± 0.24
ACN	0.20	1.0	0.38 ± 0.02	1.89 ± 0.19	0.6	3.0	0.94 ± 0.06	5.67 ± 0.57

[a]MBC: Minimum Bactericidal Concentration resulting in 3-log reduction in bacterial viability.
[b]MBC: Minimum Bactericidal Concentration resulting in bacterial viability below the limit of detection for the plating method (2.5×10^3 cfu/mL).

~0.95 μmol NO/mg in the first hour of exposure. In contrast, the ACN-modified dendrimers released a more sustained level of NO that would not reach ~0.95 μmol NO/mg until 4 h after exposure. The levels of NO generated from the ACN-modified dendrimers are likely insufficient for complete killing of the metabolically active planktonic cells. As such, more NO (~4x) is required for the same 3-log reduction in viability.[51] Of note, the control dendrimers were not toxic at planktonic *P. aeruginosa* MBCs, but were significantly toxic (~3-log reduction in bacterial viability) at MBCs for the eradication of planktonic *S. aureus*, likely due to the increased amount of scaffold.

4.3.2 Bactericidal efficacy against biofilm bacteria

In addition to exhibiting bactericidal action against planktonic bacteria, the NO-releasing PAMAM dendrimers also proved effective against *P. aeruginosa* and *S. aureus* biofilms. Interestingly, the NO-releasing dendrimer MBCs for eradication of the biofilms followed the opposite trend of that observed for planktonic cells, with the ACN-modified dendrimer exhibiting the greatest efficacy (Table 4.2). The MBC for the NO-releasing ACN-modified dendrimers against *P. aeruginosa* biofilms was 1.0 mg/mL (~1.89 μmol NO/mL), compared to MBCs of 3.0, 3.0, and 5.0 mg/mL for the 1:7 PO/ACN, 1:1 PO/ACN, and PO-modified dendrimers, respectively. *S. aureus* biofilms exhibited similar susceptibility to the NO-releasing dendrimers with MBCs of 3.0, 3.0, 3.0 and 5.0 mg/mL for the ACN, 1:7 PO/ACN, 1:1 PO/ACN, and PO-modified dendrimers, respectively. Unlike planktonic assays, the concentrations of NO-releasing dendrimers needed to eradicate *S. aureus* biofilms compared to *P. aeruginosa* biofilms were not significantly

different. Dendrimers are effective at penetrating biofilms.[52, 53] At high concentrations (≥3.0 mg/mL), dendrimer diffusion and subsequent NO-delivery may be so similar that other factors such as varying levels of antioxidant enzymes and NO cytoprotection mechanisms play a lesser role.

To further confirm that the observed biofilm eradication was a function of NO-release kinetics and not simply increased control scaffold concentration, biofilm viability was evaluated for the control ACN, 1:7 PO/ACN, 1:1 PO/ACN, and PO-modified dendrimers at the highest MBC concentration (5.0 mg/mL) for both *P. aeruginosa* and *S. aureus* (Figure 4.3). Similar killing (~1–2 logs for controls versus 4–5 logs for NO-releasing) of the biofilm bacteria was observed for the four control dendrimer scaffolds, confirming that biofilm eradication was a function of NO-release kinetics and not the control scaffold.

In comparing the eradication of planktonic bacteria to biofilms, the biofilms required ~5–100x more NO and exhibited increased susceptibility to lower, sustained NO levels over burst-release profiles. The initial NO burst from the PO dendrimers likely resulted in residual bacteria remaining embedded within the biofilm. However, the more sustained NO release from the ACN-modified dendrimers may have continued to exert both oxidative and nitrosative stresses against the bacteria throughout the duration of the assay, thus requiring less NO for complete eradication (~1.89–5.67 versus 9.45 μmol NO/mL for NO-releasing ACN- and PO-modified dendrimers, respectively).

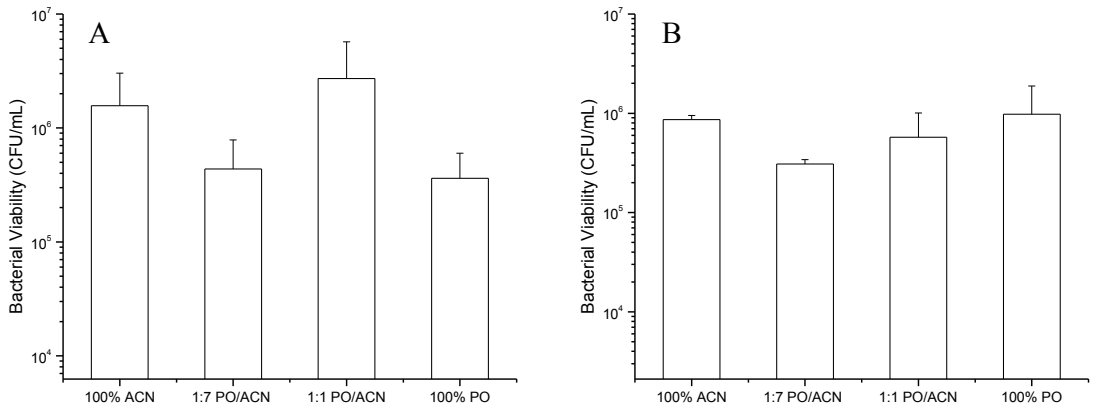

Figure 4.1 Determination of bacterial viability for (A) *P. aeruginosa* and (B) *S. aureus* biofilms exposed to control (i.e., non-NO-releasing) PAMAM dendrimers at 5.0 mg/mL. Viability is similar for the four control scaffolds at the highest MBC.

4.3.3 Confocal microscopy

Confocal microscopy was utilized to further support the results of the bactericidal assays. The eradication of both *P. aeruginosa* and *S. aureus* biofilms was most effective using scaffolds with sustained NO-release profiles. To confirm that the observed differences in scaffold efficacy were due to NO release and not scaffold penetration within the biofilm, we monitored the diffusion of RITC-labeled ACN, 1:7 PO/ACN, 1:1 PO/ACN, and PO-modified dendrimers within the *P. aeruginosa* biofilm. Microscopy studies were not conducted with *S. aureus* biofilms since the observed trends in killing were similar to *P. aeruginosa*. For evaluation of dendrimer diffusion, *P. aeruginosa* biofilms were incubated with the control RITC-labeled dendrimers (200 μg/mL) for 1 h. The biofilm cells were then stained with green nucleic acid stain (Syto 9). As shown in Figure 4.4, the *P. aeruginosa* biofilms exposed to control ACN, 1:7 PO/ACN, 1:1 PO/ACN, or PO-modified dendrimers exhibited similar red RITC fluorescence, indicating similar scaffold diffusion through the biofilm independent of the ACN or PO surface functionality. The improved anti-biofilm efficacy of the NO-releasing ACN dendrimers compared to the PO dendrimers may thus be attributed to NO-release kinetics and not differences in dendrimer association and diffusion through the biofilm.

Intracellular NO concentrations and bacterial killing in *P. aeruginosa* biofilms were also visualized with confocal microscopy. Based on results from the biofilm eradication assays, we hypothesized that greater intracellular NO concentrations (green

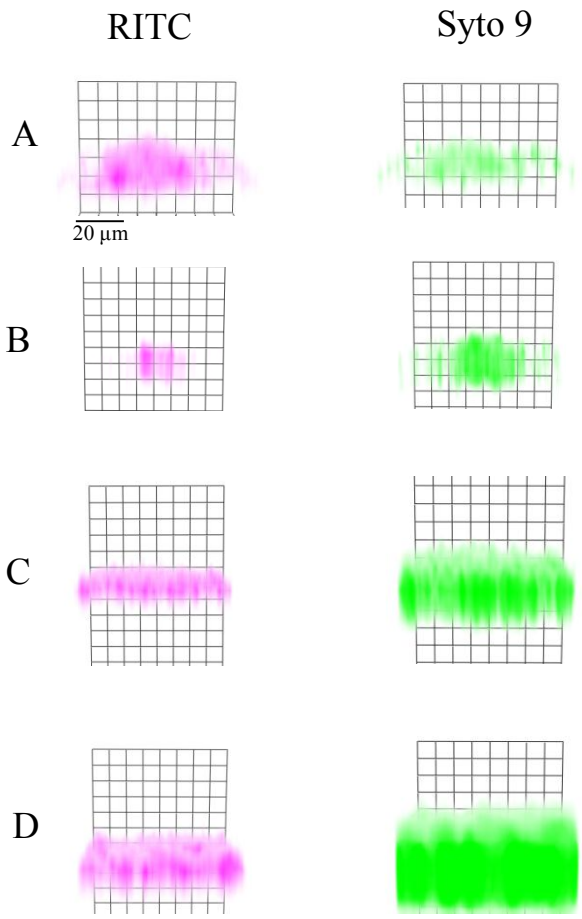

Figure 4.2 Fluorescent images of RITC-modified (A) PO, (B) 1:1, (C) 1:7, and (D) ACN control PAMAM dendrimers (200 µg/mL) diffusion in *P. aeruginosa* biofilm 1 h after dendrimer addition. Green Syto 9 fluorescence shows biofilm cells. Similar RITC red fluorescence indicates similar association and diffusion within biofilm for each scaffold.

DAF fluorescence) would likely be observed for the NO-releasing PO-modified dendrimers, but that the biofilms exposed to NO-releasing ACN-modified dendrimers would exhibit enhanced bacterial cell death (red PI fluorescence) after prolonged exposure. *P. aeruginosa* biofilms were exposed to the NO-releasing PO, 1:1, 1:7, and ACN dendrimers (200 μg/mL) for periods of 1 and 4 h. Exposure times of 1 and 4 h were selected to evaluate intracellular NO concentrations and bacterial cell death at the $t_{1/2}$ for the PO and ACN systems, respectively. As expected, the biofilms exposed to the NO-releasing PO dendrimers exhibited increased green intracellular NO and red PI fluorescence at 1 h (Figure 4.5). At this time no DAF or PI fluorescence was readily visible within the biofilms exposed to the NO-releasing 1:1 PO/ACN, 1:7 PO/ACN, or ACN-modified dendrimers since the NO-release levels were likely low and the fluorescence concomitantly below the limit of detection. After 4 h, red PI fluorescence was observed for bifiolms exposed to the NO-releasing 1:1, 1:7, and ACN-modified dendrimers in addition to the PO-modified scaffolds. However, significant DAF fluorescence was not observed for the 1:1 PO/ACN, 1:7 PO/ACN, or ACN-modified dendrimers, suggesting that NO-release amount remained below the limit of detection or that the DAF dye diffused into solution upon destruction of the bacterial cell membrane. Overall, the visualization of PI fluorescence over time confirmed that the NO-releasing ACN dendrimers exerted similar, if not better killing of *P. aeruginosa* biofilms at prolonged exposure (i.e., 4 h), even though the NO-releasing PO dendrimers disrupted some of the bacterial cell membranes within 1 h.

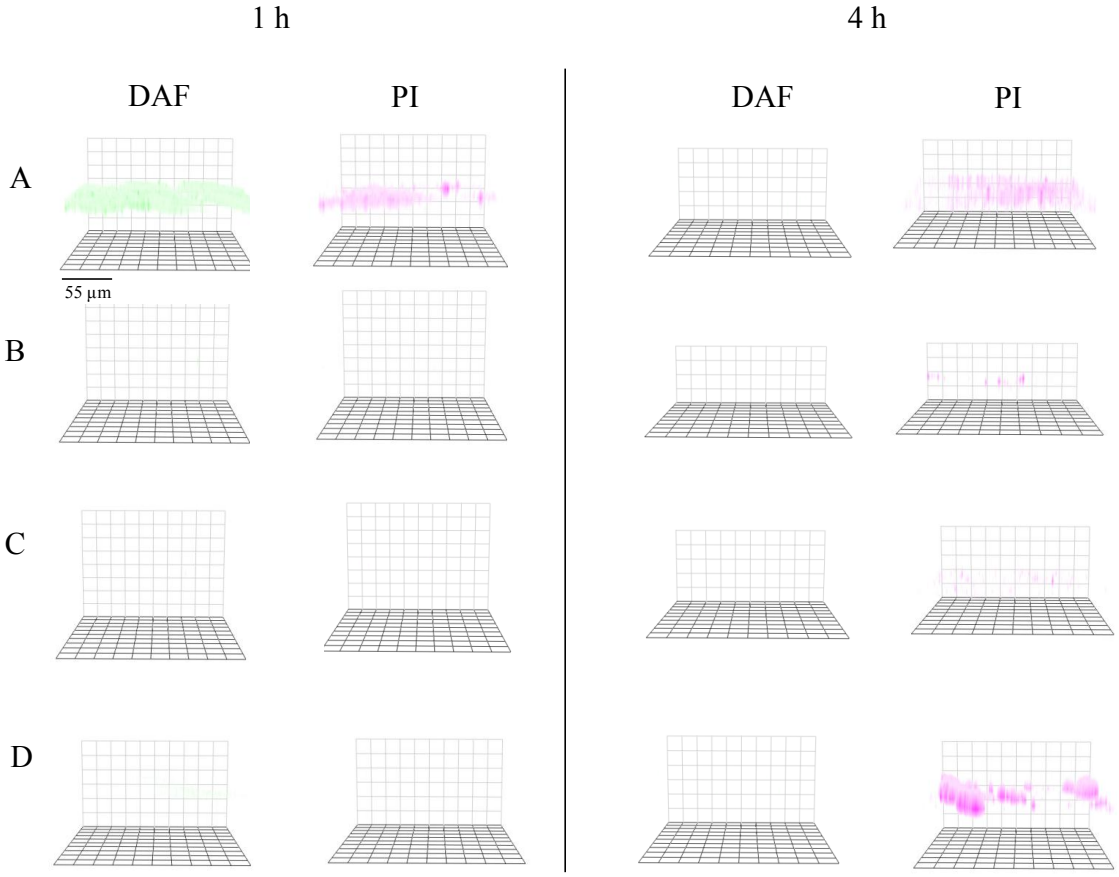

Figure 4.3. Fluorescent images of *P. aeruginosa* biofilm exposed to the same dendrimer concentration (200 µg/mL) of NO-releasing (A) PO, (B) 1:1, (C) 1:7, or (D) ACN dendrimers for 1 or 4 h. DAF-2 green fluorescence indicates increased intracellular NO and PI red fluorescence indicates compromised cell membranes (i.e., cell death).

4.3.4 Cytotoxicity of PAMAM dendrimers at therapeutic concentrations

Given the bactericidal efficacy of the NO-releasing PAMAM dendrimers presented herein, the PO, 1:1 PO/ACN, 1:7 PO/ACN, and ACN-modified scaffolds were evaluated against healthy host cells to further determine potential therapeutic utility. L929 mouse fibroblasts, which are ubiquitous in connective tissue,[54] were incubated with both control and NO-releasing dendrimers for 24 h at their respective planktonic and biofilm MBCs. Fibroblasts exposed to the dendrimers at planktonic MBCs (0.05–0.6 mg/mL) exhibited no reduction in cell viability for either the control or NO-releasing systems (Figure 4.6). Significant viability reductions (~55–84%) were observed for fibroblasts exposed to NO-releasing dendrimers at biofilm MBCs (1.0–5.0 mg/mL) even though the controls remained relatively non-toxic (~1–18% viability reduction) (Figure 4.7).

The aforementioned cytotoxicity studies demonstrate the utility of NO-releasing PO, 1:1PO/ACN, 1:7 PO/ACN, and ACN PAMAM dendrimers as antibacterial agents against planktonic bacteria, due to their potent biodical action and minimal effects toward healthy host cells. However, >99% of bacteria exist in a biofilm state and the cytotoxicity of potential therapeutics must be evaluated with these conditions in mind.[55] The control PAMAM dendrimers were not significantly cytotoxic to L929 fibroblasts regardless of the concentration tested (0.05–5.0 mg/mL). In contrast, larger NO concentrations (≥5.67 μmol NO/mL) resulted in elevated cytotoxicity (Figure 4.7 A and B). Of note, NO-releasing ACN-PAMAM dendrimers exhibited only ~3% reduction in cell viability

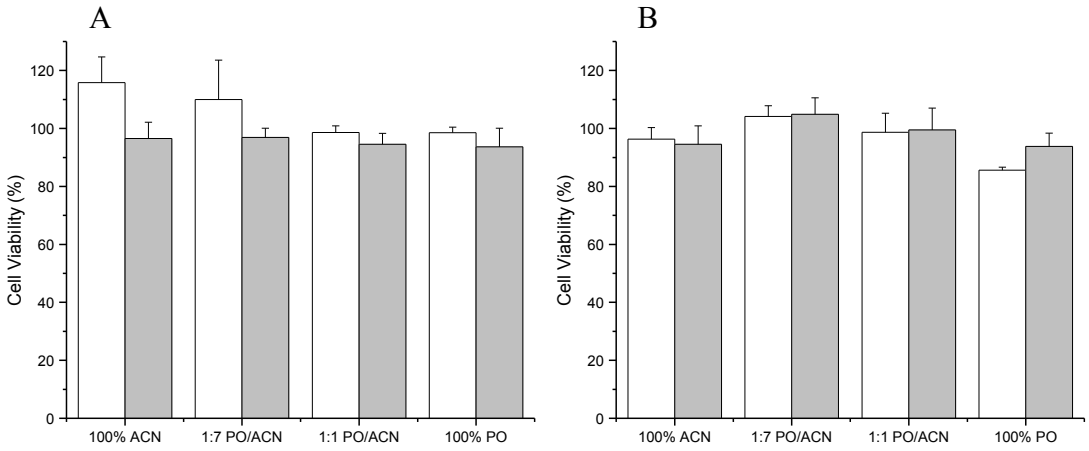

Figure 4.4 Cytotoxicity of NO-releasing (white) and control (gray) PAMAM dendrimers against L929 mouse fibroblasts at MBC concentrations required for killing of planktonic (A) *P. aeruginosa* and (B) *S. aureus* as listed in Table 4.2.

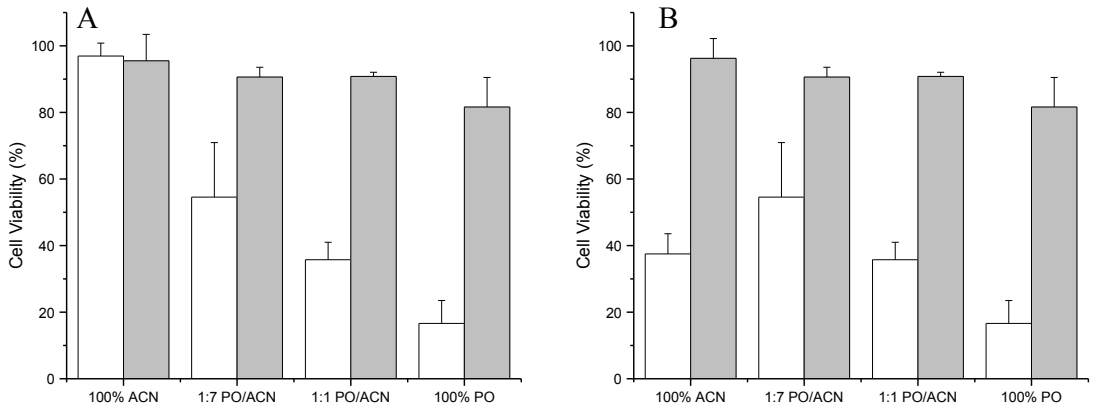

Figure 4.5 Cytotoxicity of NO-releasing (white) and control (gray) PAMAM dendrimers against L929 mouse fibroblasts at MBC concentrations required for (A) *P. aeruginosa* and (B) *S. aureus* biofilm killing as listed in Table 4.2.

at the MBC (1.0 mg/mL or ~1.89 μmol NO/mL) for *P. aeruginosa* biofilm eradication, making them a desirable therapeutic for anti-biofilm applications.

4.3.5 Cytotoxicity of PAMAM dendrimers as a function of NO-release kinetics

In addition to evaluating cytotoxicity at the dendrimer MBC concentrations, we sought to determine if NO-induced cytotoxicity was a function of NO-release kinetics. L929 mouse fibroblasts were incubated with varying concentrations (i.e., 0.2, 1.0, 3.0, and 5.0 mg/mL) of control and NO-releasing PO, 1:1 PO/ACN, 1:7 PO/ACN, and ACN-PAMAM dendrimers for 24 h. As shown in Figure 4.8B, the four control PAMAM dendrimers were minimally toxic over the entire concentration range tested (0.2–5.0 mg/mL). In contrast, the effects of NO on L929 cell viability proved to be concentration dependent (Figure 4.8A). Low levels of NO (≤1.89 μmol NO/mL) actually promoted fibroblast proliferation,[56] while larger doses (≥5.67 μmol NO/mL) resulted in significant reductions in viability. Determination of fibroblast cytotoxicity as a function of NO-release kinetics was not definitive for the systems and concentrations tested. At low concentrations of NO-releasing dendrimers (≤1.0 mg/mL), little dependence on NO-release kinetics was noted as the cell viabilities for the fibroblasts exposed to NO-releasing PO and ACN dendrimers proved similar. At 5.0 mg/mL, the burst-release profile of the NO-releasing PO dendrimers resulted in a greater reduction in cell viability (~84% reduction) compared to the lower but sustained NO release from the ACN dendrimers (~51% reduction). At larger NO concentrations, it is likely that the antioxidant enzymes (e.g., superoxide dismutase) employed by mammalian cells are

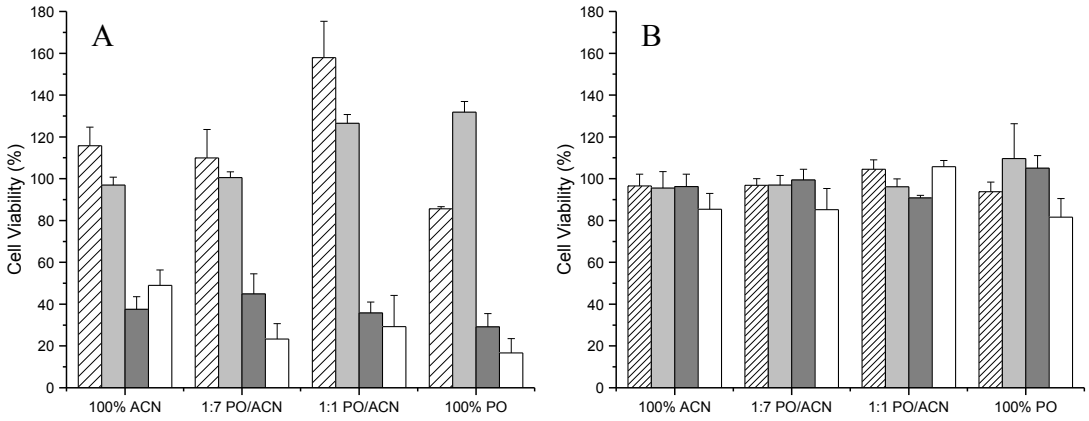

Figure 4.6 Cytotoxicity of (A) NO-releasing and (B) control PAMAM dendrimers against L929 mouse fibroblasts at concentrations of 0.2 (dashed), 1.0 (light gray), 3.0 (dark gray), and 5.0 (white) mg/mL.

unable to adequately mitigate the effects of NO. Thus, scaffolds delivering large bursts of NO exhibit slightly greater cytotoxicity compared to sustained release systems.

4.4 Conclusions

The importance of NO-release kinetics in the eradication of planktonic and biofilm-based *P. aeruginosa* and *S. aureus* bacteria was demonstrated using NO-releasing PAMAM dendrimers functionalized with PO, ACN, or both PO/ACN. Although Hetrick et al. noted improved biofilm eradication for the NO-releasing MAP3 silica particles with faster release (i.e., lower $t_{1/2}$) compared to the slower-releasing AHAP3 particles, the total NO storage between the two scaffolds was so varied (~7.6 versus 3.8 μmol/mg, respectively) that killing differences could not be due to NO-release kinetics alone.[40] While our results indicate that slower, sustained NO-release profiles are preferred for biofilm eradication, increasing total NO storage (>1.89 μmol/mg) may improve the efficacy of faster-releasing dendrimer scaffolds since fewer residual bacteria would likely remain after delivery of the intial NO burst. However, an increased NO storage may also influence cytotoxicity to healthy host cells. Previous literature has observed that scaffolds delivering sustained levels of an antibacterial over time were ultimately more effective against biofilms, with biphasic release profiles being the most ideal,[19, 27] although these systems may result in increased antibiotic resistance over time.[29] The slower NO-releasing ACN-PAMAM dendrimers presented here show therapeutic potential due to their ability to effectively eradicate *P. aeruginosa* biofilms at concentrations with minimal cytotoxicity. Eradication of *S. aureus* biofilms could be improved by further

tuning of both the NO-release profile and total NO storage, and perhaps even co-administering NO-releasing PO- and ACN- modified dendrimers.

REFERENCES

1. Bryers, J. D., Medical biofilms. *Biotechnol*. *Bioeng*. **2008,** *100*, 1-18.

2. D'Avignon, L. C.; Hogan, B. K.; Murray, C. K.; Loo, F. L.; Hospenthal, D. R.; Cancio, L. C.; Kim, S. H.; Renz, E. M.; Barillo, D.; Holcomb, J. B.; Wade, C. E.; Wolf, S. E., Contribution of bacterial and viral infections to attributable mortality in patients with severe burns: An autopsy series. *Burns* **2010,** *36*, 773-779.

3. Goswami, A. P.; Goswami, N.; Patel, T.; Tripathi, C.; Trivedi, H., Antibiotic sensitivity profile of bacterial pathogens in postoperative wound infections at a tertiary care hospital in Gujarat, India. *J*. *Pharmacol*. *Pharmacother*. **2011,** *2*, 158-164.

4. James, G. A.; Swogger, E.; Wolcott, R.; Pulcini, E. d.; Secor, P.; Sestrich, J.; Costerton, J. W.; Stewart, P. S., Biofilms in chronic wounds. *Wound Repair Regen*. **2008,** *16*, 37-44.

5. Lyczak, J. B.; Cannon, C. L.; Pier, G. B., Lung infections associated with cystic fibrosis. *Clin*. *Microbiol*. *Rev*. **2002,** *15*, 194-222.

6. Costerton, J. W.; Stewart, P. S.; Greenberg, E. P., Bacterial biofilms: A common cause of persistent infections. *Science* **1999,** *284*, 1318-1322.

7. Smith, A. W., Biofilms and antibiotic therapy: is there a role for combating bacterial resistance by the use of novel drug delivery systems? *Adv*. *Drug Delivery Rev*. **2005,** *57*, 1539-1550.

8. Aaron, S. D.; Ferris, W.; Ramotar, K.; Vandemheen, K.; Chan, F.; Saginur, R., Single and combination antibiotic susceptibilities of planktonic, adherent, and biofilm-grown *Pseudomonas aeruginosa* isolates cultured from sputa of adults with cystic fibrosis. *J*. *Clin*. *Microbiol*. **2002,** *40*, 4172-4179.

9. Anderl, J. N.; Franklin, M. J.; Stewart, P. S., Role of antibiotic penetration limitation in *Klebsiella pneumoniae* biofilm resistance to ampicillin and ciprofloxacin. *J*. *Antimicrob*. *Chemother*. **2000,** *44*, 1818-1824.

10. Nickel, J. C.; Ruseska, I.; Wright, J. B.; Costerton, J. W., Tobramycin resistance of *Pseudomonas aeruginosa* cells growing as a biofilm on urinary catheter material. *J*. *Antimicrob*. *Chemother*. **1985,** *27*, 619-624.

11. Cerca, N.; Martins, S.; Cerca, F.; Jefferson, K. K.; Pier, G. B.; Oliveira, R.; Azeredo, J., Comparative assessment of antibiotic susceptibility of coagulase-

negative staphylococci in biofilm versus planktonic culture as assessed by bacterial enumeration or rapid XTT colorimetry. *J*. *Antimicrob*. *Chemother*. **2005,** *56*, 331-336.

12. Stewart, P. S.; William Costerton, J., Antibiotic resistance of bacteria in biofilms. *The Lancet* **2001,** *358*, 135-138.

13. Smith, K.; Perez, A.; Ramage, G.; Gemmell, C. G.; Lang, S., Comparison of biofilm-associated cell survival following in vitro exposure of meticillin-resistant *Staphylococcus aureus* biofilms to the antibiotics clindamycin, daptomycin, linezolid, tigecycline and vancomycin. *Int*. *J*. *Antimicrob*. *Agents* **2009,** *33*, 374-378.

14. Eckert, R.; He, J.; Yarbrough, D. K.; Qi, F.; Anderson, M. H.; Shi, W., Targeted killing of Streptococcus mutans by a pheromone-guided "smart" antimicrobial peptide. *Antimicrob*. *Agents Chemother*. **2006,** *50*, 3651-3657.

15. Bjarnsholt, T.; Kirketerp-Muller, K.; Kristiansen, S.; Phipps, R.; Nielsen, A. K.; Jensen, P. O.; Holby, N.; Givskov, M., Silver against *Pseudomonas aeruginosa* biofilms. *APMIS* **2007,** *115*, 921-928.

16. Kostenko, V.; Lyczak, J.; Turner, K.; Martinuzzi, R. J., Impact of silver-containing wound dressings on bacterial biofilm viability and susceptibility to antibiotics during prolonged treatment. *Antimicrob*. *Agents Chemother*.**2010**, *54*, 5120-5131.

17. Kenawy, E.-R.; Worley, S. D.; Broughton, R., The chemistry and applications of antimicrobial polymers: A state-of-the-art review. *Biomacromolecules* **2007,** *8*, 1359-1384.

18. Cappelletty, D. M.; Kang, S. L.; Palmer, S. M.; Rybak, M. J., Pharmacodynamics of ceftazidime administered as continuous infusion or intermittent bolus alone and in combination with single daily-dose amikacin against *Pseudomonas aeruginosa* in an in vitro infection model. *Antimicrob*. *Agents Chemother*. **1995,** *39*, 1797-801.

19. Cheow, W.; Chang, M.; Hadinoto, K., Antibacterial efficacy of inhalable levofloxacin-loaded polymeric nanoparticles against *E*. *coli* biofilm cells: The effect of antibiotic release profile. *Pharm*. *Res*. **2010**, *27*, 1597-1609.

20. Shani, S.; Friedman, M.; Steinberg, D., In vitro assessment of the antimicrobial activity of a local sustained release device containing amine fluoride for the treatment of oral infectious diseases. *Diagn*. *Micr*. *Infect*. *Dis*. **1998,** *30*, 93-97.

21. Gunderson, B. W.; Ross, G. H.; Ibrahim, K. H.; Rotschafer, J. C., What do we really know about antibiotic pharmacodynamics? *Pharmacotherapy: The Journal of Human Pharmacol*. *Drug Ther*. **2001,** *21*, 302S-318S.

22. Kumari, A.; Yadav, S. K.; Yadav, S. C., Biogradable polymeric nanoparticles based drug delivery systems. *Colloids and Surfaces B: Biointerfaces* **2010,** *75*, 1-18.

23. Hetrick, E. M.; Schoenfisch, M. H., Reducing implant-related infections: active release strategies. *Chem*. *Soc*. *Rev*. **2006,** *35*, 780-789.

24. Li, Z.; Lee, D.; Sheng, X.; Cohen, R. E.; Rubner, M. F., Two-level antibacterial coating with both release-killing and contact-killing capabilities. *Langmuir* **2006,** *22*, 9820-9823.

25. Damm, C.; Munstedt, H., Kinetic aspects of the silver ion release from antimicrobial polyamide/silver nanocomposites. *Applied Physics A* **2008,** *91*, 479-486.

26. Kwok, C. S.; Wan, C.; Hendricks, S.; Bryers, J. D.; Horbett, T. A.; Ratner, B. D., Design of infection-resistant antibiotic-releasing polymers: I. Fabrication and formulation. *J*. *Controlled Release* **1999,** *62*, 289-299.

27. Shukla, A.; Fleming, K. E.; Chuang, H. F.; Chau, T. M.; Loose, C. R.; Stephanopoulos, G. N.; Hammond, P. T., Controlling the release of peptide antimicrobial agents from surfaces. *Biomaterials* **2010***, 31*, 2348-2357.

28. Zilberman, M.; Elsner, J. J., Antibiotic-eluting medical devices for various applications. *J*. *Controlled Release* **2008,** *130*, 202-215.

29. Andersson, D. I., Persistence of antibiotic resistant bacteria. *Curr*. *Opin*. *Microbiol*. **2003,** *6*, 452-456.

30. Campos, M. A.; Vargas, M. A.; Regueiro, V.; Llompart, C. M.; Alberti, S.; Bengoechea, J., Capsule polysaccharide mediates bacterial resistance to antimicrobial peptides. *Infect*. *Immun*. **2004,** *72*, 7107-7114.

31. Peschel, A., How do bacteria resist human antimicrobial peptides? *Trends Microbiol*. **2002,** *10*, 179-186.

32. James, G. A.; Swogger, E.; Wolcott, R.; Pulcini, E. d.; Secor, P.; Sestrich, J.; Costerton, J. W.; Stewart, P. S., Biofilms in chronic wounds. *Wound Repair and Regeneration* **2008,** *16*, 37-44.

33. Singh, P. K.; Schaefer, A. L.; Parsek, M. R.; Moninger, T. O.; Welsh, M. J.; Greenberg, E. P., Quorum-sensing signals indicate that cystic fibrosis lungs are infected with bacterial biofilms. *Nature* **2000,** *407*, 762-764.

34. Ignarro, L. J., *Nitric Oxide: Biology and Pathobiology*. Academic Press: San Diego, CA, 2000.

35. Fang, F. C., Mechanisms of nitric oxide-related antimicrobial activity. *J*. *Clin*. *Invest*. **1997,** *99*, 2818-2825.

36. Carpenter, A. W.; Schoenfisch, M. H., Nitric oxide release: Part II. Therapeutic applications. *Chem*. *Soc*. *Rev*. **2012,** *41*, 3742-3752.

37. Privett, B. J.; Broadnax, A. D.; Bauman, S. J.; Riccio, D. A.; Schoenfisch, M. H., Examination of bacterial resistance to exogenous nitric oxide. *Nitric Oxide* **2012,** *26*, 169-173.

38. Barraud, N.; Hassett, D. J.; Hwang, S.-H.; Rice, S. A.; Kjelleberg, S.; Webb, J. S., Involvement of nitric oxide in biofilm dispersal of *Pseudomonas aeruginosa*. *J*. *Bacteriol*. **2006,** *188*, 7344-7353.

39. Sulemankhil, I.; Ganopolsky, J. G.; Dieni, C. A.; Dan, A. F.; Jones, M. L.; Prakash, S., Prevention and treatment of virulent bacterial biofilms with an enzymatic nitric oxide-releasing dressing. *Antimicrob*. *Agents Chemother*. **2012,** *56*, 6095-6103.

40. Hetrick, E. M.; Shin, J. H.; Paul, H. S.; Schoenfisch, M. H., Anti-biofilm efficacy of nitric oxide-releasing silica nanoparticles. *Biomaterials* **2009,** *30*, 2782-2789.

41. Riccio, D. A.; Schoenfisch, M. H., Nitric oxide release: Part I. Macromolecular scaffolds. *Chem*. *Soc*. *Rev*. **2012,** *41*, 3731-3741.

42. Hetrick, E. M.; Shin, J. H.; Stasko, N. A.; Johnson, C. B.; Wespe, D. A.; Holmuhamedov, E.; Schoenfisch, M. H., Bactericidal efficacy of nitric oxide-releasing silica nanoparticles. *ACS Nano* **2008,** *2*, 235-246.

43. Sun, B.; Slomberg, D. L.; Chudasama, S. L.; Lu, Y.; Schoenfisch, M. H., Nitric oxide-releasing dendrimers as antibacterial agents. *Biomacromolecules* **2012,** *13*, 3343-3354.

44. Lu, Y.; Slomberg, D. L.; Shah, A.; Schoenfisch, M. H., Nitric oxide-releasing amphiphilic poly(amidoamine) (PAMAM) dendrimers as antibacterial agents. *Biomacromolecules* **2013,** *submitted*.

45. Carpenter, A. W.; Slomberg, D.L.; Rao, K.S.; Schoenfisch, M.H., Influence of scaffold size on bactericidal activity of nitric oxide-releasing silica nanoparticles. *ACS Nano* **2011,** *5*, 7235-7244.

46. Ishima, Y.; Sawa, T.; Kragh-Hansen, U.; Miyamoto, Y.; Matsushita, S.; Akaike, T.; Otagiri, M., *S*-Nitrosylation of human variant albumin liprizzi (R410C) confers potent antibacterial and cytoprotective properties. *J*. *Pharmacol*. *Exp*. *Therap*. **2007,** *320*, 969-977.

47. Lu, Y.; Slomberg, D. L.; Sun, B.; Schoenfisch, M. H., Shape- and nitric oxide flux-dependent bactericidal activity of nitric oxide-releasing silica nanorods. *Small* **2013,** *9*, 2189-2198.

48. Silhavy, T. J.; Kahne, D.; Walker, S., The bacterial cell envelope. *Cold Spring Harb*. *Perspect*. *Biol*. **2010**, 1-16.

49. Mandell, G., Catalase, superoxide dismutase, and virulence of *Staphylococcus aureus*. In vitro and in vivo studies with emphasis on staphylococcal--leukocyte interaction. *J*. *Clin*. *Invest*. **1975,** *55*, 561-566.

50. Gusarov, I.; Nudler, E., NO-mediated cytoprotection: Instant adaptation to oxidative stress in bacteria. *Proc*. *Natl*. *Acad*. *Sci*. *U*.*S*.*A*. **2005,** *102*, 13855-13860.

51. Drenkard, E., Antimicrobial resistance of *Pseudomonas aeruginosa* biofilms. *Microbes and Infection* **2003,** *5*, 1213-1219.

52. Hou, S.; Zhou, C.; Liu, Z.; Young, A. W.; Shi, Z.; Ren, D.; Kallenbach, N. R., Antimicrobial dendrimer active against *Escherichia coli* biofilms. *Bioorganic & Med*. *Chem*. *Lett*. **2009,** *19*, 5478-5481.

53. Johansson, E.; Crusz, S. A.; Kolomiets, E.; Buts, L.; Kadam, R. U.; Cacciarini, M.; Bartels, K.-M.; Diggle, S. P.; CÃ¡mara, M.; Williams, P., Inhibition and dispersion of *Pseudomonas aeruginosa* biofilms by glycopeptide dendrimers targeting the fucose-specific lectin LecB. *Chemistry & biology* **2008,** *15*, 1249-1257.

54. Alberts, B.; Johnson, A.; Lewis, J., *Molecular Biology of the Cell*. 4th ed.; Garland Science: New York, 2002.

55. Smith, A. W., Biofilms and antibiotic therapy: Is there a role for combating bacterial resistance by the use of novel drug delivery systems? . *Adv*. *Drug Deliv*. *Rev*. **2005,** *57*, 1539-1550.

56. Babaei, S.; Teichert-Kuliszewska, K.; Monge, J.-C.; Mohamed, F.; Bendeck, M. P.; Stewart, D. J., Role of nitric oxide in the angiogenic response in vitro to basic fibroblast growth factor. *Circul*. *Res*. **1998,** *82*, 1007-1015.

CHAPTER 5: SIZE- AND SHAPE-DEPENDENT SILICA NANOPARTICLE PHYTOTOXICITY AND UPTAKE IN *ARABIDOPSIS THALIANA*

5.1 Introduction

The evolution of nanotechnology is proceeding rapidly as researchers work to engineer nanomaterials with unique molecular organization, properties, and functions relative to bulk materials.[1] Indeed, engineered nanoparticles (ENPs) have already proven to be useful for drug delivery and environmental remediation.[2, 3] Engineered nanoparticles incorporated into consumer goods are now making their way into atmospheric, aquatic, and terrestrial environments due to incidental and direct release/disposal.[2, 4, 5] A better understanding of particle fate, behavior, and potential toxicity in these environments is thus warranted.

Studies have assessed the toxicity of ENPs toward mammalian cells, bacteria, aquatic invertebrates, and other terrestrial organisms. To date, plant toxicity due to nanoparticle exposure has received less attention.[6, 7] Prior work with plants has evaluated the toxicity of silica (SiO_2), zinc oxide (ZnO), nickel hydroxide ($Ni(OH)_2$), copper (Cu), cerium oxide (CeO_2), titanium dioxide (TiO_2), iron oxide (Fe_3O_4), gold (Au), silver (Ag), iron (Fe), and CdSe/ZnS quantum dot nanoparticles to *Arabidopsis thaliana*,[4, 8] rye grass,[9, 10] mesquite,[11] and select edible plant species including wheat and mung bean,[5] alfalfa, tomato, corn, and cucumber.[12, 13]

Silica nanoparticles (SiNPs) have received special interest due to their prominence in cosmetic and biomedical applications.[14-16] In one study, the toxicity of 12.5 and 27.0 nm SiNPs (20.0 and 28.8 mg L^{-1}, respectively) to green alga was shown to reduce growth by 20% after 72 h.[17] Silica particles (10–20 nm) were also shown to exhibit toxicity to *Scenedesmus obliquus* (green algae) after 72 and 96 h, as evidenced by a 20% reduction in growth (388.1 and 216.5 mg L^{-1}, respectively) and decreased chlorophyll content.[18] In contrast, phytotoxicity assays with *Cucurbita pepo* (zucchini) showed no significant difference in germination percent, root elongation, or biomass after exposure to 1000 mg L^{-1} bulk silicon powder and SiNPs (< 100 nm) for 5–14 d.[19] Lee et al. found that 42.8 nm SiNPs promoted *Arabidopsis thaliana* root elongation at a low concentration (400 mg L^{-1}), but resulted in toxicity at higher concentrations (≥ 2000 mg L^{-1}).[4] Likewise, an increase in shoot/root ratio has been reported in *Lactuca sativa* (lettuce) plants after 15 d exposure to 0.066% (w/w) SiNPs (~100 nm).[20] Nair and coworkers examined the use of SiNPs (~25 nm) labeled with fluorescein isothiocyanate (FITC) as potential biolabels in plants.[21] They confirmed uptake of the SiNPs into rice seedlings and determined that the particles had no effect on germination up to 50 mg L^{-1}. The importance of nanoparticle shape and surface charge in phytotoxicity have also been noted, but studies systematically investigating these parameters are not currently available.[22] While work thus far on the phytotoxicity of SiNPs to higher plants has established a strong foundation, we sought to examine toxicity over an increased SiNP size range (i.e., < 42.8 nm and > 100 nm) and growth duration (i.e., 6 weeks), with evaluation of particle surface charge and shape. In addition, the literature currently lacks

visualization of SiNPs in *A. thaliana* cells and information about where SiNPs are uptaken (i.e., roots, rosette, and stem).

Herein, the phytotoxicity of 14, 50, and 200 nm SiNPs at concentrations of 250 and 1000 mg L^{-1} (ppm) to *Arabidopsis thaliana* over 3 and 6 weeks in a hydroponic growth medium was evaluated. Additionally, SiNPs of various shape (i.e., aspect ratios 1 and 3) were examined for phytotoxic effects and uptake. The objective was to determine how size, surface charge, composition, and shape play a role in SiNP phytotoxicity while assessing particle uptake in the roots, rosette, and stems. *A. thaliana* is a universal model plant due primarily to its rapid life-cycle and relevance for toxicity implications on edible food crops.[4, 13] Multiple plant growth parameters were evaluated including rosette diameter, biomass, and length of the main stem. Transmission electron microscopy (TEM) and inductively coupled plasma-optical emission spectroscopy (ICP-OES) were used to visualize SiNP localization and quantify uptake.

5.2 Materials and Methods

Note: Silica particle synthesis and characterization (AR1 and AR3) were supported by other members of the Schoenfisch lab

Tetraethylorthosilicate (TEOS) was purchased from Gelest (Morrisville, PA). Ethanol (EtOH), ammonium hydroxide (28 wt%), and a silicon reference standard solution (1000 ppm) were purchased from Fisher Scientific (Fair Lawn, NJ). Cetyltrimethylammonium bromide (CTAB) was obtained from Acros Organics (Geel, Belgium). Organosilicasol MT-ST silica particles (14 nm) in methanol were obtained

from Nissan Chemical Corp. (Houston, TX). Wild-type *Arabidopsis thaliana* (Col-0) seeds were purchased from Carolina Biological Supply Company (Burlington, NC). Triton X-100, agar, Hoagland's No. 2 Basal Salt Mixture, triethanolamine, and glutaraldehyde (50% v/v in water) were purchased from Sigma-Aldrich (St. Louis, MO). A hydroponic plant growth system was acquired from Araponics (Liège, Belgium). Hydrofluoric acid (48–51 wt%) and osmium tetroxide (2.5 wt% in *t*-butanol) were purchased from Acros Organics (Morris Plains, NJ). Cacodylate buffer was purchased from Electron Microscopy Sciences (Hatfield, PA). LR White Resin was purchased from Polysciences, Inc. (Warrington, PA). Argon (Ar) gas was obtained from Airgas National Welders (Raleigh, NC). Other solvents and chemicals were analytical-reagent grade and used as received. A Millipore Milli-Q UV Gradient A10 System (Bedford, MA) was used to purify distilled water to a final resistivity of 18.2 MΩ·cm and a total organic content of ≤6 parts per billion (ppb).

5.2.1 Silica nanoparticle synthesis and characterization

Organosilicasol MT-ST particles (14 nm) were dried under vacuum before use. Tetraethylorthosilicate SiNPs (50 and 200 nm) were synthesized by the Stöber method following conditions reported by Bogush et al.[23] Briefly, 50 nm SiNPs were made by adding TEOS (3.792 mL) to a stirred solution of EtOH (91.378 mL),ammonium hydroxide (3.378 mL), and water (1.452 mL). After 5 h, the particles were collected by adding hexane to the solution in a 2:1 ratio (v/v) and centrifugation (3645*g* for 5 min). The particles were resuspended in EtOH via sonication and collected again by

centrifugation (3645*g* for 5 min). This washing procedure was repeated and the particles were then dried under vacuum. The 200 nm SiNPs were made by adding TEOS (3.792 mL) to a stirred solution of EtOH (88.351 mL), ammonium hydroxide (6.757 mL), and water (1.101 mL). These particles were collected, washed, and dried after 2 h using the aforementioned procedure. For select studies, the silica particles were calcined at 1000 °C for 24 h in a muffle furnace.

Silica particles of two distinct aspect ratios (AR1 and AR3) were synthesized via a surfactant-templated approach as previously described by varying reaction temperature and ammonia concentration.[24] Elevated temperature (50 vs. 20 °C) was used to increase the aspect ratio of the particles (AR3), while a greater ammonia concentration (1.0 vs. 0.5 M) allowed for the synthesis of a more spherical particle (AR1). Tuning these reaction parameters, silica particles with aspect ratios of 1 (62 ± 8 nm) and 3 (241 ± 32 nm length and 78 ± 6 nm width), but similar particle volume (~10^6 nm^3) were achieved. Of note, cetyltrimethylammonium bromide (CTAB) removal was confirmed via CHN analysis prior to surface grafting.

Particle size, shape, and morphology were characterized with a JEOL 100 CX II transmission electron microscope (TEM) at 80 kV or Hitachi S-4700 scanning electron microscope (Tokyo, Japan). Hydrodynamic diameters and zeta potentials were determined by dynamic light scattering (DLS) using a Malvern Zetasizer Nano ZS (Worcestershire, UK). Measurements were performed in solutions of the plant growth medium at pH 5.8. To assess the relative amount of silanols and/or unreacted silane on the particle surface, CHN elemental analysis was performed using a 2400 Series II

CHNS/O analyzer from Perkin Elmer to determine both wt% H and C for each particle size.

5.2.2. Plant growth

A. thaliana seeds were sterilized prior to use with a solution of 95% (v/v) EtOH (73.7 mL), water (26 mL), and Triton X-100 (50 μL) for 10 min, and rinsed with 95% (v/v) EtOH twice. Seeds were pretreated via dispersal on filter paper moistened with water, then "incubating" at 4 °C for 6 d in the dark to simulate winter and encourage germination.[25] The hydroponic system, including seed holders, was sterilized with a 10% (v/v) sodium hypochlorite solution and rinsed copiously with water. The seed holders were filled with 0.65 wt% agar support, and seeds sown by dropping one seed (in a suspension of 0.2 wt% agar) into each holder.[25] The SiNPs 14, 50, and 200 nm SiNPs were dispersed in the hydroponic troughs at concentrations of 250 or 1000 ppm with Hoagland's No. 2 Basal Salt Mixture (400 mg L^{-1}), while the AR1 and AR3 particles were dispersed at 250 ppm. Control plants were grown in blank solutions of Hoagland's No. 2 Basal Salt Mixture (400 mg L^{-1}). Studies were carried out by either allowing the pH of the hydroponic solution to fluctuate naturally or maintaining the pH at pH 5.8 via addition of dilute hydrochloric acid or sodium hydroxide. Seeds were grown at room temperature under fluorescent light (GE Pro-Line Watt-Miser F40T12) with a 12 h photoperiod and 78–91 $\mu molm^{-2}s^{-1}$ photosynthetically active radiation for 3 or 6 weeks. During the first two weeks of germination and growth, transparent lids were used to increase the relative humidity (~50–60%) surrounding the seedlings and establish

plantlets.[26] For each experiment, at least 6 separate plants were harvested and examined. Significant differences in growth were determined based on the Student's *t*-test at the 95% confidence level.

5.2.3 Transmission electron microscopy

Plant samples were fixed with 4% (v/v) glutaraldehyde in 0.1 M cacodylate buffer for 3 h at room temperature.[9] Specimens were then rinsed with 0.1 M cacodylate buffer for 10 min and post-fixed with 1% (v/v) osmium tetroxide in 0.1 M cacodylate buffer for 2 h. After two additional 10 min rinses in 0.1 M cacodylate buffer, samples were dehydrated in a series of graded ethanol solutions (30, 50, 70, 95, and 100% v/v), with 10 min incubation per solution. LR White Resin was used to infiltrate the plant tissue with a series of resin solutions (25, 50, 75, 100, and 100% v/v in EtOH), with 1 h incubation per solution. Plant samples were then embedded in 100% LR White Resin in gelatin capsules at 60 °C for 40 h. An ultramicrotome was used to cut thin sections (~100 nm) that were post-stained with 2% (v/v) uranyl acetate and 0.5–1% (v/v) lead citrate. Samples were then characterized using a JEOL 100 CX II TEM at 80 kV.

5.2.4 Silicon elemental analysis

Several plant samples from the same exposure group (6 weeks) were homogenized by grinding with a mortar and pestle, digested with acid, and analyzed via ICP-OES to determine Si content. Briefly, plant samples were digested with 10% (v/v) HNO_3 (10 mL) in a microwave accelerated reaction system (CEM Corporation; Matthews, NC) for 15 min at 200 °C. Following digestion, samples were prepared further

for Si elemental analysis by adding aqua regia (2.5 mL) and hydrofluoric acid (1 mL) to dissolve any remaining material. Triethanolamine (3.575 mL of 40% v/v) was used to neutralize this solution. The solution was then diluted to 50 mL with water. CAUTION: hydrofluoric acid is extremely corrosive and requires special handling. Silicon elemental analysis was carried out in triplicate using a Prodigy ICP-OES (Teledyne Leeman Labs; Hudson, NH). The instrument was calibrated from 0.1–10 ppm in the axial configuration at 251.611 nm using a silicon reference standard solution.

5.3 Results and Discussion

5.3.1 Size-dependent phytotoxicity and uptake

5.3.1.1 Synthesis and characterization of silica nanoparticles with varied size

The physicochemistry of nanoparticles in the environment is influenced by their shape, size, surface area, degree of aggregation, adsorption, and local pH and ionic strength.[7] To enable the study of particle phytotoxicity over a range of sizes spanning ~2 orders of magnitude and compare results to previous work, we purchased 14 nm SiNPs and synthesized both 50 and 200 nm SiNPs via the Stöber process.[4, 17, 19, 20] Particle size of the SiNPs (50 and 200 nm) is easily tuned in the Stöber process by varying water and ammonia concentrations and/or overall reaction time.[23]

Prior to studying phytotoxicity, we sought to understand the shape and morphology of the native SiNPs. As expected, the silica particles were spherical and monodisperse upon TEM analysis (14.8 ± 2.4, 51.4 ± 5.3, and 211.5 ± 24.3 nm for the 14, 50, and 200 nm SiNPs, respectively) while the hydrodynamic diameters of the particles in

the hydroponic growth medium were larger due to solvation (Figure 5.1 and Table 5.1).[27] Of note, the particles remained monodisperse in the growth medium, indicating their suitability for evaluating size-dependent phytotoxicity.

Surface charge, a parameter that influences particle stability, was evaluated by measuring the zeta potential in the plant growth medium at pH 5.8. Interestingly, the zeta potentials for the 50 and 200 nm SiNPs synthesized in-house with the Stöber method were highly negative in magnitude at -20.3 ± 0.4 and -31.9 ± 0.9 mV, respectively, while the zeta potential for the 14 nm MT-ST SiNPs was less negative (Table 5.1). The difference in measured surface charge is attributed to the synthesis and drying conditions employed during particle preparation (e.g., in-house vs. commercial). Elemental analysis (CHN) was performed to elucidate any relationship between zeta potential variation and surface composition of the particles. The 14 nm particles were characterized with a lower wt% H and C than the 50 and 200 nm SiNPs (Table 5.2). Unreacted but stable silane and silanol groups on the particle surfaces are suspected contributors to the highly negative zeta potential of the 50 and 200 nm SiNPs.

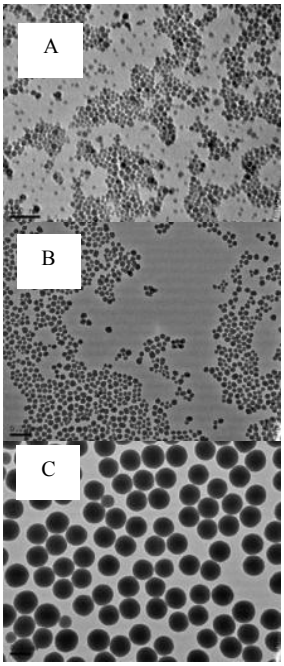

Figure 5.1 TEM of SiNPs with sizes of 14.8 ± 2 nm (A), 51.4 ± 5 nm (B), and 211.5 ± 24 nm (C). Scale bar is 100 nm (A) or 200 nm (B and C).

Table 5.1 Size and charge characterization of SiNPs via TEM, DLS, and zeta potential. Measurements were made in Hoagland's #2 nutrient solution (400 mg L^{-1}) with SiNP concentration of 250 ppm unless noted. Measurement of 14 nm SiNPs made in ethanol.[a]

	TEM Size (nm)	**DLS Size (nm)**	**Zeta Potential (mV)**
14 nm	14.8 ± 2	139.4 ± 9.6 12.4 ± 0.1[a]	-15.3 ± 1.1
50 nm	51.4 ± 5	135.2 ± 1.1	-20.3 ± 0.4
200 nm	211.5 ± 24	291.6 ± 2.3	-31.9 ± 0.9

Table 5.2 Carbon and hydrogen weight percents for unmodified and calcined SiNPs as determined by CHN analysis.

	14 nm		**50 nm**		**200 nm**	
	Unmodified	Calcined	Unmodified	Calcined	Unmodified	Calcined
% C	1.18	-0.03	3.46	-0.03	3.08	-0.05
% H	0.40	-0.05	1.28	-0.05	1.45	-0.06

5.3.1.2 Plant growth

In initial experiments, *A. thaliana* seeds were grown in solutions of 250 and 1000 ppm SiNPs (i.e., 14, 50, and 200 nm) without adjusting the pH of the growth medium. These experiments were intended to mimic an environment where the pH is not maintained at a given level. Of note, terrestrial environments often do contain buffers that influence pH of the bulk soil and root-mediated pH changes in the rhizosphere.[28, 29] In our studies, 50 and 200 nm SiNPs at 250 and 1000 ppm over 3 weeks (Figure 5.2) and 6 weeks (Figure 5.3) resulted in reduced plant development with respect to rosette diameter, biomass, and stem length. Plants exposed to 50 and 200 nm SiNPs were also chlorotic, exhibiting a yellowish color due to insufficient production of chlorophyll (Figure 5.4).[30] Compared to the larger particles, no chlorosis or reduction in growth was observed for the 14 nm SiNPs at 3 or 6 weeks for the concentrations studied. The lack of phytotoxicity for the 14 nm SiNPs may be attributed to the particles not significantly altering the pH of the growth medium, whereas the 50 and 200 nm SiNPs raised the pH over 3 units (e.g., pH 5.24, 5.98, 8.31, and 8.59 for the blank, 14, 50, and 200 nm SiNP solutions at 1000 ppm, respectively). The variation in pH over the 6 weeks for these exposure groups is provided in Supporting Information (Table 5.3). The wt% H values for the 14, 50, and 200 nm SiNPs were 0.4, 1.28, and 1.45%, respectively, corresponding to fewer silanols on the particle surface for the 14 nm SiNPs and thus a lessened capacity to alter solution pH (Table 5.2). As has been reported previously, a more basic

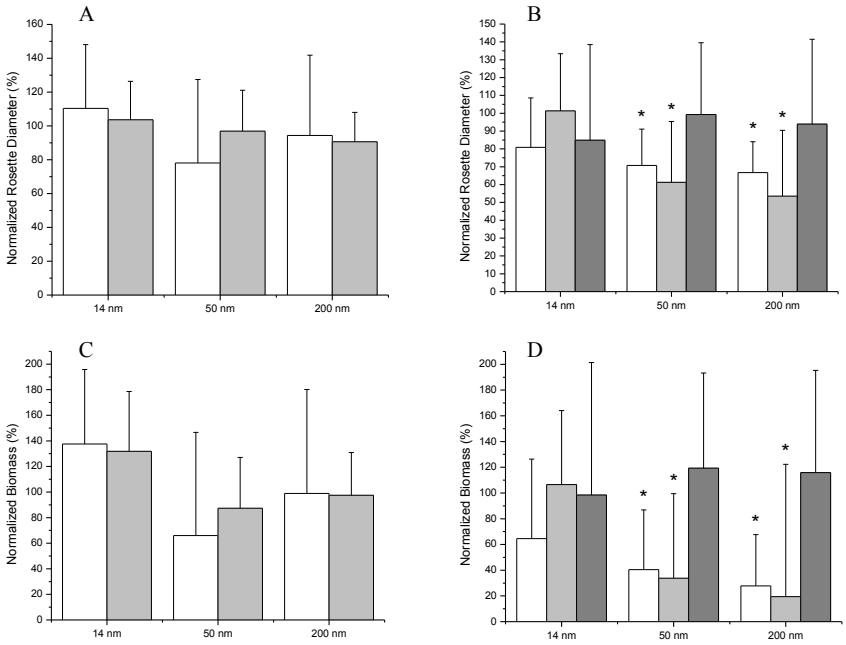

Figure 5.2 Growth data for plants harvested at 3 weeks with (A, C) pH 5.8 and (B, D) pH unadjusted after exposure to 250 ppm (white), 1000 ppm (light gray), or calcined (dark gray) SiNPs. Values are normalized to plants grown in blank solution. *Significant difference at 95% relative to blank. Of note, stems were not developed by 3 week harvest for measurement.

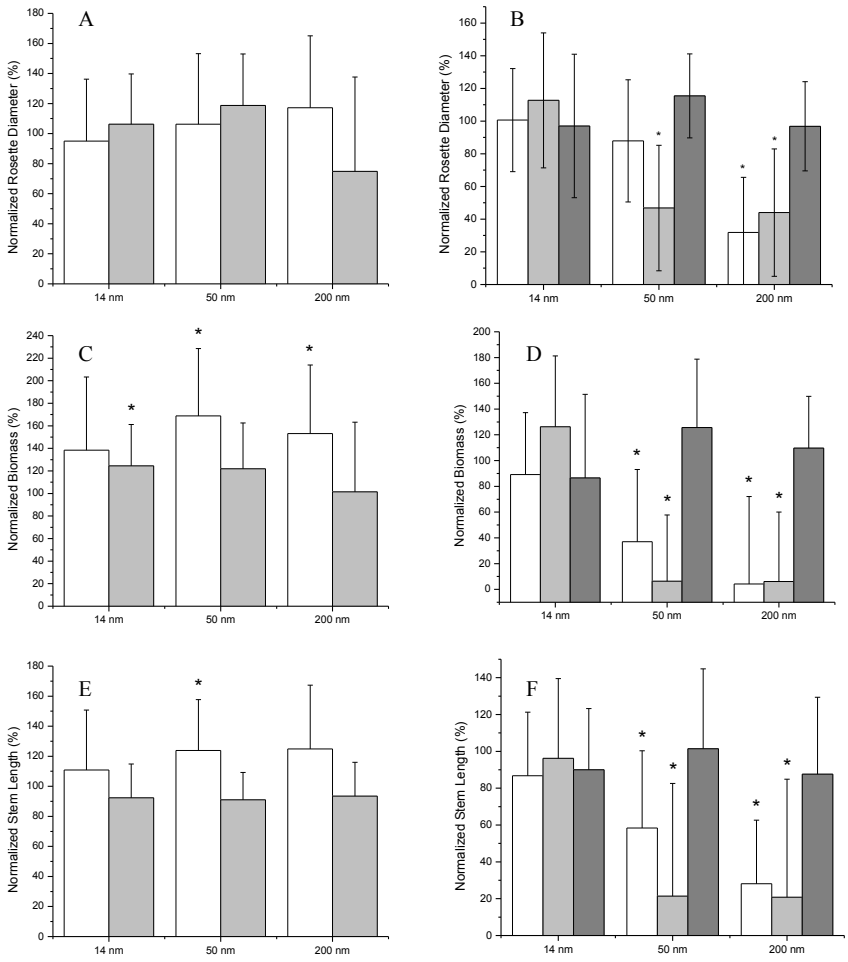

Figure 5.3 Growth data for plants harvested at 6 weeks with (A, C, E) pH 5.8 and (B, D, F) pH unadjusted after exposure to 250 ppm (white), 1000 ppm (light gray), or calcined (dark gray) SiNPs. Values are normalized to plants grown in blank solution. *Significant difference at 95% relative to blank.

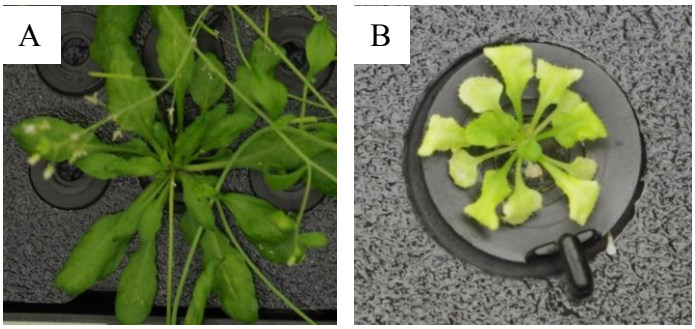

Figure 5.4 Growth after 6 weeks in (A) blank nutrient solution with no pH adjustment and (B) after exposure to 250 ppm of 200 nm SiNPs with no pH adjustment. Seed holder diameter is 2 cm.

Table5.3 Variation in pH for exposure groups where pH was not adjusted over 6 weeks. Blank exposure groups were grown in a solution of Hoagland's #2 Basal Salt Mixture (400 mg L^{-1}).

	Initial	1 Week	3 Weeks	6 Weeks
		250 ppm		
Blank	5.24	5.27	5.38	7.11
14 nm	5.67	5.51	5.26	7.4
50 nm	6.99	6.76	6.70	5.64
200 nm	7.26	7.12	6.98	6.6
		1000 ppm		
Blank	5.24	4.88	5.34	6.49
14 nm	5.98	4.91	5.40	7.05
50 nm	8.31	7.30	7.48	7.27
200 nm	8.59	7.89	7.75	7.25
		Calcined		
Blank	5.39	5.68	5.52	6.81
14 nm	6.78	6.91	6.98	7.15
50 nm	4.69	4.72	6.23	7.03
200 nm	5.19	4.41	5.32	6.38

pH may limit the availability of nutrients and result in growth deficiencies.[31] Indeed, *A. thaliana* plants grow optimally at pH 5.8 where the necessary nutrients are more biologically available for uptake.[4] To understand the role of pH on nanoparticle phytotoxicity, plants were grown at pH 8 in absence of the SiNPs. *A. thaliana* plant growth (i.e., rosette number, biomass, and length of main stem) was reduced by the more basic medium relative to the control (pH 5.8) at 3 or 6 weeks (Figure 5.5), but not to the same degree as with 50 and 200 nm SiNPs and concomitant greater pH medium. Indeed, previous reports have noted that alkaline stress (pH $\geq$ 8.0) in *Arabidopsis* can reduce root growth and begin de-polymerization of microfilaments.[30] Thus, the question was raised as to whether the observed reduction in growth for the highly negative 50 and 200 nm SiNPs could be reversed if their surface charge was mitigated by maintaining the growth medium at pH 5.8.

Arabidopsis seeds were then exposed to the same concentrations of SiNPs while maintaining the solution pH at 5.8 and we hypothesized that by holding the growth medium pH constant, plant development would be less affected due to protonation of the silanol groups on the SiNP surface. As expected, phytotoxic effects at 3 (Figure 5.2) or 6 (Figure 5.3) weeks were not observed relative to plants grown in the blank solution regardless of particle size. Furthermore, neither the rosette diameter, biomass, nor length of the main stem was reduced compared to blanks. In fact, plants showed similar flowering behavior upon maturation relative to the blanks. In some cases, the presence of the SiNPs even aided growth. At 6 weeks at pH 5.8, several of the 14, 50, and 200 nm SiNP exposure groups exhibited increased development relative to the blank.

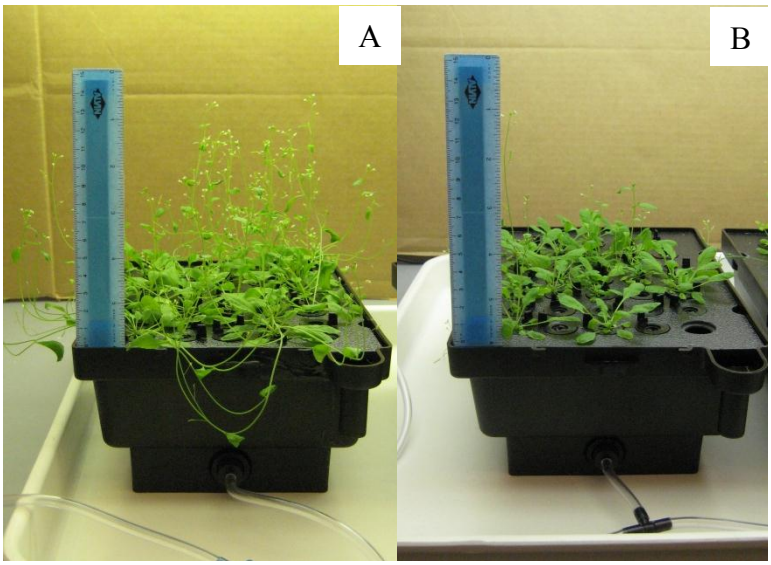

Figure 5.5 Plants grown for 6 weeks in (A) pH 5.8 nutrient solution and (B) nutrient solution adjusted to pH 8. Scale bar is 15 cm.

For example, the normalized biomass of 50 nm SiNPs at 250 ppm was 168.8 ± 59.7%. The role of silicon in plant nutrition and alleviating stress has been argued as essential, increasing the plausibility that exposure to the SiNPs strengthens plant structure.[31, 32] In total, the data suggest that allowing the pH to naturally fluctuate leads to nanoparticle phytotoxicity at 250 ppm over 3 weeks for the 50 and 200 nm SiNPs. Conversely, no toxicity is noted for even the 1000 ppm exposure groups regardless of size when pH is maintained at 5.8.

The particles were also calcined to validate that the surface charge of the 50 and 200 nm particles, rather than the SiNP scaffold itself, resulted in the observed phytotoxicity. In this method, the silica surface was dehydrated by prolonged heating at 1000 °C resulting in the removal of unreacted alkoxy silane groups and silanols while maintaining particle composition, size, and morphology.[33] To confirm that calcining the particles resulted in surface modification, the pH of each particle solution (calcined and unmodified) was measured in the growth medium at a concentration of 1000 ppm SiNPs. The pH of the calcined 14, 50, and 200 nm SiNPs was 5.74, 5.40, and 5.35, respectively, versus 5.98, 8.31, and 8.59 for the unmodified particles. As expected, calcining the SiNPs reduced pH values to within 0.2 pH units of the blank for 50 and 200 nm SiNP solutions. Removal of unreacted silane and silanol groups from the calcined SiNPs was confirmed with CHN where the wt% H and C values decreased for the calcined particles (Table 5.2).

Arabidopsis seeds were exposed to the resulting calcined SiNPs at 1000 ppm with the assumption that if no phytotoxicity were observed at the higher concentration of 1000

ppm, growth reductions would not be observed at 250 ppm. In this case, the pH of the growth medium was not adjusted to allow for comparison to the phytotoxicity of the unmodified SiNPs (50 and 200 nm) without pH adjustment. At both 3 and 6 weeks, no reduction in plant development was observed for the any of the calcined SiNP exposure groups, supporting our hypothesis that the SiNPs alone are not phytotoxic at concentrations up to 1000 ppm. Maintaining the growth medium pH at 5.8 or removing the surface charge of the SiNPs thus eliminated the SiNP toxicity (Figure 5.6).

To further confirm that the 14, 50, and 200 nm silica scaffolds themselves are not phytotoxic even in cases where high pH growth medium resulted, *Arabidopsis* plants were grown in the presence of the calcined SiNPs at 1000 ppm with the growth medium maintained at pH 8. As noted above, some reduced development for plants grown in the blank pH 8 medium was noted at 3 and 6 weeks, but the plants exposed to 1000 ppm calcined 14, 50, and 200 nm SiNPs were not significantly different from these blanks (Figure 5.7). The presence of the calcined SiNPs in the higher pH medium did not further reduce plant growth and development, validating that the SiNP scaffold is not toxic up to 1000 ppm.

We hypothesize that the observed phytotoxicity arises from a combination of the high pH of the growth medium and the ability of the negative SiNPs (i.e., 50 and 200 nm) to adsorb nutrients, making them unavailable for plant uptake.[34] Plant development problems (e.g., reduced growth and chlorosis) resulting from deficiencies of macro- (e.g., nitrogen, phosphorus, and potassium) and micro-nutrients (e.g., iron, zinc, and manganese) are well-known.[31] Silica particles with a greater number of silanols on the

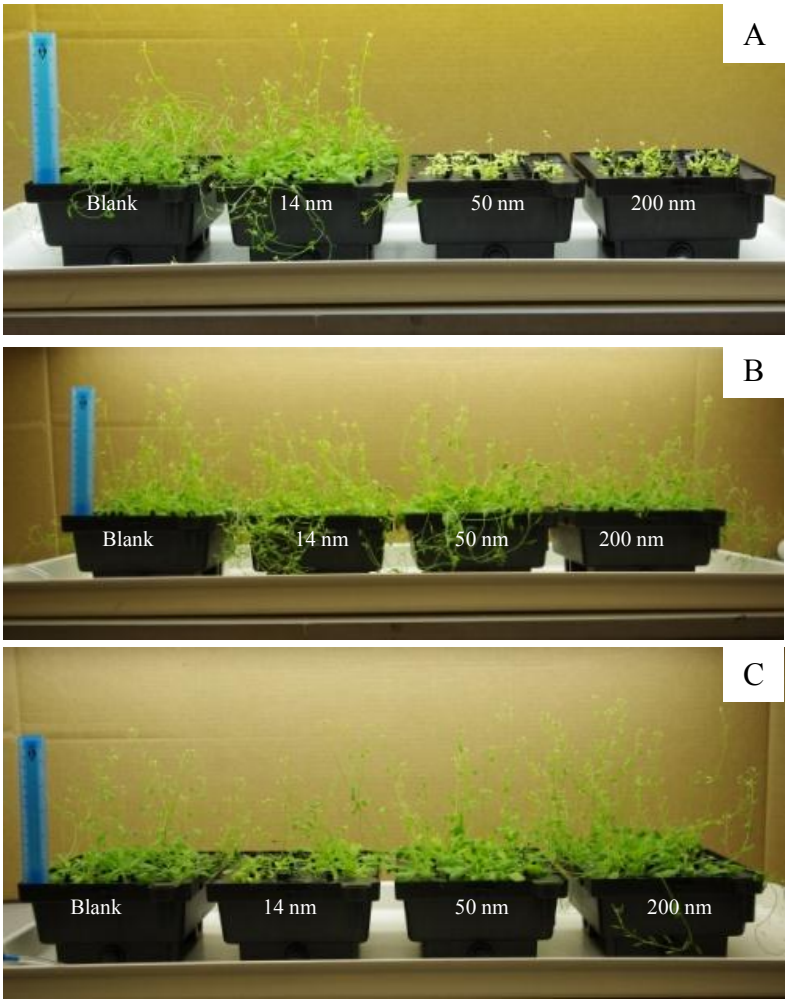

Figure 5.6 Growth of plants exposed to 1000 ppm SiNPs after 6 weeks showing development with (A) no pH adjustment; (B) pH 5.8; and (C) pH unadjusted with calcined SiNPs. Scale bar is 15 cm.

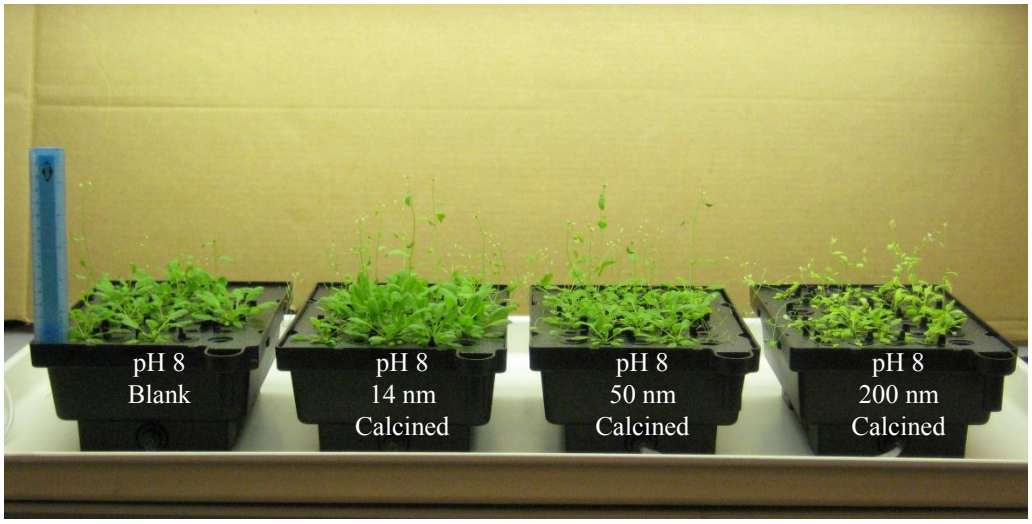

Figure 5.7 Growth of plants after 6 week exposure to 1000 ppm calcined SiNPs with growth medium maintained at pH 8. Scale bar is 15 cm.

particle surface adsorb these nutrients and restrict plant uptake, thus resulting in reduced plant growth and chlorosis.[29, 34-36] Upon adjusting the pH of the growth medium to 5.8, the nutrients adsorbed to silanols on the 50 and 200 nm particles are likely displaced by H^+ ions, making them available for uptake.[36] Likewise, the SiNPs no longer adsorb nutrients and the toxicity is eliminated when the surface charge is removed through calcination.

The results presented herein build upon prior work evaluating SiNP phytotoxicity. Characterization of the SiNP surface charge proved important since phytotoxicity, likely due to nutrient adsorption, was observed for the highly negative 50 and 200 nm SiNPs. When the silanols on the SiNPs are capable of altering the growth medium pH and/or nutrient availability, phytotoxicity may be observed at concentrations even as low as 250 ppm, a marked difference from previous work showing no reduction in *A. thaliana* growth at SiNP concentrations below 400 ppm.[4] Modifying the charge of the 50 and 200 nm SiNPs or adjusting the pH of the medium to that for favorable growth conditions resulted in no phytotoxic effects, even at exposure concentrations of 1000 ppm. Similar to Lee and Shah's report,[4, 20] we also noted cases of increased plant growth and development after exposure to 14, 50, and 200 nm SiNPs when pH effects were not a factor.

5.3.1.3 Transmission electron microscopy

Transmission electron microscopy was used to determine SiNP localization within the plant cells. Samples were exposed to the SiNPs at 1000 ppm with the growth medium maintained at pH 5.8 for a period of 6 weeks to simulate high exposure levels

and assess particle uptake for experiments that did not result in phytotoxicity. The resulting TEM images revealed that the 14, 50, and 200 nm SiNPs each were taken up into the roots of *A. thaliana* (Figures 5.8 and 5.9). Within the root cells, the SiNPs were localized in the cytoplasm of the cell surrounding organelles. Fewer particles were observed with increasing particle size as a result of fewer particles and/or the inability of the larger particles to enter the cells as readily. Of note, the TEM sizes of the particles in the roots (11.7 ± 1.4, 52.9 ± 15.7, and 162.9 ± 19.0 nm for the 14, 50, and 200 nm SiNPs, respectively) differed slightly from sizes observed in TEM micrographs taken before the exposure experiments (14.8 ± 2.4, 51.4 ± 5.3, and 211.5 ± 24.3 nm for the 14, 50, and 200 nm SiNPs, respectively; Figure 5.1). We attribute this disparity to degradation of the particles in solution (or plant) over the 6-week period. Indeed, particle sizes determined by DLS were reduced by 46.2, 23.6, and 22.3% for the 14, 50, and 200 nm SiNPs, respectively, after 6 weeks immersion in the plant nutrient solution (pH 5.8), likely indicating some SiNP dissolution. This corroborates previous results by Zhang et al. in which small NPs were found to dissolve more readily than their larger counterparts.[37] Although dissolution has been shown to increase with pH,[38] we do not believe Si dissolution to be the cause of observed phytotoxicity with the highly negative 50 and 200 nm SiNPs because the toxicity was mitigated by adjusting the pH to 5.8 or calcination. If the toxicity resulted from dissolved silicon species, a significant reduction in development would have been noted in the treatment of the *Arabidopsis* plants at pH 8 with the caclined SiNPs. In addition, Stampoulis and coworkers previously reported that bulk Si powder (1000 ppm) was non-toxic to *Cucurbita pepo* (zucchini).[19]

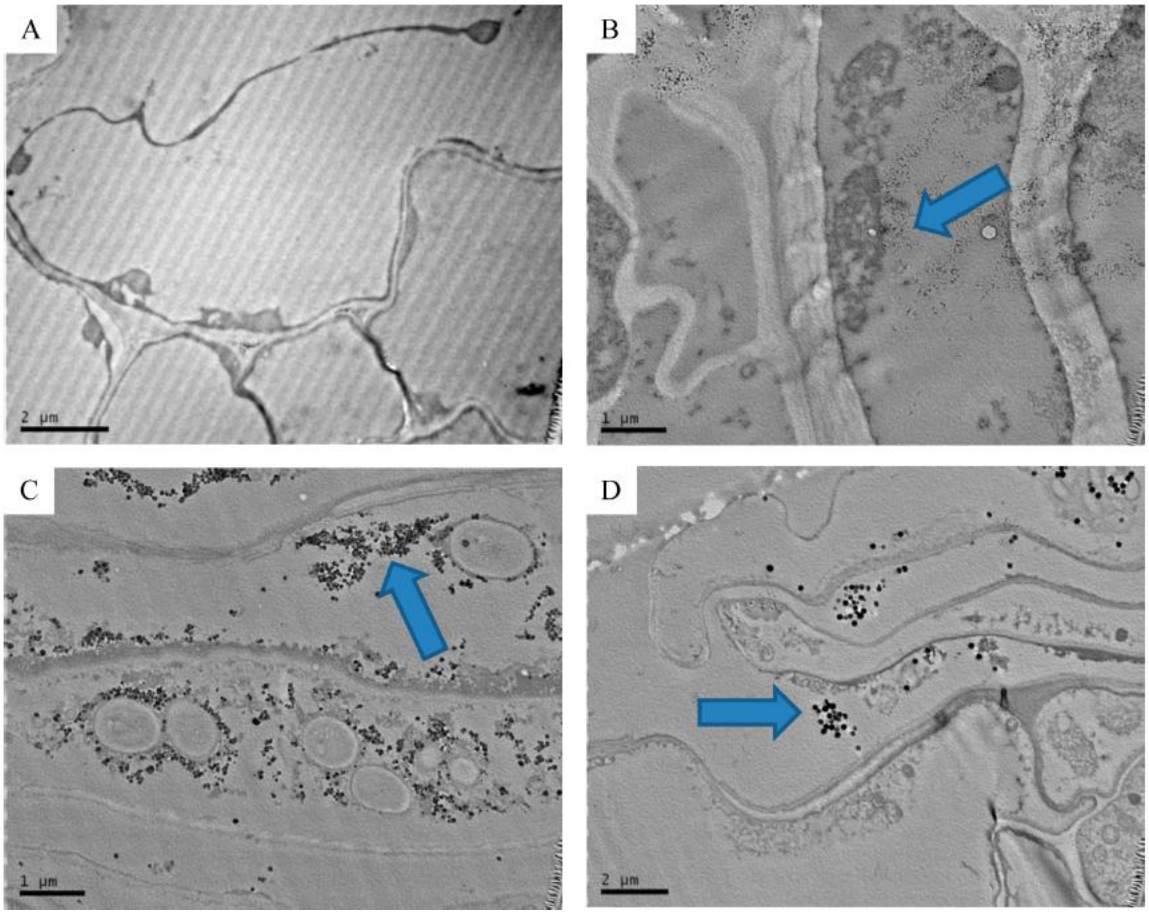

Figure 5.8 Transmission electron microscopy images of roots from (A) blank solution and from 1000 ppm exposure after 6 weeks with SiNP sizes of (B) 14 nm; 14 kx magnification; (C) 50 nm; 29 kx; and (D) 200 nm; 14 kx. Arrows point to SiNPs in each image.

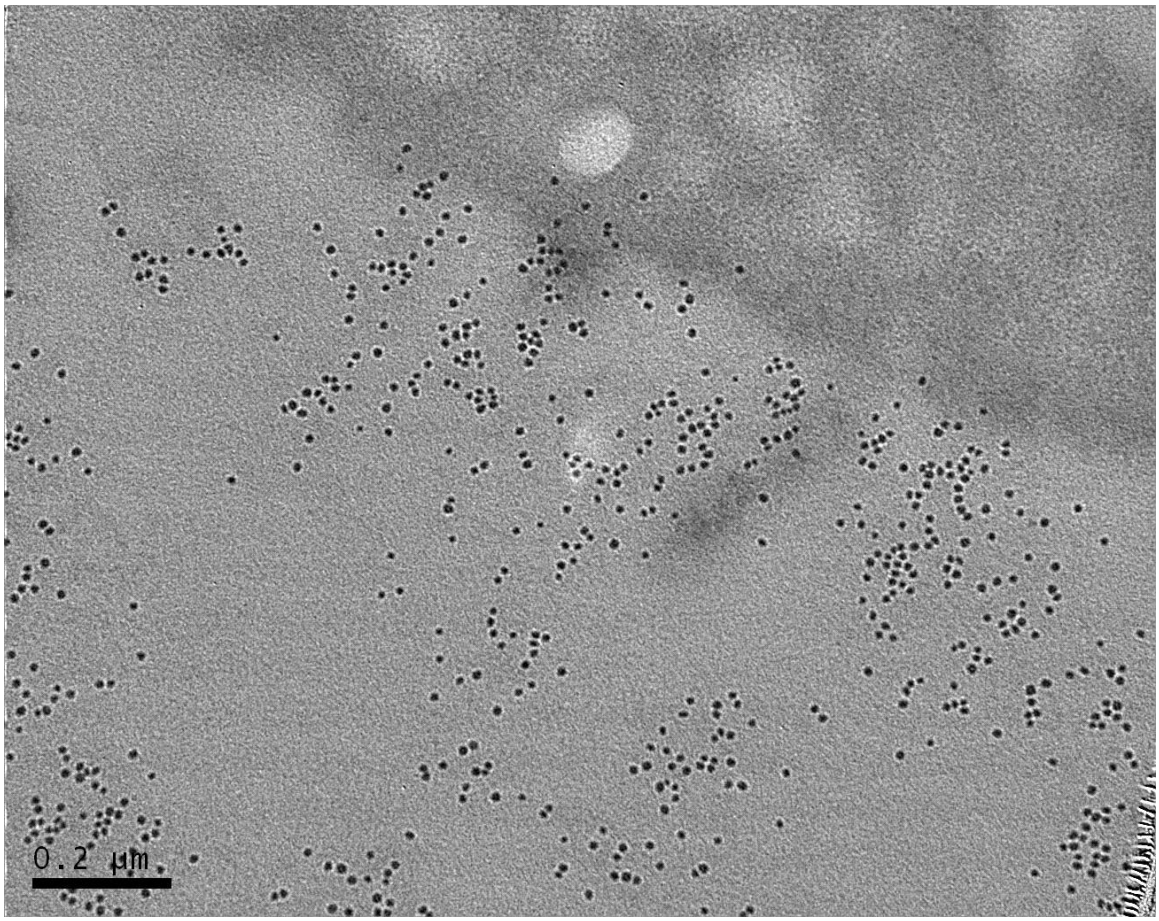

Figure 5.9 Transmission electron microscopy image of roots from 1000 ppm exposure to 14 nm SiNPs after 6 weeks. Magnification is 72 kx and scale bar is 0.2 µm.

Lastly, sections of the leaves and stems exposed to SiNPs during plant growth were examined with TEM to ascertain particle localization. No nanoparticles were visible in the leaves and stems examined, a potentially anticipated result since the leaves and stems do not come into direct contact with the nanoparticle solution and should therefore have a lower distribution of the SiNPs than the roots.

5.3.1.4 Silicon elemental analysis

Silicon (Si) elemental analysis was carried out to provide a more quantitative understanding of particle uptake and interaction with *A. thaliana*. Silicon content was expected to be greatest in the roots since they were directly exposed to the SiNP solution. If possible, the SiNPs would then translocate to the leaves of the rosette and finally into the stem.

Prior to analysis, the optimal conditions for complete digestion of the plants and SiNPs were determined. Plant tissue was first digested with 10% (v/v) HNO_3 in a microwave accelerated reaction system.[39] Initial ICP-OES experiments showed that concentrated HNO_3 alone did not completely dissolve the SiNPs and as a result, we explored other digestion protocols. The combination of aqua regia and hydrofluoric acid (HF) has been used previously to dissolve coal fly ash, a material with high silica content.[40] However, we observed surprisingly large Si readings for our blank calibration sample (a solution of HNO_3, aqua regia, and HF in water) under these acidic conditions, which we could only attribute to the hydrofluoric acid. The large Si readings from the calibration blank result from HF reaction with the quartz ICP torch, necessitating a neutralization step to remove excess HF.[41] Triethanolamine, an organic base, was used to

neutralize the HF instead of boric acid to avoid etching of the ICP torch. Digestion of the SiNPs in solution was concluded complete when recovered Si levels (via ICP-OES) approached the theoretical Si content based on SiNP mass analyzed (Equation 5.1).

Silicon in the plants was then quantified by ICP-OES. As expected, plants exposed to SiNPs exhibited increased Si levels relative to plants grown in blank hydroponic solutions (Tables 5.4 and 5.5). The Si concentrations observed in the roots and rosettes were greater than in the stems, likely due to the minimal translocation of the SiNPs into the stem. This observation corroborates the lack of particles found in the stems via TEM. Due to limited sample mass and nontrivial solution preparation, the silicon elemental analysis data was determined using a single SiNP exposure treatment, with 3 replicate analyses from the ICP-OES.

The data was subsequently normalized to depict SiNP uptake per unit of nanoparticle volume and determine the extent of particle uptake as a function of SiNP size (Tables 5.6 and 5.7). Using the particle sizes from TEM data (Table 5.1), the nanoparticle volumes were determined to be 1.70×10^3, 7.11×10^4, and 4.95×10^6 nm^3 for the 14, 50, and 200 nm SiNPs, respectively. As expected, increased uptake of the smaller, 14 nm particles was observed upon normalizing the data relative to the 50 and 200 nm particles for all exposure conditions. Overall, these results indicate that the 14, 50, and 200 nm SiNPs are in fact taken up through the root system of *A. thaliana*, followed by translocation into the rosette and stem in a size-dependent manner.

The extent of SiNP uptake was also analyzed as a function of SiNP charge and exposure concentration. Although the charges of the 50 and 200 nm SiNPs were

Equation 5.1 Equation for determining theoretical Si content from known SiNP concentration.

$$\text{Theoretical Si Content} = \text{Original SiNP Concentration} \times 0.467^{a} \times \%\,SiO_2{}^{b}$$

[a] Mass % Si in SiO_2

[b] Obtained by subtracting organic content determined with CHN

Table 5.4 Silicon determination in roots, rosette, and stems for 250 ppm exposure group after 6 weeks using ICP-OES. Results are reported in mg Si per kg plant tissue. Error represents variation between three instrument integrations.

	Blank		**14 nm**		**50 nm**		**200 nm**	
Sample	pH 5.8	pH unadjusted	pH 5.8	pH unadjusted	pH 5.8	pH unadjusted	pH 5.8	pH unadjusted
Roots (mg Si/ kg tissue)	378 ± 14	1045 ± 8	43, 992 ± 939	47,575 ± 291	70,442 ± 176	26,384 ± 49	60,217 ± 482	71,186 ± 671
Rosette (mg Si/ kg tissue)	168 ± 9	112±13	890 ± 10	412 ± 5	737 ± 9	1,087 ± 15	1,242 ± 3	3,143 ± 34
Stem (mg Si/ kg tissue)	84 ± 2	58 ± 3	123 ± 3	119 ± 2	300 ± 2	342 ± 6	94 ± 2	1,759 ± 53

Table 5.5 Silicon determination in roots, rosette, and stems for 1000 ppm exposure group after 6 weeks using ICP-OES. Results are reported in mg Si per kg plant tissue. Error represents variation between three instrument integrations.

	Blank		**14 nm**		**50 nm**		**200 nm**	
Sample	pH 5.8	pH unadjusted	pH 5.8	pH unadjusted	pH 5.8	pH unadjusted	pH 5.8	pH unadjusted
Roots (mg Si/ kg tissue)	483 ± 3	418 ± 26	54,281 ± 424	32,297 ± 139	131,515 ± 815	115,528 ± 209	37,267 ± 232	68,000 ± 396
Rosette (mg Si/ kg tissue)	72 ± 3	138 ± 5	707 ± 11	1,316 ± 17	1,084 ± 35	1,746 ± 7	2,244 ± 22	3,564 ± 81
Stem (mg Si/ kg tissue)	66 ± 3	92 ± 2	280 ± 7	200 ± 1	344 ± 1	2,538 ± 5	394 ± 3	3,109 ± 59

Table 5.6 Si determination in roots, rosette, and stem for 250 ppm exposure group after 6 weeks using ICP-OES. Results are normalized for the nanoparticle volume.

	14 nm		50 nm		200 nm	
Sample	pH 5.8	pH unadjusted	pH 5.8	pH unadjusted	pH 5.8	pH unadjusted
Roots (mg Si·kg tissue^{-1}/nm^3)	25.9 ± 0.6	28.0 ± 0.2	9.90 x 10^{-1} ± 0.002	3.70 x 10^{-2} ± 7.0 x 10^{-4}	1.20 x 10^{-2} ± 1.0 x 10^{-4}	1.40 x 10^{-2} ± 1.0 x 10^{-4}
Rosette (mg Si·kg tissue^{-1}/nm^3)	5.20 x 10^{-1} ± 0.01	2.4 x 10^{-1} ± 0.003	1.00 x 10^{-2} ± 1.0 x 10^{-4}	2.00 x 10^{-2} ± 2.0 x 10^{-4}	3.00 x 10^{-4} ± 6.1 x 10^{-7}	6.00 x 10^{-4} ± 7.0 x 10^{-6}
Stem (mg Si·kg tissue^{-1}/nm^3)	7.00 x 10^{-2} ± 0.002	0.07 x 10^{-2} ± 0.001	4.00 x 10^{-3} ± 3.0 x 10^{-5}	4.00 x 10^{-3} ± 3.0 x 10^{-5}	2.00 x 10^{-5} ± 4.0 x 10^{-7}	4.00 x 10^{-4} ± 1.0 x 10^{-5}

Table 5.7 Si determination in roots, rosette, and stem for 1000 ppm exposure group after 6 weeks using ICP-OES. Results are normalized for the nanoparticle volume.

	14 nm		**50 nm**		**200 nm**	
Sample	pH 5.8	pH unadjusted	pH 5.8	pH unadjusted	pH 5.8	pH unadjusted
Roots (mg Si·kg tissue^{-1}/nm^3)	32.0 ± 0.3	19.0 ± 0.1	1.85 ± 0.01	1.62 ± 0.003	$7.00 \times 10^{-3} \pm 5.0 \times 10^{-5}$	$1.40 \times 10^{-2} \pm 8.0 \times 10^{-5}$
Rosette (mg Si·kg tissue^{-1}/nm^3)	$4.20 \times 10^{-1} \pm 0.01$	$7.80 \times 10^{-1} \pm 0.01$	$2.00 \times 10^{-2} \pm 5.0 \times 10^{-4}$	$2.00 \times 10^{-2} \pm 1.0 \times 10^{-4}$	$4.00 \times 10^{-4} \pm 4.0 \times 10^{-6}$	$7.00 \times 10^{-4} \pm 2.0 \times 10^{-5}$
Stem (mg Si·kg tissue^{-1}/nm^3)	$1.60 \times 10^{-1} \pm 0.004$	$1.10 \times 10^{-1} \pm 5.0 \times 10^{-4}$	$5.00 \times 10^{-3} \pm 1.0 \times 10^{-5}$	$4.00 \times 10^{-2} \pm 7.0 \times 10^{-5}$	$8.00 \times 10^{-5} \pm 6.0 \times 10^{-7}$	$6.00 \times 10^{-4} \pm 1.0 \times 10^{-5}$

significantly negative (Table 5.1) and resulted in phytotoxicity when the pH of the medium was not controlled, for the most part SiNP uptake was not significantly different in plants where the pH was maintained at pH 5.8 (Tables 5.4 and 5.5). Likewise, charge did not readily influence uptake of the 14 nm SiNPs. While an increase in SiNP uptake was observed upon increasing exposure concentration from 250 to 1000 ppm, this trend was not linear. The non-linear increase suggests that there is an upper limit to the degree of SiNP uptake in the *Arabidopsis* plant.

Generally, plant biologists believe that cellular uptake of particles less than ~300 nm involves endocytosis.[42] The idea of nanoparticle endocytosis in plant cells was originally dismissed because of the high turgor pressure in plant cells combined with the presence of the rigid cell wall hindering internalization. Rather, it was believed that nanoparticles must passively pass through cell wall pores (<50 nm).[43] As such, many studies excluded nanomaterials larger than ~20 nm.[44] Recent research has shown that plant cells are able to endocytose matter from the extracellular environment in a process resembling mammalian cell endocytosis.[42] Indeed, plant cells can bioaccumulate nanomaterials including single-walled carbon nanotubes (length <500 nm),[45] magnetite NPs (40 nm),[46] Cu NPs (50 nm),[5] and tannate-coated gold NPs (10–50 nm).[47] *A. thaliana*, specifically, has been shown to take up ultrasmall anatase TiO_2[48] (<5 nm) and AgNPs[49] (20 and 40 nm). However, other nanomaterials (e.g., CdSe/ZnS quantum dots[8]) are not internalized indicating somewhat selective bioaccumulation.

Uptake of SiNPs into plants cells has also been previously observed. For example, mesoporous silica nanoparticles have been shown to penetrate tobacco mesophyll plant

cells and facilitate intracellular delivery of DNA.[50] Accumulation of FITC-labeled SiNPs in rice seedlings represents a future use for SiNPS in biolabeling of plant cells.[21] Similarly, our work has shown that a range of SiNPs (i.e., 14–200 nm) will accumulate in *A. thaliana* root cells in a size-dependent manner, although translocation to other regions of the plant is minimal. Future studies should focus on understanding the endocytic pathway for SiNP internalization, identifying possible translocation mechanisms that enable movement of the SiNPs to other regions of the plant, and determine whether uptake is species dependent.

5.3.2 Shape-dependent phytotoxicity and uptake

5.3.2.1 Synthesis and characterization of silica nanoparticles with varied shape

Given the size-dependent uptake of silica nanoparticles in *A. thaliana*, the potential for shape-dependent SiNP phytotoxicity and uptake was also evaluated. A surface-templated method was utilized to synthesize both spherical (AR1) and rod-like (AR3) particles. The AR1 particles exhibited a length and width of ~ 62 ± 8 nm, while the AR3 particles exhibited a length of 241± 32 nm and width of 78 ± 6 nm (Figure 5.10). Despite the varied aspect ratios of the AR1 and AR3 SiNPs, they were appropriate candidates for examining shape-dependent effects since they had similar particle volume (~10^6 nm^3) and thus similar interaction volume with the plant cells.

5.3.2.2 Plant growth

Based on the previous studies with SiNPs of varied size (i.e., 14–200 nm), *A. thaliana* plants were grown in the presence of AR1 and AR3 particles at a concentration of 250 ppm for 6 weeks. The nutrient solution was maintained at pH 5.8 to mitigate any

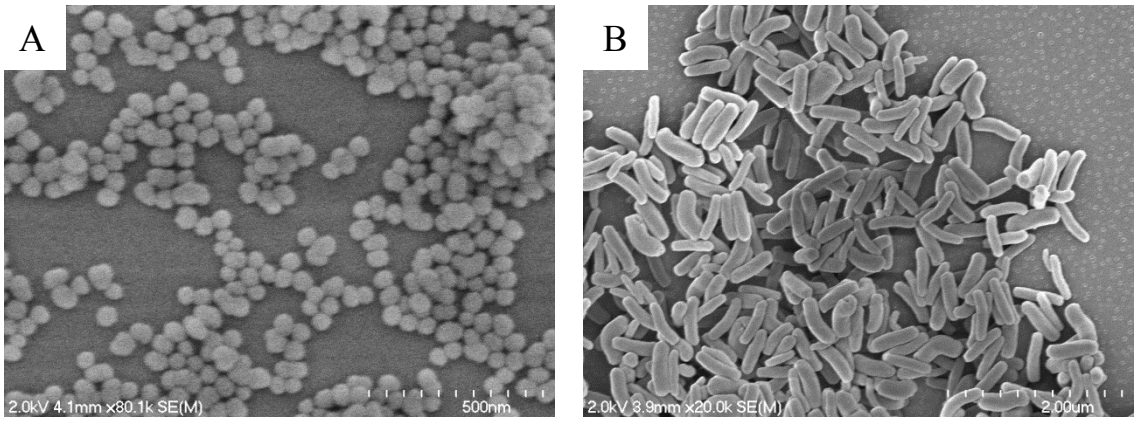

Figure 5. 10 Scanning electron micrographs of (A) AR1 and (B) AR3 silica particles. Scale bar is 500 nm (A) or 2 μm (B).

potential silanol effects. Plants exposed to the AR1 particles exhibited some reduced development, with biomass and rosette diameters of 52 ± 24 and 77 ± 18% relative to plants grown in blank nutrient solution, respectively. However, the stem length for plants exposed to the AR1 particles was similar to blanks (88 ± 25% normalized to blank). For the AR3 particles, neither the biomass, rosette diameter, nor length of the main stem was reduced compared to blanks (84 ± 64, 101 ± 40, 77 ± 45% normalized to blank). Plants grown in the presence of AR1 and AR3 particles were non-chlorotic and showed similar flowering behavior upon maturation. Thus, although the AR1 particles exhibited some growth reduction at 250 ppm over the 6 weeks, they were not deemed toxic. Overall, a significant dependence of shape on phytotoxicity was not observed.

5.3.2.3 Transmission electron microscopy

Shape-dependent uptake of the AR1 and AR3 particles was subsequently examined with TEM. Root samples from plants exposed to the AR1 or AR3 particles were prepared according to the aforementioned protocol. As shown in Figure 5.11, the AR1 particles were observed in the root cells, while there was no indication for AR3 particle uptake. The lack of AR3 particle uptake is not surprising given the lower exposure concentration, plant cell wall barrier, and the increased length (i.e., 241 ± 32 nm) of the AR3 particles.[32] Of note, some dissolution of the AR1 particles (~35%) was observed over the 6 week exposure based on TEM images.

5.3.2.4 Silicon elemental analysis

Silicon elemental analysis of the plant tissue (i.e., roots, rosette, stem) was employed to quantitatively determine any uptake of the AR1 and AR3 silica particles.

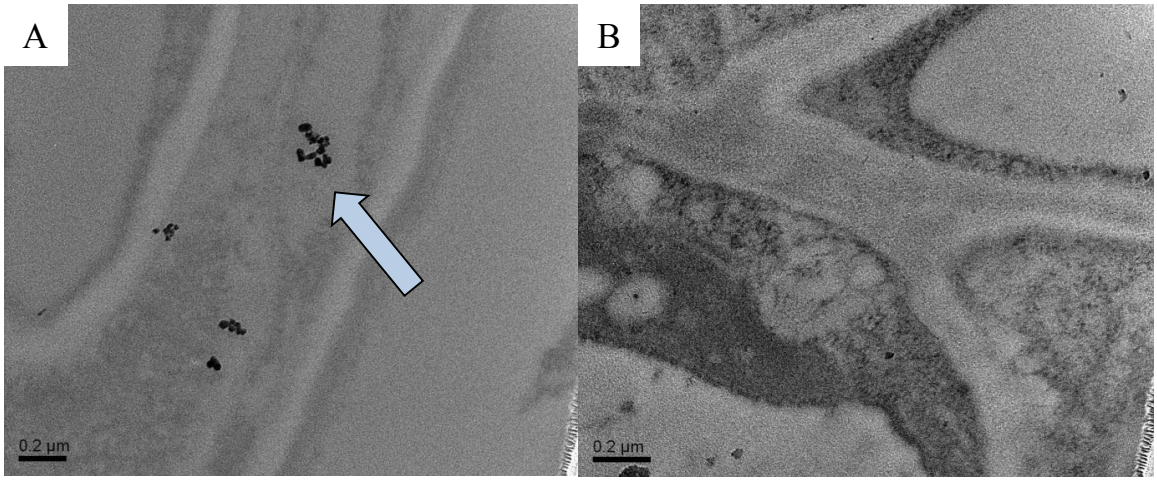

Figure 5.11 Transmission electron micrographs of root cells after exposure to 250 ppm (A) AR1 or (B) AR3 particles. Scale bar is 0.2 µm. Arrow points to AR1 particles.

Analysis via ICP-OES confirmed little uptake of these particles into the plant roots, rosettes, or stems using the conditions studied (Table 5.8). However, silicon measurements for the blanks were also lower than previous experiments with similar growth conditions (e.g., 4 ± 3 vs. 378 ± 14 mg Si/kg plant tissue). Future experiments should examine increased exposure concentrations for the AR1 and AR3 particles to see if uptake is concentration dependent, while also utilizing more biomass for ICP-OES analysis.

5.4 Conclusions

The results suggest that SiNPs will not exhibit significant phytotoxicity upon mitigating any pH effects and/or silanol-nutrient adsorption, although significant uptake of smaller SiNPs (e.g., 14 and 50 nm) into the plant is still likely. Any pH-dependent phytotoxic effects of the SiNPs are expected to be further reduced in terrestrial environments where natural buffers aid in maintaining an ideal pH for plant growth.[29] Although nanoparticle shape has been shown to have significant influence over particle–cell adhesion strength, internalization rate, and toxicity in mammalian cell drug delivery,[33] the presence of a cell wall reduces the likelihood of uptake for plants.[32] However, nanoparticles of varied shape can be delivered to plant cells via bombardment strategies and continued evaluation of phytotoxicity is thus warranted.[34] With respect to terrestrial environments, soil provides a large reactive sink for nanoparticles, and thus the applied dose employed in our study is greater than doses that may reach soil-based organisms.[7] Notwithstanding, nanoparticles will undergo dissolution, sorption/aggregation, and migration in real environments. For those nanoparticles that

Table 5.8 Silicon determination in roots, rosette, and stems for 250 ppm exposure to AR1 and AR3 particles after 6 weeks using ICP-OES. Results are reported in mg Si per kg plant tissue. Error represents variation between three instrument integrations.

Sample	Roots (mg Si/kg tissue)	Rosette (mg Si/kg tissue)	Stem (mg Si/kg tissue)
Blank	4.4 ± 3.1	0.2 ± 0.1	0.3 ± 0.1
AR1	4.8 ± 0.2	0.5 ± 0.1	0.0 ± 0.1
AR3	0.6 ± 0.5	1.2 ± 0.1	1.1 ± 0.4

remain bioavailable in the soil, future work should focus on entry modes and mechanisms into the terrestrial food chain while continuing to evaluate phytotoxicity and potential biomagnification.

REFERENCES

1. Alvarez, P. J., Nanotechnology in the environment - The good, the bad, and the ugly. *J*. *Envir*. *Engrg*. **2006**, *132*, 1233.

2. Navarro, E. B., A.; Behra, R.; Hartmann, N. B.; Filser, J.; Miao, A.; Quigg, A.; Santschi, P.H.; Sigg, L., Environmental behavior and ecotoxicity of engineered nanoparticles to algae, plants, and fungi. *Ecotoxicol*.**2008**, *17*, 372-386.

3. Alexiou, C. J., R.; Schmid R.; Hilpert, A.; Bergemann, C.; Parak, F.; Iro, H., In vitro and in vivo investigation of targeted chemotherapy with magnetic nanoparticles. *J*. *Magn*. *Magn*. *Mater*. **2005**, *293*, 389-393.

4. Lee, C. W. M., S.; Zodrow, K.; Li, D.; Tsai, Y.; Braam, J.; Alvarez, P. J. J. , Developmental phytotoxicity of metal oxide nanoparticles to *Arabidopsis thaliana*. *Environ*. *Toxicol*. *Chem*. **2010**, *29*, 669-675.

5. Lee, W.; An, Y.; Yoon, H.; Kweon, H., Toxicity and bioavailability of copper nanoparticles to the terrestrial plants mung bean (*Phaseolus radiatus*) and wheat (*Triticum aestivum*): Plant agar test for water-insoluble nanoparticles. *Environ*. *Toxicol*. *Chem*. **2008**, *27*, 1915-1921.

6. Peralta-Videa, J. R. Z., L.; Lopez-Moreno, M. L.; de la Rosa, G.; Hong, J.; Gardea-Torresdey, J.L., Nanomaterials and the environment: A review for the biennium 2008-2010. *J*. *Hazard*. *Mater*. **2011**, *186*, 1-15.

7. Klaine, S. J. A., P. J. J.; Batley, G. E.; Fernandes, T. F.; Handy, R. D.; Lyon, D. Y.; Mahendra, S.; McLaughlin, M. J.; Lead, J. R., Nanomaterials in the environment: Behavior, fate, bioavailability, and effects. *Environ*. *Toxicol*. *Chem*. **2008**, *27*, 1825-1851.

8. Navarro, D. A. B., M. A.; Aga, D. S., Investigating uptake of water-dispersible CdSe/ZnS quantum dot nanoparticles by *Arabidopsis thaliana* plants. *J*. *Hazard*. *Mater*. **2012**, *211-212*, 427-435.

9. Lin, D.; Xing, B., Root uptake and phytotoxicity of ZnO nanoparticles. *Environ*. *Sci*. *and Technol*. **2008**, *42*, 5580-5585.

10. Yin, L. C., Y.; Espinasse, B.; Colman, B. P.; Auffan, M.; Wiesner, M.; Rose, J.; Liu, J.; Bernhardt, E. S. , More than the ions: The effects of silver nanoparticles on *Lolium multiflorum*. *Environ*. *Sci*. *and Technol*. **2011**, *45*, 2360-2367.

11. Parsons, J. G. L., M. L.; Gonzalez, C. M.; Peralta-Videa, J. R.; Gardea-Torresdey, J. L., Toxicity and biotransformation of uncoated and coated nickel hydroxide nanoparticles on mesquite plants. *Environ*. *Toxicol*. *Chem*. **2010**, *29*, 1146-1154.

12. Lopez-Moreno, M. L.; de la Rosa, G.; Hernandez-Viezcas, J. A.; Peralta-Videa, J. R.; Gardea-Torresdey, J. L., X-ray absorption spectroscopy (XAS) corroboration of the uptake and storage of CeO_2 nanoparticles and assessment of their differential toxicity in four edible plant species. *J*. *Agric*. *Food Chem*. **2010**, *58*, 3689-3693.

13. Rico, C. M.; Majumdar, S.; Duarte-Gardea, M.; Peralta-Videa, J. R.; Gardea-Torresdey, J. L., Interaction of nanoparticles with edible plants and their possible implications in the food chain. *J*. *Agric*. *Food Chem*. **2011**, *59*, 3485-3498.

14. Xu, H. Y., F.; Monson, E. E.; Kopelman, R., Room-temperature preparation and characterization of polyethylene-glycol coated silica nanoparticles for biomedical applications. *J*. *Biomed*. *Mater*. *Res*., *Part A* **2003**, *66A*, 870-879.

15. Anselmann, R., Nanoparticles and nanolayers in commercial applications. *J*. *Nanopart*. *Res*. **2001**, *3*, 329-336.

16. Meyer, D. E.; Curran, M. A.; Gonzalez, M. A., An examination of existing data for the industrial manufacture and use of nanocomponents and their role in the life cycle impact of nanoproducts. *Environ*. *Sci*. *and Technol*. **2009**, *43*, 1256-1263.

17. Hoecke, K. V.; de Schamphelaere, K. A. C.; van der Meeren, P.; Lucas, S.; Janssen, C. R., Ecotoxicity of silica nanoparticles to the green alga *Psuedokirchneriella subcapitata*: Importance of surface area *Environ*. *Toxicol*. *Chem*. **2008**, *27*, 1948-1957.

18. Wei, C. Z., Y.; Guo, J.; Han, B.; Yang, X.; Yuan, J., Effects of silica nanoparticles on growth and photosynthetic pigment contents of *Scenedesmus obliquus*. *J*. *Envir*. *Sci*. **2010**, *22*, 155-160.

19. Stampoulis, D. S., S.; White, J., Assay-dependent phytotoxicity of nanoparticles to plants. *Environ*. *Sci*. *and Technol*. **2009**, *43*, 9473-9479.

20. Shah, V. B., I., Influence of metal nanoparticles on the soil microbial community and germination of lettuce seeds. *Water, Air, Soil, Pollut*. **2009**, *197*, 143-148.

21. Nair, R. P., A. C.; Nagaoka, Y.; Yoshida, Y.; Maekawa, T.; Kumar, D. S., Uptake of FITC-labeled silica nanoparticles and quantum dots by rice seedlings: Effects on seed germination and their potential as biolabels for plants. *J*. *Fluorescence* **2011**, *21*, 2057-2068.

22. Ma, X.; Geiser-Lee, J.; Deng, Y.; Kolmakov, A., Interactions between engineered nanoparticles (ENPs) and plants: Phytotoxicity, uptake and accumulation. *Sci. Total Environ*. **2010**, *408*, 3053-3061.

23. Bogush, G. H.; Tracy, M. A.; Zukoski Iv, C. F., Preparation of monodisperse silica particles: Control of size and mass fraction. *J. Non-Cryst. Solids* **1988**, *104*, 95-106.

24. Lu, Y.; Slomberg, D. L.; Sun, B.; Schoenfisch, M. H., Shape- and nitric oxide flux-dependent bactericidal activity of nitric oxide-releasing silica nanorods. *Small* **2013**, *9*, 2189-2198.

25. Tocquin, P.; Corbesier, L.; Havelange, A.; Pieltain, A.; Kurtem, E.; Bernier, G.; Périlleux, C., A novel, high efficiency, low maintenance, hydroponic system for synchronous growth and flowering of *Arabidopsis thaliana*. *BMC Plant Biol*. **2003**, *3*.

26. Araponics: hydroponic growing system for *Arabidopsis thaliana*. http://www.araponics.com/products.php. (accessed December 7, 2009).

27. Xu, R., Shear plane and hydrodynamic diameter of microspheres in suspension. *Langmuir* **1998**, *14*, 2593-2597.

28. Hinsinger, P.; Plassard, C.; Tang, C.; Jaillard, B., Origins of root-mediated pH changes in the rhizosphere and their responses to environmental constraints: A review. *Plant Soil* **2003**, *248*, 43-59.

29. Magdoff, F. R.; Bartlett, R. J., Soil pH buffering revisited. *Soil Sci. Soc. Am. J*. **1985**, *49*, 145-148.

30. Taiz, L. Z., E., *Plant Physiology*. 3rd ed.; Sinauer: Sunderland, MA, 2002.

31. Van Patten, G. F., *Hydroponics Basics*. Van Patten Publishing: 2004.

32. Martin-Ortigosa, S.; Valenstein, J. S.; Sun, W.; Moeller, L.; Fang, N.; Trewyn, B. G.; Lin, V. S.-Y.; Wang, K., Parameters affecting the efficient delivery of mesoporous silica nanoparticle materials and gold nanorods into plant tissues by the biolistic method. *Small* **2012**, *8*, 413-422.

33. Champion, J. A.; Katare, Y. K.; Mitragotri, S., Particle shape: a new design parameter for micro-and nanoscale drug delivery carriers. *J. Controlled Release* **2007**, *121*, 3-9.

34. Taylor, N. J.; Fauquet, C. M., Microparticle bombardment as a tool in plant science and agricultural biotechnology. *DNA Cell Biol*. **2002**, *21*, 963-977.

CHAPTER 6: SUMMARY AND FUTURE DIRECTIONS

6.1 Summary

Nanomaterial physicochemical properties (e.g., size, shape, surface hydrophobicity, drug-release kinetics) were shown to influence association/fate and toxicity in both bacterial pathogens and terrestrial plants. Chapter 1 reviewed the rising societal use of nanomaterials and addressed the importance of understanding the impact of nanomaterial properties on cellular interaction and toxicity, whether deemed beneficial (e.g., bacterial pathogen killing) or detrimental (e.g., plant death). The design of NO-releasing silica nanoparticles, dendrimers, and chitosan oligosaccharides with controlled size, shape, surface hydrophobicity, molecular weight, and NO-release kinetics was discussed for the eradication of clinically-relevant planktonic bacteria and biofilms. The effects of nanomaterial properties (e.g., composition, size, shape) on phytotoxicity toward terrestrial plants were also presented. Overall, the introduction served to address the challenges in evaluating engineered nanomaterial toxicity to biological systems.

In Chapter 2, nanomaterial (i.e., silica nanoparticle, dendrimer, chitosan) properties (e.g., size, shape, exterior functionality, and molecular weight) were found to significantly impact planktonic bacterial killing. Nitric oxide-releasing silica nanoparticles of three different sizes (i.e., 50, 100, and 200 nm) and similar total NO storage were utilized to evaluate biocidal action against *P. aeruginosa* as a function of

nanoparticle size. Particles with decreased size exhibited increased bactericidal efficacy due to improved nanoparticle–cell association. The shape (i.e., aspect ratio) of NO-releasing silica nanoparticles also proved important in the killing of planktonic *P. aeruginosa* and *S. aureus*. Particles with increased aspect ratio (i.e., 8) had lower MBCs than particles with aspect ratios of 1 or 4 due to enhanced NO delivery, likely from increased particle surface area in contact with the cell.

Killing of planktonic *P. aeruginosa* and *S. aureus* was also demonstrated for NO-releasing PPI dendrimers as a function of exterior functionality and size (i.e., generation). The higher generation NO-releasing dendrimers (5 versus 2) exhibited increased biocidal action due to a greater concentration of *N*-diazeniumdiolates at the dendrimer surface. Additionally, NO-releasing-dendrimers modified with the more hydrophobic SO group exhibited lower MBCs than those functionalized with PO or PEG as a result of improved electrostatic interactions with the bacterial cell membrane.

Lastly, the bactericidal efficacy of NO-releasing chitosan oligosaccharides was evaluated against *P. aeruginosa* as a function of molecular weight and exterior functionality. Of the three NO-releasing chitosan oligosaccharide molecular weights (i.e., 2.5k, 5k, and 10k) examined, no significant differences in planktonic killing were observed. Rapid association of the positively-charged chitosan with the negatively-charged bacterial cell membrane likely occurred independent of any potential molecular weight-related diffusion limitations. Similar to observations with the NO-releasing PPI dendrimers, the more neutral PEG-modified NO-releasing chitosan oligosaccharides

exhibited reduced biocidal action. Differences in susceptibility to NO from both silica and dendrimer scaffolds were noted between Gram-negative *P*. *aeruginosa* and Gram-positive *S*. *aureus*, with *S*. *aureus* generally requiring increased NO doses for eradication. Furthermore, cytotoxicity against L929 mouse fibroblasts was evaluated for both control and NO-releasing scaffolds at their respective MBCs, with many of the scaffolds proving non-toxic at the concentrations necessary for killing planktonic bacteria.

Chapter 3 built upon the NO-releasing therapeutics utilized in Chapter 2 to understand the effects of nanomaterial properties on the eradication of clinically-relevant bacterial biofilms. The eradication of *P*. *aeruginosa* and *S*. *aureus* biofilms was evaluated as a function of NO-releasing silica nanoparticle size (i.e., 14, 50, and 150 nm) and shape (i.e., aspect ratio 1, 4, and 8). Similar to planktonic studies, NO-releasing silica nanoparticles of reduced size or increased aspect ratio were most effective. However, NO doses ~3–31x those for planktonic assays were required for biofilm killing, resulting in more significant toxicity toward healthy host cells. Despite cytotoxicity concerns for the silica scaffolds at the higher biofilm MBCs, the benefits of NO as an anti-biofilm agent, as well as the importance of particle size and shape were demonstrated. Differences in susceptibility to NO between Gram-negative *P*. *aeruginosa* and Gram-positive *S*. *aureus* biofilms were again observed, with *S*. *aureus* biofilms requiring increased NO doses for eradication.

Similarly, NO-releasing amphiphilic PAMAM dendrimers were evaluated as anti-biofilm agents as a function of size and exterior functionality (i.e., PO/ED ratio). As

expected, size-dependent killing of *P. aeruginosa* biofilms was observed, with improved efficacy of the generation 3 dendrimers over generation 1. The role of surface hydrophobicity in biofilm eradication was also prominent. Enhanced bactericidal efficacy was observed for the hydrophobic ED-modified dendrimers compared to the more hydrophilic PO-modified dendrimers. However, the ED-modified dendrimers were significantly cytotoxic at MBC concentrations necessary for biofilm killing. Thus, the PO to ED ratio was optimized (7:3 and 5:5) to obtain maximum biofilm eradication and minimal cytotoxicity.

In addition to their utility in planktonic studies, NO-releasing chitosan oligosaccharides were evaluated for therapeutic potential against *P. aeruginosa* biofilms. Anti-biofilm efficacy of the NO-releasing chitosan oligosaccharides was demonstrated to be a function of both molecular weight (2.5k, 5k, and 10k) and exterior functionality. In contrast to planktonic studies, an increased MBC for the 10k chitosan oligosaccharide was observed and attributed to more restricted diffusion of the scaffold through the biofilm. Cationic chitosan oligosaccharides rapidly associated with bacterial cells and penetrated the *P. aeruginosa* biofilms, thus exhibiting improved efficacy compared to the neutral PEG-modified scaffolds. Of note, none of the NO-releasing chitosan oligosaccharides studied were cytotoxic to L929 mouse fibroblasts at concentrations necessary for biofilm eradication.

In Chapter 4, the role of NO-release kinetics on biocidal action was investigated against both *P. aeruginosa* and *S. aureus* planktonic bacteria and biofilms. Dendrimers

were synthesized with different ratios of PO and ACN to exhibit varied NO-release profiles (i.e., burst versus sustained release) and similar total NO storage (~1.89 μmol NO/mg). Planktonic cells exhibited greater susceptibility to NO-releasing PO-modified dendrimers (i.e., burst release). However, NO-releasing ACN-modified dendrimers (i.e., sustained release) were more effective at biofilm eradication. Control and NO-releasing PO, 1:1 PO/ACN, 1:7 PO/ACN, and ACN-modified dendrimers were non-toxic to healthy host cells at concentrations required for planktonic bacterial killing. Control dendrimers were also non-toxic at concentrations necessary for biofilm eradication, but significant reductions in fibroblast viability were observed at these concentrations for the NO-releasing dendrimers. Although cytotoxicity did not show a dependence on NO-release kinetics, a clear association exists between high doses of NO and reduced fibroblast viability.

Chapter 5 investigated the effects of silica nanoparticle size and shape toward the terrestrial plant, *Arabidopsis thaliana*. Three sizes (i.e., 14, 50, and 200 nm) of silica nanoparticles with varied surface charge and composition were evaluated for phytotoxicity and plant uptake. Phytotoxic effects (up to 1000 ppm) were mitigated by adjusting the pH of the plant-growth nutrient solution or removal of the particle surface charge. However, size-dependent uptake of the silica particles was observed, with the smaller 14nm particles showing increased uptake in *A. thaliana* root cells. Silicon elemental analysis confirmed particle uptake into the rosettes and stems as well, although to a lesser extent. Silica particle phytotoxicity and uptake were also evaluated as a function of shape (i.e., aspect ratio 1 and 3). *A. thaliana* growth was not significantly

reduced after exposure to AR1 and AR3 particles at 250 ppm for 6 weeks. While AR1 particles were observed in the root cells with TEM, silicon elemental analysis of the roots, rosette, and stems confirmed little uptake of the AR1 and AR3 particles. The minimal uptake observed was likely due to the low exposure concentration. Overall, the silica nanoparticles examined were found to be relatively non-toxic to *A. thaliana* plants.

6.2 Future Directions

The true realization of the potential for engineered nanomaterials is still in its infancy. Nanomaterial use continues to increase rapidly, but much remains to learn about the behavior of these systems in clinical settings and the environment. Ultimately, a predictive approach for determining nanomaterial structure-activity relationships is desired for evaluating toxicity risk, whether beneficial or detrimental. The research presented in this thesis indicates the importance of nanomaterial physicochemical properties (e.g., size, shape, exterior hydrophobicity, drug-release kinetics) in improving the antibacterial action of NO-releasing therapeutics (e.g., silica particles, dendrimers, chitosan oligosaccharides) while minimizing cytotoxicity. In addition, we have initiated work to evaluate the effects of nanomaterial properties on other organisms (i.e., plants) and understand their broader environmental impact. Continued examination of the nanomaterial-bio interface is warranted for extending the utility of NO-releasing therapeutics to additional clinically-relevant infections and for determining the potential for nanomaterial toxicity, transformation, and biomagnification within the environment.

6.2.1 Tuning nanomaterial surface charge and hydrophobicity

With increasing antibiotic resistance, combination antibacterial therapies have become increasingly attractive. Ideally, combining two agents that exert biocidal action via differing mechanisms would prolong their utility and even result in synergistic killing. Long chain cationic quaternary ammoniums compounds have proven effective at both preventing bacterial adhesion and killing adhered bacteria.[1, 2] The positively-charged ammonium group promotes association with the negatively-charged bacterial cell membrane, whereby the long alkyl chains are then able to insert into the membrane and cause disruption. Carpenter et al. reported on the bactericidal efficacy of quaternary ammonium-functionalized silica nanoparticles both with and without NO-release capabilities.[3] The quaternary ammonium-functionalized silica particles were modified with varying chain lengths (i.e., methyl, buytl, octyl, and dodecyl). Scaffolds with longer chain lengths (i.e., octyl and dodecyl) exhibited potent antibacterial efficacy both with and without NO-release, however many of the scaffolds were cytotoxic to fibroblasts. Combining quaternary ammonium-functionalized silica particles with NO-release is thus attractive for the dual-mechanistic killing, reduced risk of antibacterial resistance, and ability of low levels of NO to help mitigate cytotoxic effects and promote fibroblast proliferation.

Based on the work presented in Chapters 2 and 3, it is hypothesized that decreasing the size of the quaternary ammonium/NO-functionalized scaffold (<180 nm) would further improve bactericidal efficacy. As such, quaternary ammonium-modified dendrimers (~2 nm) both with and without NO-release capabilities should be evaluated for bacterial killing. Nitric oxide-releasing dendrimers were previously shown to

associate readily with both planktonic bacteria and biofilms,[4, 5] thus coupling this scaffold with long chain (i.e., octyl and dodecyl), non-depleting quaternary ammoniums may further enhance bacterial eradication. Although quaternary ammonium-functionalized scaffolds previously demonstrated cytotoxicity to fibroblast cells, improved bacterial eradication for quaternary ammonium/NO-modified dendrimers (i.e., reduced material doses) would also likely reduce potential cytotoxicity. Thus, further tuning of the scaffold charge and hydrophobic chain length should be completed to enhance bacterial eradication, while minimizing toxicity to healthy host cells.

6.2.2 Effects of nitric oxide against additional clinically-relevant bacterial strains

Clinically-relevant infections are comprised of diverse communities of bacteria, and thus differential susceptibility to NO may play a significant role in overall bactericidal efficacy.[6-8] As detailed in Chapters 2 and 3, planktonic *P. aeruginosa* and *S. aureus* exhibited differential susceptibility to NO, with *S. aureus* requiring increased doses for eradication. Hetrick et al. previously investigated the anti-biofilm efficacy of NO-releasing silica nanoparticles against Gram-negative *P. aeruginosa* and *E. coli*, as well as Gram-positive *S. aureus* and *S. epidermidis*.[7] At the same concentration of NO-releasing particles, a 5-log reduction in viability was observed for the Gram-negative bacteria (i.e., *P. aeruginosa* and *E.coli*), while only a 2-log reduction in viability was noted for the Gram-positive bacteria (i.e., *S. aureus* and *S. epidermidis*). Varied bacterial membrane structure may be a partial cause for these differences in antibacterial susceptibility.[9] However, other properties of the bacteria may govern NO susceptibility as

well, including antioxidant enzyme levels[10] and production of NO for cytoprotection.[11] The potential Gram-class dependence for NO susceptibility should be further evaluated as a function of scaffold properties, total NO storage, NO-release kinetics, and nutrient conditions for a greater number of bacterial strains (e.g., Gram-negative *A. baumannii* and Gram-positive *E. faecalis*).

Furthermore, additional disease-related (e.g., cystic fibrosis) bacterial strains should be studied for susceptibility to NO-induced killing.[12] Cystic fibrosis (CF) patients exhibit chronic lung inflammation with increased mucus in their respiratory system.[13] Normal clearance of bacteria from the CF respiratory system is prevented and bacterial biofilms readily form. Specifically, antibiotic-resistant, alginate-producing, mucoid *P. aeruginosa* biofilms are associated with the persistence of CF.[14, 15] Inhaled, gaseous NO has shown promise in eradicating CF-relevant *P. aeruginosa*, but continuous exposure to the high NO concentrations required (~160–200 ppm) would lead to methemoglobinemia.[16] As such, NO-releasing macromolecular scaffolds utilizing localized NO delivery should be studied for eradication of CF-relevant *P. aeruginosa* strains. Pulmonary delivery necessitates that the scaffold be biodegrable and thus the NO-releasing chitosan oligosaccharides discussed in Chapters 2 and 3 are promising candidates for therapeutic evaluation.

6.2.3 Effects of nitric oxide against polymicrobial biofilms

In considering the effects of NO against clinically-relevant bacteria, future research should focus on the NO-induced eradication of polymicrobial biofilms.[17] For

example, infected burn wounds are often comprised of *Pseudomonas* and *Staphylococcus* bacterial strains as well as the fungi, *Candida* and *Aspergillus*. Hammond et al. demonstrated the differential efficacy of common antibiotics toward polymicrobial biofilms.[18] Both species in the *P. aeruginosa* and *S. aureus* polymicrobial biofilms were eradicated with gentamycin, however mupirocin readily eradicated only *S. aureus* and triple antibiotic ointment was more effective against *P. aeruginosa*. Thus, examination of NO's broad-spectrum antibacterial action against polymicrobial biofilms is warranted. Preliminary studies determined the effects of NO-releasing G1 PE 73 dendrimers (discussed in Chapter 3) against *P. aeruginosa* and *S. aureus* polymicrobial biofilms. As shown in Figure 6.1, *P. aeruginosa* was preferentially eradicated over *S. aureus*. This result is expected given the differential NO susceptibility observed for the individual bacterial strains, however future work should focus on varying properties of the NO-release scaffold and the initial ratio of *P. aeruginosa* and *S. aureus* within each biofilm. Additionally, eradication should be examined as a function of biofilm age and maturity.

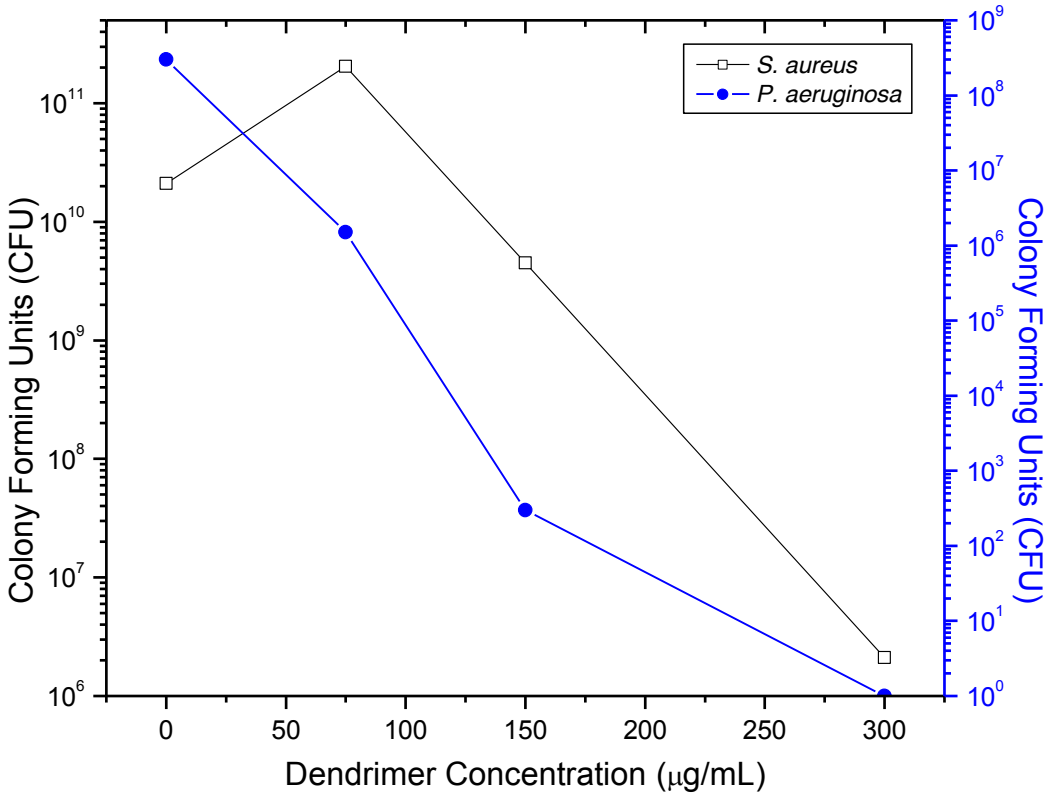

Figure 6.1 Bacterial viability of *P*. *aeruginosa* (circle, right scale) and *S*. *aureus* (square, left scale) after 24 h exposure to NO-releasing G1 PE 73 dendrimers (Chapter 3). *P*. *aeruginosa* was fully eradicated at 300 μg/mL, but ~10^6 colony forming units of *S*. *aureus* remained.

6.2.4 Phytotoxicity as a function of plant species and nanomaterial characteristics

Due to the increased prevalence of new nanomaterials, continued evaluation of phytotoxicity as a function of nanomaterial physicochemical properties is critical. Screening of additional plant types for phytotoxicity is also warranted since nanomaterial uptake and translocation may differ between species and some plants may be more susceptible to toxicity than others.[19] Hydroponic plant growth is suitable for initial toxicity determinations,[20] however if substantial toxicity nanomaterial toxicity is noted, more relevant soil-based experiments should be conducted. The potential for nanomaterial biodistribution and biomagnification should also be examined. For example, gold nanoparticles taken up into tobacco plants were passed onto hornworms through ingestion.[21] A myriad of nanomaterials and plant species exist for phytotoxicity testing, and thus researchers should carefully consider nanomaterial exposure routes, possible nanomaterial transformations, and the potential end organisms when developing their studies.

6.3 Conclusions

The work presented here detailed the importance of nanomaterial physicochemical properties in evaluating biological interactions and toxicity. Silica, dendrimer, and chitosan oligossacharide NO-releasing scaffolds with varied size, shape, and exterior functionality were demonstrated to be effective against common pathogenic bacteria. Nitric oxide-releasing nanomaterials with small size, increased aspect ratio, and hydrophobic exteriors proved the most toxic to bacteria, albeit cytotoxicity to healthy

host cells was also observed in some cases. The determinations made in the preceding chapters will aid in designing future NO-releasing scaffolds to exhibit maximum bactericidal action, while preventing unwanted cytotoxic effects. Furthermore, the evaluation of nanoparticle phytotoxicity in relation to size, surface composition, and shape showed that even if plants exhibit significant particle uptake, extensive toxicity may not be observed. These studies also emphasized the need to evaluate the potential for nanomaterial biodistribution and biomagnification in the environment, especially with regard to the food chain.

REFERENCES

1. Song, J.; Kong, H.; Jang, J., Bacterial adhesion inhibition of the quaternary ammonium functionalized silica nanoparticles. *Colloids and Surfaces B: Biointerfaces* **2011**, *82*, 651-656.

2. Oosterhof, J. J. H.; Buijssen, K. J. D. A.; Busscher, H. J.; van der Laan, B. F. A. M.; van der Mei, H. C., Effects of quaternary ammonium silane coatings on mixed fungal and bacterial biofilms on tracheoesophageal shunt prostheses. *Appl.Environ. Microbiol.* **2006,** *72*, 3673-3677.

3. Carpenter, A. W.; Worley, B. V.; Slomberg, D. L.; Schoenfisch, M. H., Dual action antimicrobials: Nitric oxide release from quaternary ammonium-functionalized silica nanoparticles. *Biomacromolecules* **2012,** *13*, 3334-3342.

4. Sun, B.; Slomberg, D. L.; Chudasama, S. L.; Lu, Y.; Schoenfisch, M. H., Nitric oxide-releasing dendrimers as antibacterial agents. *Biomacromolecules* **2012,** *13*, 3343-3354.

5. Lu, Y.; Slomberg, D. L.; Shah, A.; Schoenfisch, M. H., Nitric oxide-releasing amphiphilic poly(amidoamine) (PAMAM) dendrimers as antibacterial agents. *Biomacromolecules* **2013,** *submitted*.

6. James, G. A.; Swogger, E.; Wolcott, R.; Pulcini, E. d.; Secor, P.; Sestrich, J.; Costerton, J. W.; Stewart, P. S., Biofilms in chronic wounds. *Wound Repair Regen*. **2008,** *16*, 37-44.

7. Hetrick, E. M.; Shin, J. H.; Paul, H. S.; Schoenfisch, M. H., Anti-biofilm efficacy of nitric oxide-releasing silica nanoparticles. *Biomaterials* **2009,** *30*, 2782-2789.

8. Privett, B. J.; Deupree, S. M.; Backlund, C. J.; Rao, K. S.; Johnson, C. B.; Coneski, P. N.; Schoenfisch, M. H., Synergy of nitric oxide and silver sulfadiazine against gram-negative, gram-positive, and antibiotic-resistant pathogens. *Mol. Pharm*. **2010,** *7*, 2289-2296.

9. Nikaido, H.; Vaara, M., Molecular basis of bacterial outer membrane permeability *Microbiol. Rev*. **1985,** *49*, 1-32.

10. Mandell, G., Catalase, superoxide dismutase, and virulence of *Staphylococcus aureus*. In vitro and in vivo studies with emphasis on staphylococcal--leukocyte interaction. *J. Clin. Invest*. **1975,** *55*, 561-566.

11. Gusarov, I.; Nudler, E., NO-mediated cytoprotection: Instant adaptation to oxidative stress in bacteria. *Proc*. *Natl*. *Acad*. *Sci*. *U.S.A*. **2005,** *102*, 13855-13860.

12. Treggiari, M. M.; Rosenfeld, M.; Retsch-Bogart, G.; Gibson, R.; Ramsey, B., Approach to eradication of initial *Pseudomonas aeruginosa* infection in children with cystic fibrosis. *Pediatric Pulmonology* **2007,** *42*, 751-756.

13. Nichols, D.; Chmiel, J.; Berger, M., Chronic inflammation in the cystic fibrosis lung: alterations in inter- and intracellular signaling. *Clinic*. *Rev*. *Allergy Immunol*. **2008,** *34*, 146-162.

14. Lister, P. D.; Wolter, D. J.; Hanson, N. D., Antibacterial-resistant *Pseudomonas aeruginosa*: Clinical impact and complex regulation of chromosomally encoded resistance mechanisms. *Clin*. *Microbiol*. *Rev*. **2009,** *22*, 582-610.

15. Pedersen, S. S., Lung infection with alginate-producing, mucoid *Pseudomonas aeruginosa* in cystic fibrosis. *APMIS* **1991,** *28*, 1-79.

16. Miller, C.; McMullin, B.; Ghaffari, A.; Stenzler, A.; Pick, N.; Roscoe, D.; Ghahary, A.; Road, J.; Av-Gay, Y., Gaseous nitric oxide bactericidal activity retained during intermittent high-dose short duration exposure. *Nitric Oxide* **2009,** *20*, 16-23.

17. Peleg, A. Y.; Hogan, D. A.; Mylonakis, E., Medically important bacterial-fungal interactions. *Nat*. *Rev*. *Microbiol*. **2010,** *8*, 340-349.

18. Hammond, A. A.; Miller, K. G.; Kruczek, C. J.; Dertien, J.; Colmer-Hamood, J. A.; Griswold, J. A.; Horswill, A. R.; Hamood, A. N., An in vitro biofilm model to examine the effect of antibiotic ointments on biofilms produced by burn wound bacterial isolates. *Burns* **2011,** *37*, 312-321.

19. Ma, X.; Geiser-Lee, J.; Deng, Y.; Kolmakov, A., Interactions between engineered nanoparticles (ENPs) and plants: Phytotoxicity, uptake and accumulation. *Sci*. *Total Environ*. **2010,** *408*, 3053-3061.

20. Tocquin, P.; Corbesier, L.; Havelange, A.; Pieltain, A.; Kurtem, E.; Bernier, G.; Perilleux, C., A novel high efficiency, low maintenance, hydroponic system for synchronous growth and flowering of *Arabidopsis thaliana*. *BMC Plant Biology* **2003,** *3*, 2.

21. Judy, J. D.; Unrine, J. M.; Bertsch, P. M., Evidence for biomagnification of gold nanoparticles within a terrestrial food chain. *Environ*. *Sci*. *Technol*. **2011**, *45*, 776-781.